Nanopatterned PLGA for Anti-cancer Implant Applications

by

Lijuan Zhang

B. Eng., Polymer Science and Engineering,

Sichuan University, Chengdu, 2007

A dissertation submitted in partial fulfillment of the

requirements for the Degree of Doctor of Philosophy

in the Department of Chemistry at Brown University

Providence, Rhode Island

May 2012

This dissertation by Lijuan Zhang is accepted in its present form

by the Department of Chemistry as satisfying the

dissertation requirement for the degree of Doctor of Philosophy.

Date_____ _____

Professor Thomas J. Webster, Advisor

Recommended to the Graduate Council

Date_____ _____

Professor Shouheng Sun, Reader

Date_____ _____

Professor Sarah Delaney, Reader

Approved by the Graduate Council

Date_____ _____

Professor Peter M. Weber, Dean of the Graduate School

Curriculum Vitae

Lijuan Zhang was born in Sichuan, China, grown up in a beautiful city - Suining. In 2003, she entered into Sichuan University for higher education in the School of Polymer Science and Engineering, from which she was awarded the B. Eng. in 2007. She joined the PhD program in the Department of Chemistry at Brown University in 2008 and joined Dr. Thomas Webster's lab in the School of Engineering at Brown. Her research focused on nanopatterned PLGA for anti-cancer applications. She has published a number of articles in peer-reviewed journals and presented her research results at more than 13 conferences.

Publications

1. Zhang L, Webster TJ. Poly-lactic-glycolic-acid surface nanotopographies selectively decrease breast adenocarcinoma cell functions. *Nanotechnology* 2012; 23; 155101.
2. Zhang L, Webster TJ. Decreased lung carcinoma cell functions on select polymer nanometer surface features. *Journal of Biomedical Materials Research A* 2012; 100A; 94-102
3. Yang L, Zhang L, Webster TJ. Carbon nanostructures for orthopedic medical applications. *Nanomedicine* 2011; 6(7); 1231-1244
4. Yang L, Zhang L, Webster TJ. Nanobiomaterials: State of the art and future trends. *Advanced Engineering Materials* 2011; 13(6); B197-B217

5. Zhang L, Chun YW, Webster TJ. Decreased lung carcinoma cell density on select polymer nanometer surface features for lung replacement therapies. *International Journal of Nanomedicine* 2010; 5; 269-275

6. Zhang L, Webster TJ. Decreased breast adenocarcinoma cell functions on select polymer nanometer surface features. *Bioengineering Conference Proceedings* 2011; 1-2

7. Zhang L, Webster TJ. Decreased lung carcinoma cell density on select polymer nanometer surface features for lung replacement therapies. *Materials Research Society Symposium Proceedings* 2009; 1209; 1209-YY07-08

Preface and Acknowledgements

I would like to thank my advisor, Dr. Thomas J. Webster for his support throughout my PhD study at Brown. He gave me constructive guidance and enormous support in my research. I would also like to thank my thesis committee: Dr. Souheng Sun and Dr. Sarah Delaney for reviewing my dissertation and providing valuable advice. I also want to thank the Hermann Foundation for funding.

I thank all the members from Dr. Webster's laboratory for their assistance with many of the experiments that I conducted over the years. I would like to express my appreciation to Lei Yang, Bo Li, Stephanie Terrizzi, and Vera Fonseca for their important contributions to my research.

I want to give my thanks to my wonderful host family, Shari Weinberger, Zachary Weinberger and Amanda Weinberger. Their kindness and hospitality have given me unforgettable experience in US. I also want to thank all my friends, Hongming Zhu, Esther Boucher-Yip, Lijia Zhao, *etc*., for their support and encouragement.

Lastly, I am most grateful to my family, Yonghao Wang, Honghui Zhang, Zhenyu Tang, and Jian Zhang who have gave me tremendous support.

Table of Contents

List of Tables

List of Figures

Chapter 1 Introduction

1.0. Preface

In the past decade, it has been clear that the development of the next generation of biomaterials has entered the era of nanotechnology. The interface between biomaterials and nanotechnology has enormous potential for the development of novel biomaterials to improve the prevention, diagnosis, and treatment of numerous diseases. This field has become one of the fastest emerging and developing arenas at the intersection of all of materials science and biology. Nano biomaterials, a term describing biomaterials with constituent feature sizes less than 100 nm (10^{-7} m), are not only extraordinary materials with unique structures and properties to solve our most traditional biomedical puzzles, but they also provide unprecedented knowledge towards understanding biology, medicine and materials science. Thus, nanotechnology-derived biomaterials have been widely used in a broad spectrum of biological and biomedical applications, from artificial implants to drug delivery to medical imaging. These nano biomaterials include (but are not limited to) metals, ceramics, polymers, hydrogels, and novel self-assembled materials with structures from 0-D (i.e., dots and particles) to 3-D (i.e., tissue engineering scaffolds).

Undoubtedly, the rapid development of nano biomaterials has been creating a new multidisciplinary area across biology, chemistry, materials science and medicine. The reason behind the establishment of this new area is that nanotechnology has not only provided novel materials and tools for biological and medical purposes, but it is also

reshaping our thinking towards applying these materials in science and technology. Today, studies on nanostructured biomaterials have evolved into more comprehensive and systematic studies, resulting in the further understanding of the mechanisms behind biological responses to materials and the consequent better design of such materials. It is clear that the great potential and now well-known benefits of nanostructured biomaterials will be widely applied in numerous clinical practices. Representative nano biomaterials used in disease prevention, diagnosis and treatment are listed in Table 1.1.

The interaction between cells and their extracellular matrix (ECM) is complicated, drawing much attention for biomaterial interfacial research since understanding this interaction will significantly contribute to the design of better implants. In principle, cell adhesion to the ECM plays a crucial role in regulating cell functions, including cell proliferation, differentiation, morphology, apoptosis and gene expression. Thus, it is desirable to control cell responses at the cell-biomaterial interface in an expected manner. One approach to achieve controlled regulation of cellular functions is to modulate the ECM by designing specific biomaterial surface characteristics [1]. Nanoscale topographies on biomaterial surfaces are, thus, expected to provide a platform of regulating cell functions by the fact that most proteins involved in the ECM have dimensions in the range of several nanometers such as integrins, talin, fibronectin, laminin, and paxillin. Many studies have shown that cells (such as bladder smooth muscle cells, chondrocytes (cartilage forming cells) and osteoblasts (bone forming cells)) respond differently to nano-structured poly (lactic-co-glycolic acid) (PLGA) surfaces compared to nano-smooth surfaces. For example, Rosenberg claimed (as early as 1962) that nanometer sized features may influence cell functions [2, 3]. As

another example, Arnold *et al.* created nanometer Au nanodot arrays separated by various distances (specifically 28, 58, 73 and 85 nm) and found that a separation of 73 nm or more inhibited MC3T3-osteoblast spreading, affording a good cue to create nanostructured patterns to decrease osteoblast functions [4].

However, little attention has been paid to determine cancer cell responses to nano-patterned surfaces. A study by Tzvetkova-Chevolleau *et al.* [5] found that nanopillars and nanolines can strongly modify the dynamics of cancerous (SaI/N) fibroblastic cell spreading, suggesting that nanofeatured surfaces may regulate cancer cell functions. Moreover, the significantly altered surface properties of nanomaterials (i.e., the smaller feature size, increased surface area, surface energy) can control initial protein adsorption from blood, cell spreading, and cell-biomaterial signal pathways, providing the potential of nanofeatures to decrease cancer cell functions. Therefore, this dissertation, for the first time, investigated lung and breast cancer cell adhesion, proliferation, morphology, apoptosis and vascular endothelial growth factor (VEGF) secretion on nanopatterned surfaces compared to conventional nanosmooth surfaces. This dissertation documents the methods, findings, analyses and conclusions of these pioneering studies. But first, in order to understand the role nanopatterns may play in regulating cancer cell functions, it is necessary to introduce all relevant background including how cancer is formed, is currently treated, how cancer implants are used (including their promises and current failures), material properties pertinent to control cellular responses, and cell sensing to nanostructured surfaces that can be exploited to decrease cancer cell functions.

Table 1.1. Nano biomaterials for disease prevention, diagnosis and treatment

Material category	Chemical or structural features	Examples of applications
Ceramics	Iron oxide nanoparticles	MRI agents for a large variety of imaging and sensing purposes, such as *in vitro* location and pathway imaging, *in vivo* cancer detection and diagnosis, drug/cell/gene tracking, sentinel lymph node (SLN) imaging [6-13]
	Dye-doped silica nanoparticles	Low-photobleaching, high-stable imaging agent [14]
	Nanoporous ZrO_2/chitosan composite	Glucose detection [15]
Quantum dots	Cd/Se/Te-based quantum dots	Imaging cancer cells, for example, SLN imaging [16]
	CdSe/ZnS	In vitro imaging [17]
Polymers	Dox-loaded nanoparticles	Over 8-fold increase in breast cancer cell death [18]
	Self-assembling nanoparticles with siRNA	Selective tumor uptake, siRNA sequence-specific inhibition of protein expression and inhibition of both tumor angiogenesis and growth rate [19]
Metals	Gold nanoparticles	Cancer detection, imaging and diagnosis [20]
	Silver nanoparticles, nanofilms, etc.	Fluorescence enhancing agents, cancer detection and diagnosis [21, 22]
Other nanomaterials	Single fluorescent nanodiamond	Low-photobleaching labeling agent [23]
	Perfluorocarbon	MRI contrast agent for fibrin clots [24]
	Fluorescent polystyrene nanobeads	Visualizing SLN [25]
	Carbon nanotubes (CNT)	Protein detection [26], antigen and DNA detection [21]
	Si nanowires	Streptavidin detection [27]

1.1. Lung and breast cancer formation and current treatments

Cancer is, in essence, a genetic disease. Alterations in three types of genes are responsible for tumorigenesis: oncogenes, tumor-suppressor genes and stability genes. However, mammalian cells have multiple safeguards to protect them against the potentially lethal effects of cancer gene mutations, and only when several genes are defective does an invasive cancer develop [28]. When cancer develops, cells grow and proliferate in an uncontrollable way and eventually forms a mass beyond some size limit known as a tumor. Moreover, tumor cells can grow aggressively and invade other tissues of the body, which is termed metastasis.

Lung cancer is one of the most difficult cancers to treat, responsible for the highest percentage of cancer death. Clinical evidence indicated that lung cancers have accumulated numerous (perhaps 20 or more) clonal genetic and epigenetic alterations as a multistep process, including the classical genetic abnormalities of tumor suppressor gene (TSG) inactivation and overactivity of growth promoting oncogenes [29]. Moreover, tumor acquired promoter hypermethylation has been recognized as a mechanism for the epigenetic inactivation of gene expression [29]. Currently, the most common three treatments for lung cancer include surgical removal of the tumor, chemotherapy and radiation therapy. In the medical community, there is general agreement that the definitive surgical treatment is the first choice of therapy for all patients with non-small cell lung cancer limited to the lung, whether intrapulmonary nodes are involved or not (stages I and II) [30]. Radiation therapy uses high-energy ionizing radiation (i.e., X-rays and gamma rays) to control or kill cancer cells. Chemotherapy involves the use of medicines or drugs to kill cancer cells or stop the proliferation of cancer cells. Until now,

surgical removal is still the leading method for lung cancer treatment and especially, for end-stage lung cancer, it is the only way for a patient to survive.

Breast cancer is the second leading cause of cancer death after lung cancer. It has been observed that elevated levels of serum estrogens preceded the occurrence of breast cancer which bind to estrogen receptors and stimulate the transcription of genes involved in cell proliferation, creating potential errors in DNA replication and potential mutations [31]. In breast cancer, overexpression of leptin stimulated cancer cell proliferation [32]. Six types of standard treatments have been developed for saving one's life from breast cancer, including surgery, sentinel lymph node biopsy followed by surgery, radiation therapy, chemotherapy, hormone therapy, and targeted therapy [33]. Most patients with breast cancer have surgery to remove the cancer from the breast. Normal types of breast surgery include lumpectomy (remove a tumor and a small amount of normal tissue around it), partial mastectomy (remove the part of the breast that has cancer and some normal tissue around it), total mastectomy (remove the whole breast that has cancer), modified radical mastectomy (remove the whole breast that has cancer, many of the lymph nodes under the arm, and the lining over the chest muscles), and radical mastectomy (remove the breast that has cancer, chest wall muscles under the breast, and all of the lymph nodes under the arm) [33].

With this in mind, after the removal of the cancer (whether lung or breast), it is important to develop implants to maintain the original organ's function while at the same time to inhibit cancer cell growth which may be not totally removed by the surgical process to keep cancer from regrowing.

1.2. Implants after tumor removal

Implants are frequently used after tumor removal (in particular for cancers of the lung, breast and skin) and have been widely applied to rebuild the corresponding functions of the excised tissue for saving the life of cancer patients. The development of artificial lungs and the replacement of breast tissue are two of the most common cancer implants currently being developed due to the high incidence of these two cancer types. Currently, lung transplantation is currently the only treatment option for patients with end-stage lung disease [34]. Procedures include wedge resection (removal of part of a lobe), segmentectomy (removal of an anatomical division of a particular lobe of the lung), lobectomy (one lobe), bilobectomy (two lobes), or pneumonectomy (whole lung) [35].

Similarly, most patients with breast cancer have surgery to remove the cancer from the breast. Thus, in order to effectively replace the resected tissues of these cancer patients, it is necessary to design an ideal replacement construct that will decrease interactions with cancer cells should they have not been completely removed during surgery or if they return to the lung/breast tissue. For example, according to the American Cancer Society (ACS), 11% of women will suffer from breast cancer recurrence within five years and 20 percent in 10 years. The Lung Cancer Study Group (LCSG) reported a recurrence rate of 10.6% per year for patients with non-small cell cancer [36]. In this manner, biomaterials with anti-cancer properties would be an ideal implant after cancer resection. It is clear that the current plethora of materials used for breast reconstruction (i.e., saline implant, silicone gel, or polyurethane foam coating) were not originally designed to inhibit the return of cancer. For example, silicone implants are dangerous to the brain as silicone rupture can leak into the brain and lead to brain tumors in some cases.

On the other hand, most implants used for other tissues (such as metallic cobalt, metallic nickel, silicone breast implants, and ceramic implants) have a cancerogenic danger, so it is necessary to have anticancer properties for implants. For example, reports of local malignancy after hip and knee joint replacements with metal implants suggest a carcinogenic possibility with long-term risks [37]. Concern regarding the risk of cancer in women with implants is raised by findings that the polyurethane foam cover used to coat some implants has been found to have the potential for releasing 2,4-toluene diamine, a demonstrated carcinogen of liver cancer in laboratory animals [38, 39]. Also, another study found that after intratracheal instillation of nickel, significant numbers of squamous-cell carcinomas and adenocarcinomas of the lung were observed in rats [40].

According to a meeting held to evaluate the carcinogenic risks to humans of surgical implants and other foreign bodies, groups of possibly carcinogenic materials to humans were classified as: (1) polymeric implants (such as silicones, poly-urethanes, polymethacrylates, polyethylene terephthalate, polypropylene, and polyethylene) prepared as thin smooth films (but not poly (glycolic acid) or poly (lactic acid), the focus of this study); (2) metallic implants (such as stainless steel) prepared as thin smooth films; and (3) implanted foreign bodies consisting of cobalt, nickel and a particular alloy powder consisting of 66±67% nickel, 13±16% chromium and 7% iron [40]. Thus, in order to decrease such cancer risks, designing an implant with anticancer properties (i.e., inhibition of cancer cell responses while still promoting healthy cell functions) could be an effective way to prevent the occurrence of cancer involved in surgical implants. There are many reasons towards why nanotechnology may decrease cancer cell functions and increase cell functions.

1.3. Cell sensing and responses to nanostructured surfaces

Since the in vivo contact between cells are not smooth but are nano (5-200 nm) textured, nanotopographies on current implanted materials could present a biomimetic cell-stimulating environment in mediating cell responses and behaviors [1]. Basement membranes are composed of extracellular matrix proteins and are found throughout the vertebrate body, serving as substrata for overlying cellular structures. The topography of basement membranes is a complex mixture of pores, ridges, and fibers which have sizes in the nanometer range [41]. Therefore, nanotopographies could be an effective extracellular physical milieu affecting cell behaviors, without involving biomolecules. Representative surface nanotopographical features affecting cell behaviors are listed in Table 1.2.

Many studies [42-46] have demonstrated different cell sensing and responses to micro- and nanotopographies with regards to both isotropic and anisotropic topographies. However, in terms of anisotropic topographies such as grooves, ridges and waves, cell orientation and migration along the anisotropic direction have long been observed and examined. As for isotropic topographies, such as pores, spheres, dots and pillars, studies have found significant effects of these topographies on collective cell functions and they have revealed that topographical patterns determine what cell functions are regulated and the topographical scale affects the degree to which function is regulated [1].

Table 1.2. The effects of surface nanotopographical features on cell functions

Material category	Nano biomaterials	Structural feature	Applications
Self-assembly structures	Peptide-amphiphiles (PA)	Branched-PA self-assembling coatings	Promoting initial adhesion of primary human bladder smooth muscle cells [47]
	Polyelectrolyte multilayer assemblies	Nanoscale porous multilayers (poly(allylamine hydrochloride) (PAH), poly(acrylic acid) (PAA))	Significantly promoting corneal epithelial cell proliferation and migration speeds [48]
Polymers	Poly(lactic-co-glycolic acid) (PLGA)	Nanostructured film	Enhancing endothelial, smooth muscle and bladder smooth muscle cell attachment [49, 50]
		Nano-structured PLGA scaffolds	Enhancing cell adhesion and growth, promoting elastin and collagen production [51]
		NaOH-treated PLGA scaffolds	Increasing chondrocyte attachment, total intracellular protein and extracellular matrix synthesis [52]
		PLGA/nano-hydroxyapatite hybrid scaffolds	Increasing MSC attachment, viability and proliferation [53]
	Poly(ether urethane) (PU)	Nanostructured films	Increasing bladder smooth muscle cell attachment [49]
	Poly(Ɛ-caprolactone) (PCL)	Honeycomb-patterned film	Enhancing cell survival and yield of rat small hepatocytes [54]
	Poly(dimethyls-iloxane) (PDMS)	Nanorough film	Increasing endothelial cell adhesion and elongation [55]
Ceramic	Alumina	Nanoporous membranes	Decreasing platelet adhesion [56]

Metals	Titanium	Nanotubular anodized titanium	Enhancing chondrocyte adhesion [57]
	Gold	Thin films with nanoscale roughness	Increasing embryonic stem-cell-derived neural precursors adhesion and differentiation [58]
Semiconductor	Silicon	Nano-island silicon	Increasing insulinoma cell adhesion and insulin secretion [53]
		Silica nanoparticle-modified surfaces	Enhancing osteogenic differentiation of human mesenchymal progenitor cells [59]
Carbon nanostructures	Diamond	Ultra-nanocrystalline diamond films	Induction and regulation of the differentiation of neural stem cells [60]

Many studies [42-44, 61] have also demonstrated cell orientation and migration along the anisotropic direction of surface topographies such as grooves and ridges. For example, a study found that rat dermal fibroblasts on 2 and 5 µm grooves on a poly (dimethylsiloxane) (PDMS) cast of silicon were elongated and aligned parallel to grooves [42, 62]. Moreover, Dunn et al. indicated that ridge width was more important that groove width in determining fibroblast alignment and the alignment of cells inversely proportional to ridge width [43]. In addition to cell orientation, orientation and alignment of actin filaments and microtubules have also been identified as the first and primary event in contact-guided cell alignment [1]. Oakley *et al.* reported that on V-shaped 15 µm wide, 3 µm deep grooves on Ti-coated silicon, microtubules of human gingival fibroblasts were the first element to become aligned at the bottom of grooves after 20 mins, actin alignment was observed first at the wall-ridge edges after 40-60 mins and after 3 h most of the cells exhibited aligned focal contacts [61]. Another study also demonstrated that microfilaments and vinculin from rat dermal fibroblasts oriented along 2 µm grooves on PDMS casts of silicon and bovine and endogeneous fibronectin and vitronectin were also oriented along the direction of grooves [44]. However, most of these early studies used topographies with µm scales due to the limitation of fabrication techniques for nano sized topographies.

Recently, some advances have been made concerning nanotopography regulation of cell functions. For example, Webb *et al.* [63] prepared 130 nm-4.01 µm wide, 100 nm-1.17 µm deep grooves on poly-D-lysine coated chrome plated quartz using a laser holographic technique. It was found that rat optic nerve oligodendrocytes were highly aligned along surface contours as small as 100 nm deep and a 260 nm repeat spacing.

Moreover, oligodendrocytes showed no high-order F-actin cytoskeletal network but aligned optic nerve astrocytes showed a striking arrangement of actin stress fibers.

The size scales of anisotropic topographies play an important role in determining the degree of cell orientation. Generally, cell orientation and alignment increase with increasing groove depth but decrease with increasing width. For example, Clark *et al.* [64] observed that BHK (baby hamster kidney) cells aligned on all groove topographies with features 130 nm wide and 100, 210, or 400 nm deep grooves, but the degree of alignment increased with increasing groove depth; MDCK (Madin-Darby canine kidney) cells aligned and elongated to grooves, but elongation only increased with increasing depth. Another study also found that human corneal epithelial cells elongated and aligned along patterns of grooves and ridges with feature dimensions as small as 70 nm and the percentage of aligned cells increased with groove depth. Also, actin microfilaments and focal adhesions aligned along the substrate topographies and the width of focal adhesions was determined by the width of the ridges in the underlying substrate [65]. Fredrik *et al.* investigated axonal outgrowth on nano printed patterns in polymethylmethacrylate (PMMA)-covered silicon chips consisting of parallel grooves with depths of 300 nm and varying widths of 100-400 nm. Axons from neurons displayed contact guidance on all patterns, but the nerve cell processes preferred to grow on ridge edges and elevations in the patterns rather than in grooves [66]. These studies indicated that anisotropic topographies from micro- to nanoscale can profoundly affect cell shapes. However, cell functions at the molecular level, such as gene expression, differentiation, apoptosis and examination of cancer cells as well on such cell features need to be more extensively examined.

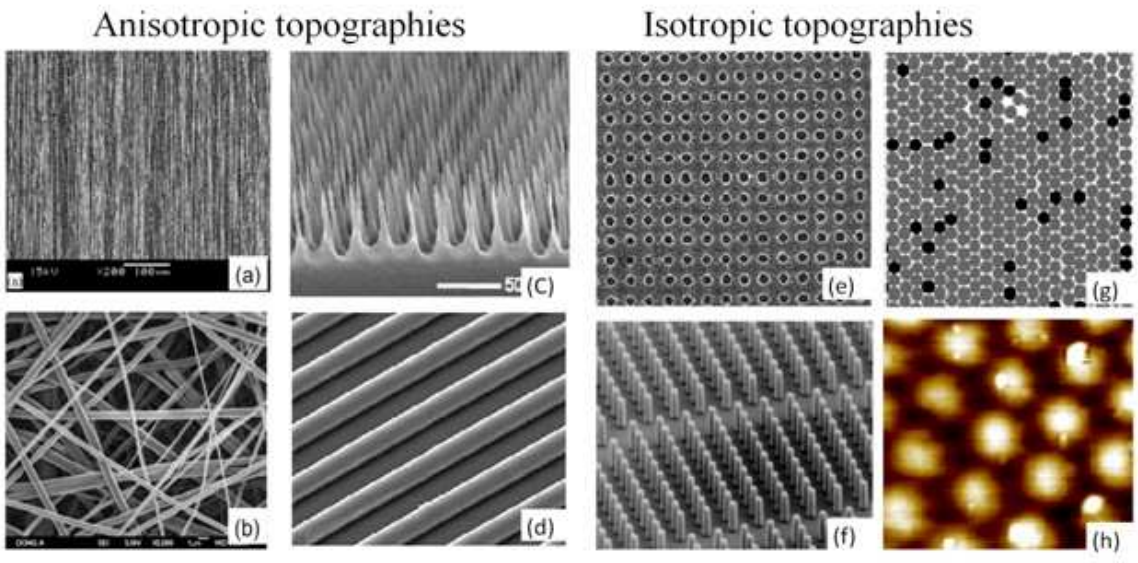

Fig. 1.1. Examples of surface topographical features: (a) poly(L-lactic acid) (PLLA) aligned nanofibers, (b) poly(lactic-co-glycolic) acid (PLGA) nanofiber scaffold, (c) silicone sharp-tip nanotopography, (d) quartz surface with grooves, (e) silicon nanopits, (f) polystyrene (PS) nanopillar surfaces, (g) arginine-glycine-aspartic acid (RGD) nanoislands and (h) PLGA nanospheres (images adapted and redraw from [67-73]).

In regards to isotropic micro- and nanotopographies (including uniformly or randomly distributed pits, nods, pillars, pores, spheres, cylinders, etc.) with no directional guidance, cell orientation and alignment have not been observed, however, the control of other cell functions, such as cell proliferation, morphology and apoptosis, has been revealed [1]. Moreover, the topographical scale has determined whether and to what degree cells alter specific functions and, thus, accurate control of topographical size is an important consideration in regulating cell functions. For example, human abdomen fibroblasts on 2 μm and 5 μm diameter nodes showedan increased rate of proliferation and increased cell density than that on 2 μm and 5 μm wells on PDMS casts of silicone

[74]. However, another study by Hunt *et al.* [75] found no significant stimulation on neutrophil movement with no effects on fibroblast spreading on uniformly arrayed nodes 7, 25, or 50 µm wide and 0.5, 1.5, 2.5 µm high. Fujimoto *et al.* [46] fabricated a micropatterned polystyrene surface with settling particles in diameters of 0.86-0.63 µm when the temperature raised from 25 to 37 ^{o}C and found that neutrophil-like induced HL-60 cells loosely adhered but did not spread on the spherical coated surfaces.

Recently, the development of polymer demixing and colloidal lithography has made it possible to produce large areas of nanotopographical surfaces with reasonable uniformity. Jung *et al.* [76] investigated human foetal osteoblastic cell responses to randomly distributed nanoisland topographies with varying heights (11, 38 and 85 nm) produced by a polystyrene (PS)/polybromostyrene polymer-demixing techniques. Cells cultured on 11 nm high islands displayed significantly enhanced cell adhesion, cell proliferation, cell spreading, cell dimensions, and alkaline phosphatase (non-specific metalloenzyme which hydrolyzes phosphate esters) activity than cells on larger nanoislands or flat PS control. Also, cell signal transmission (such as focal adhesive vinculin proteins and cytoskeletal actin stress fibers) was more pronounced for cells cultured on the smaller nanoisland surfaces. Other studies by Dalby *et al.* [77] demonstrated increased fibroblast responses (such as cell signaling, proliferation, cytoskeleton, and production of extracellular matrix proteins) to 13 nm high polymer demixed islands than on planar controls. However, the control of phase separation in polymer mixtures is difficult and results in some randomly arrayed nanopatterns.

In a much more simple and versatile process of colloidal lithography, colloidal particles can be arranged into an array (an ordered structure) through self-organization

and have been used as templates to produce nanotopographies [78]. Specifically, Ann-Sofie *et al.* [79] reported that human bladder carcinoma cells cultured on hemispherically structured surfaces prepared by colloidal lithography (100 nm high, 168 nm in diameter) decreased IL-6 (mediator of acute inflammatory responses) and IL-8 (induction of chemotaxis) cellular production and were less spread, less round and more stellate (larger dispersion) compared to flat control surfaces. In another study, human fibroblasts were observed trying to endocytose nanocolumns (160-nm high, 100-nm diameter, and 230-nm center-center spacing) produced by colloidal lithography and a small population of the cells changed to unusual morphologies with macrophage-like processes and a highly disrupted cytoskeleton [80]. These results implied the potential of nanotopography on decreasing cancer cell functions.

Some other randomly oriented nanometer rough surfaces can also be fabricated by acid etching, electropolishing, sandblasting, and plasma spraying, demonstrating large effects on cell functions. For example, Martin *et al.* studied rough titanium (Ti) surfaces and observed that electropolished surfaces had more MC63 osteoblast cells while Ti-plasma-sprayed surfaces had less cells than tissue culture polystyrene (TCPS), thymidine incorporation, and alkaline phosphatase production except on coarse blasted Ti [41, 46]. Peritoneal macrophages accumulated preferentially on roughened polystyrene surfaces while fibroblasts preferred smooth surfaces [81]. In summary, micro- and nanotopographical features can clearly mediate cell-biomaterial interactions controlling cell functions for specific applications. A tentative trend can be drawn that smaller nanotopographical features can stimulate cell functions greater than smooth surfaces and such effects decrease with increasing topographical features [1]. However, all of these

studies have not provided a systematic, extensive insight into the effects of nanotopography on cancer cell behaviors and whether nanotopographical features could be used as an implant to regenerate healthy tissue after cancerous tissue is removed.

A thorough review of the effects of surface topographical features on various cell functions has implied the potential applications of nanotopography on regulating cancer cell functions. In order to better understand the cell-biomaterial interactions, we first must examine several important material properties related to cell biological behaviors.

1.4. Surface properties of nanomaterials relevant to biological effects

1.4.1. Brief overview of biological responses to implants

Nanomaterials possess numerous unique properties compared to bulk conventional materials (e.g., materials with microstructured features in the micron or larger sizes) that can influence cell functions: (i) much larger surface areas and resulting increased surface reactivity; (ii) greatly enhanced mechanical properties (such as high ductility and high yield strength) due to various mechanisms depending on their chemistry (such as increased grain boundary sliding and short–range diffusion-healing); (iii) exceptional magnetic, optical and electrical properties due to stacking, alignment and orientation of nanoscale building blocks (grains, supermolecules, etc.); and (iv) homogeneity and high purity in composition and structure because of reaction or mixing at the molecular and atomic levels. Specifically, nanoscale materials and structures provide a few other important properties to a biomaterial. First is their structural similarity to natural tissues or biological systems which have nanoscale hierarchical

components. Second is the comparable size of nanoscale materials to biomolecules and bio-microstructures, which enables researchers to detect, manipulate and mediate these bio-components. Lastly, nanostructured materials can be readily tailored to reveal extraordinary variations in surface properties.

Compared to the understanding of nanomaterial properties and the ability to control these properties, what occurs at the interface between nanomaterials and biological systems (e.g., cells and tissues) has not been completely understood to date. A general consensus is that there are a sequence of events which occurs at the interface between biomaterials and a cell [82, 83]: (a) adsorption of proteins from blood and tissue fluids onto the nanomaterial surface (usually protein desorption also occurs at the same time); (b) tissue cells and/or inflammatory cells approach the material; (c) possible targeted release of matrix proteins from the biomaterial and selected adsorption of specific proteins; and (d) adhesion of cells and commencement of subsequent cell functions (e.g., proliferation, differentiation, phagocytosis, etc.). These events happen at a time scale from milliseconds (e.g., protein adsorption) to even years (foreign body granuloma reaction). Besides these host responses towards nanomaterials, conversely, material responses to the host (like material decomposition and release) also exist at the cell-biomaterial interface [83]. All of these interfacial events are crucial for the success of nano biomaterials, because they are closely related to material cytocompatibility properties and immune or inflammatory host responses that ultimately determine the efficacy and safety of nano biomaterials.

For cancer implants, there are several important host responses or mechanisms which occur after implantation. These responses include inflammatory processes,

coagulation and hemolysis, adaptation, chemical and foreign-body carcinogenesis and an allergic foreign-body response. Inflammation is a response to trauma, infection, local cell death, presence of cancer cells, intrusion of foreign materials, or an adjunct to immune responses [84]. During tissue responses to implants, a sequence of events arise such as acute and chronic inflammation, granulation tissue generation (the proliferation of new small blood vessels and fibroblasts), foreign body reaction (composed of foreign body giant cells, macrophages, fibroblasts, and capillaries in varying amounts, depending upon the form and topography of the implanted material), and fibrous encapsulation (scar formation) [85]. The chronic inflammatory response to biomaterials is confined to the implant site, whereas the foreign body reaction with granulation tissue development is considered the normal wound healing response to implanted biomaterials (i.e., the normal foreign body reaction).

For implants, the surface properties (such as chemistry, topography and roughness, rigidity, surface energy and surface charge) of the medical device, prosthesis, or biomaterial can determine the composition and extent of the foreign body reaction [86]. Thus, surface modification strategies of biomaterials have been developed to reduce implant failure. Besides inflammation, implant materials (especially smaller-sized materials such as particles) may trigger responses from immune cells (such as monocytes, macrophages, dendritic cells and natural killer cells) which recognize and differentiate these “foreigners” from the host, and protect the host from exposure by destroying these foreign substances through acid chemical secretions. At present, immune responses to implants have been widely reported including hypersensitivity related to peacemakers,

dental implants, artificial organ, and orthopedic implants [87-89]. Therefore, suppressing inflammation and an immunological response of implants is a topic of great interest.

In addition, infection is another common problem associated with an implant. Normally, three types of infection are distinguishable including a superficial immediate infection, deep infection and late infection [90]. A superficial infection is the growth of organisms on the skin in association with an implant, such as suture infections. A deep infection is usually seen after surgery as the bacteria (mostly skin dwelling bacteria) are carried into the implant site during the surgical procedure. A late infection may happen years after surgery in sites with no history of infection. It represents a major problem in many procedures, such as total joint replacements and orthopedic implantation and great difficulty may be encountered in treatment of this infection once established.

Another consideration when using implants is their role in carcinogenesis. A startling finding was that many agents not previously thought to be carcinogens could incite dramatic neoplasm (an abnormal proliferation of cells) formation when implanted in a solid form rather than injected or fed in a soluble or dispersed form, which is called foreign body carcinogenesis [90]. As early as the 1940s and 1950s, investigators found that solid materials without chemical carcinogenic activity can induce a variety of neoplasms and the induction activity generally increases with the size of the implant. Furthermore, the induction activity varies inversely as the inflammatory response; that is, well-tolerated materials are better foreign-body carcinogens in the long term [90]. Alexander and Horning proposed that the most likely process for foreign-body materials to be carcinogenic would appear to be that the implant alters the normal environment of the neighboring cells in such a way as to favor the induction (or selection) of

discontinuous variations leading to malignancy [90, 91]. That is, the viable products of normally occurring cell damage or mutation are somehow favored by the presence of the implants and protected from physiological processes until they are ready to enter the rapid growth phase characteristic of malignancy [90]. Two conditions have been recognized to impact the carcinogenesis of implants: geometric (including topography and roughness) condition and the chemical and electrical conditions near an implant-tissue interface [90]. For example, a very high gradient electric field has been suggested to play a role in carcinogenesis. Therefore, the surface modification of biomaterials can control these interface properties, rendering the implants less carcinogenic.

Although understanding the interfacial interactions between nanomaterials and biological systems is still under progress, mediating cellular or tissue responses on nanomaterials is not a complete mystery. Generally, cells and tissues recognize (subsequent to initial protein interactions) both surface and bulk properties of nanostructured materials *in vivo* and *in vitro*, so cell and tissue responses can be altered or controlled to some extent by manipulating these material properties [92-94]. Surface properties often refer to surface chemistry and charge, material topography and surface energetics, while bulk properties are closely related to cell or tissue responses including inherent chemistry, stiffness, porosity and so on [92-99]. Fig. 1.2. illustrates the nanomaterial-cell interface and the interactions between cells, proteins and material properties. Nanomaterials have successfully demonstrated the ability to modulate cell and tissue responses *in vitro* and *in vivo* due to their extraordinary properties. Here, we first review several important surface properties of nanobiomaterials relevant to biological responses.

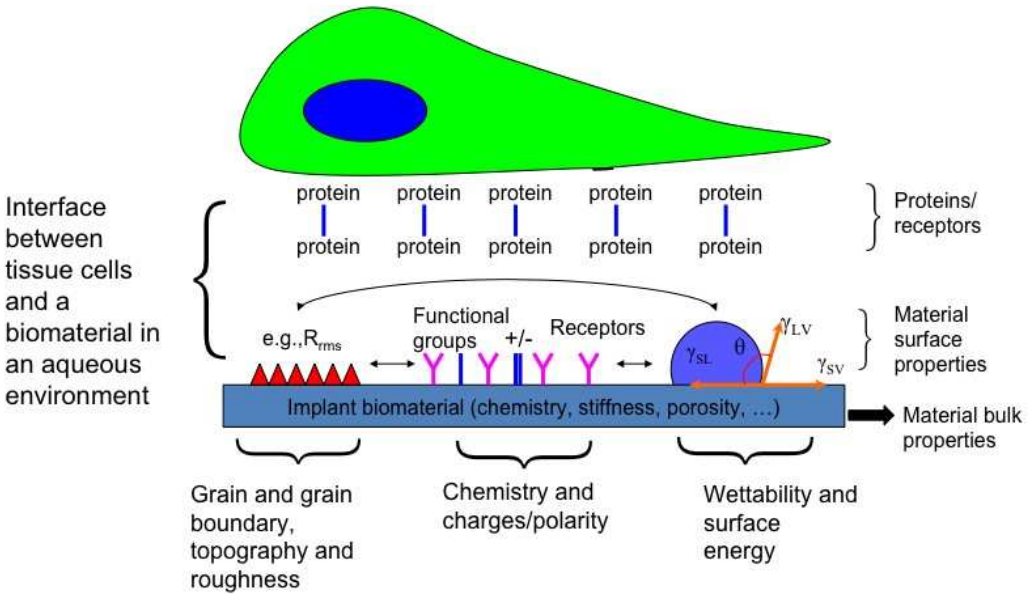

Fig. 1.2. Schematic illustrating the potential interfacial interactions between a cell (or tissue) and nano biomaterials. Double arrows indicate interactions among surface properties of nano biomaterials. In the schematic, examples of nanomaterial surface properties include: root mean square roughness (R_{rms}), surface electrical charges (+/-), contact angles (θ), interfacial tension between solids and vapors (γ_{SV}), interfacial tension between solids and liquids (γ_{SL}), and interfacial tension between liquids and vapors (γ_{LV}).

1.4.2. Size and surface area of nanobiomaterials

Nanomaterials is a field that studies materials with morphological features on the nanoscale dimensions, which is usually defined as smaller than one hundred nm in at least one dimension, though it is sometimes also used for materials smaller than one micrometer. A basic aspect of nanomaterials is the dramatically increased surface area to volume ratio as a result of such small feature sizes. The increased surface area of materials creates some specific material properties (such as high plasticity, enhanced

catalytic property, superparamagnetism, etc.) on the nanoscale, enabling unique applications for nanomaterials compared to conventional micron-scale materials. For nano biomaterials, the specific surface properties may result in numerous distinct biological responses, including the adsorption of proteins, cell and bacteria adhesion and subsequent proliferation, and enzymatic biological reactions. Therefore, due to the specific properties related to the nanoscale, biomaterials may have potential for anti-cancer, anti-infection, cardiac, and other tissue growth applications as will be described next.

1.4.3. Topography and roughness of nanobiomaterials

Surface topography is an important property towards controlling cell behavior and responses as discussed in Section 1.2. Topography involves various anisotropic or isotropic micro- and nanostructures, such as grooves, ridges, wells, pores, pillars, and columns, in mediating cell-biomaterial interfaces. Generally, roughness is a widely used parameter to describe surface topography, such as root mean square (RMS) height which is a statistical variation in the height of the surface around some mean value. Many studies have demonstrated the extensive roles of micro- and nanotopographied surfaces in regulating cell behaviors such as adhesion, proliferation, differentiation, migration, and apoptosis. Specially, anisotropic surface topography (such as grooves, ridges) has been widely identified in regulating cell orientation and migration along the anisotropic direction; while isotropic surface topography (such as islands, dots, wells, and spheres) is recognized to affect collective cell functions and the topography scale determines the

degree to which the specific function is affected. Thus, surface topography is an effective physical method in affecting cell behaviors without involving biomolecules.

Currently, the mechanisms behind topographically regulated cell behavior and responses are still not clear because of the complicated combination of cell type, topography style and substrate material. However, it has been proposed that the adsorption and conformation of cell adhesive proteins (such as fibronectin and vitronectin) may be altered on nanotopographical surfaces. Increased surface area of nanotopographical features could contribute to increased select protein adsorption. On the other hand, nano topographies may induce alterations of surface wettability and surface energy, possibly affecting local protein adsorption. Also, cell adaptation may be an important process in mediating cell response to topographies. Cells may adapt to physical topographical cues by conditioning growth environments such as secreting and modulating ECM proteins [1]. For example, Chou *et al.* proposed that substratum surface topography alters cell shape and modulates fibronectin synthesis at the transcriptional and post-transcriptional levels, as well as the amount of fibronectin assembled into the ECM [100].

1.4.4. Surface chemistry of nanobiomaterials

Biomaterial surface chemistry is another important cue in directing cell behavior since it is highly related to other surface properties like surface wettability, surface free energy and surface charge. Thus, surface chemistry modulates in vitro and in vivo cell responses and further regulates cell and host responses to implanted devices, biological integration of biomaterials and tissue-engineered constructs [101]. For example,

biologically active surfaces can be produced by altering surface chemistry with ECM proteins such as fibronectin, vitronectin, laminin, and collagen to render the surface biofouling. Keselowsky *et al.* [102] produced different surface chemistries using self-assembled monolayers of alkanethiols on gold and found that OH- and NH_2-terminated surfaces enhanced osteoblast-specific gene expression, alkaline phosphatase enzymatic activity, and matrix mineralization compared with surfaces presenting -COOH and -CH_3 groups. Surface chemistry is also involved in cell adhesive protein adsorption (i.e., fibronectin and vitronectin) and subsequently affects cell functions. For example, low protein adsorption has been observed on a chitosan/alginate multilayer, for both chitosan and alginate as top layers [103].

1.4.5. Surface wettability and surface energy of nanobiomaterials

Surface wettability and surface energy play an important role on protein adsorption and subsequent cell adhesion. Water contact angles (θ) have been used to determined surface wettability (i.e., the surface is hydrophilic or hydrophobic) and a θ less than 65° suggests a hydrophilic surface [104]. The conformation and biological activities of cell adhesive proteins (such as fibronectin and vitronectin) can be altered by surface wettability and resultant cell functions changed. For example, Altankov *et al.* [105] showed that fibroblasts on hydrophilic surfaces may reorganize fibronectin in an extracellular matrix-like structure whereas on hydrophobic surfaces no rearrangement of fibronectin occurs. Moreover, it was demonstrated that there are significant differences in the morphology of fibroblasts adhering to hydrophilic and hydrophobic surfaces.

Surface wettability and surface energy can be easily changed by surface chemistry. However, surface topography may also interfere with surface wettability. For instance, roughening a hydrophobic surface can enhance its nonwetting properties into superhydrophobicity and topographical effects can also enhance partial wetting by a given liquid into complete wetting to create superwetting [106]. Moreover, surface energy demonstrates a close relationship with surface wettability. The most common methods for the calculation of the surface free energy of solids are to use the results of the contact angle measurements. A greater surface energy may involve more hydrophilic surfaces for hydrophilic materials but more hydrophobic surfaces for hydrophobic materials. Hydrophilic surfaces (higher surface energy relative to hydrophobic) have indicated a higher affinity for cell adhesive proteins and subsequently, a strong ability to affect cell behavior.

1.4.6. Surface charge of nanobiomaterials

Surface charge has been correlated to protein adsorption and cell adhesion since most proteins and cell membranes are charged. Proteins contain both carboxyl and amine groups which are ionizable to render proteins charged. Cell member charge is determined by the cumulative effect of charged lipid headgroups within the plasma membrane itself. Both cationic and anionic functional groups contained in the lipid headgroups contribute to the net electric field at membrane surfaces [107]. Studies have demonstrated that charged surfaces can affect the adhesion and morphology of a variety of cell types through the mediation of electric charge and/or adsorption of biological molecules. For

example, Qiu *et al.* [108] reported that rat marrow stromal cell attachment was enhanced in serum-supplemented and serum-free media on positively charged substrate. However, cell spreading, alkaline phosphatase activity, and osteopontin were observed to decrease in cells grown on positively charged surfaces. This study also revealed that although cell adhesion is critical in subsequent cell development, cell adhesion alone is not an adequate indicator of biocompatibility when a specific function is required [83]. Another study by Hallab *et al.* [109] measured the adhesion strength of fibroblasts over a range of charge densities and the fibroblasts showed charge and electrical potential-dependent adhesion maxima.

In summary, surface properties of biomaterials play an important role in regulating and mediating the cellular and subsequent tissue responses. In this dissertation, cancer/healthy cell responses to nanotopographical substrates were completely investigated on PLGA surfaces and were correlated to substrate surface properties, providing insights towards inhibiting cancer cell behaviors by manipulating precise surface nanotopography.

1.5. Outline of the dissertation

The goals of this dissertation were to: (i) fabricate controllable PLGA nanopatterned substrates and investigate their various properties; (ii) investigate lung/breast cancer/healthy cell responses on nanopatterned substrates; (iii) chemically modify nanopatterned substrates to optimize substrate anti-cancer properties; (iv) investigate the correlation of surface properties with various cell functions; and (v)

provide guidance and cues to design ideal biomaterial interfaces for specific purposes. The central hypothesis of this dissertation is that due to altered surface properties, specific PLGA nanopatterns could decrease lung and breast cancer cell functions whiling increasing respective healthy cell functions and, thus, could be used as anti-cancer implants after tumor removal. To verify this hypothesis, biological responses (including cancer cell and healthy cell) on various nano-smooth and nanopatterned PLGA surfaces with altering surface properties were investigated. Furthermore, this dissertation determined which specific PLGA nanopattern size could regulate which cancer cell function and for the first time, provided a thorough understanding of cancer cell responses to nanotopographic surfaces. The dissertation consists of the following parts.

In Chapter 2, a simple and effective process will be described to prepare nanopatterned PLGA surfaces with an orderly array of spherical patterns on a large surface area. More importantly, cytocompatibility properties and lung carcinoma cell and lung healthy cell functions (including adhesion, proliferation, viability, apoptosis and vascular endothelial growth factor (VEGF) secretion) will be described on various nano-smooth and nanopatterned PLGA surfaces. The effects of the surface properties (including roughness, pattern size and wettability) on such biological responses will be discussed, providing insights towards controlling lung cancer cell responses by changing PLGA surface nanotopography.

Chapter 3 will systematically report on another cancer cell line, breast adenocarcinoma cell functions (including adhesion, proliferation, apoptosis, viability and VEGF secretion) and healthy breast epithelial cell proliferation on PLGA surfaces with altered pattern sizes. This part of the study will provide an understanding towards the

generality of nanotopographically controlling cancer cell functions, which will enable the determination of topographical effects of PLGA surfaces on other cancer cell lines.

In Chapter 4, chemical modification of nanopatterned PLGA surfaces by using a layer by layer (LBL) self assembly method (specifically, alginate and chitosan monolayers) will be reported. The impact of PLGA surface chemistry-induced property alteration on cancer cell and healthy cell proliferation and VEGF secretion *in vitro* will also be reported.

In Chapter 5, various surface properties (including roughness, pattern size, surface area, surface chemistry, surface charge, surface wettability and surface free energy) of nanopatterned PLGA surfaces will be described to understand the role nanotopographies play in mediating cancer cell functions and the factors behind the observed biological responses to biomaterials. More importantly, protein adsorption (fibronectin and vitronectin) will be reported to elucidate the way surface topography mediates cell responses. This part of the study will help to further understand how surface topography regulates cell functions and will provide insights towards the design of ideal implants after tumor removal.

Chapter 6 will conclude with the major scientific findings of this dissertation and provide the future directions of this work towards developing implants that can decrease cancer cell functions and promote healthy cell functions without the use of chemotherapeutics.

Chapter 2 Lung Carcinoma Cell Functions on Polymer Nanometer Surface Features

2.0. Preface

Since nanotopographies play an important role in mediating cellular behavior and tissue responses, for the first time, lung carcinoma cell functions on polymer nanometer surface features were investigated in this chapter. Poly (lactic-co-glycolic acid) (PLGA) has been widely used as a biomaterial in regenerative medicine due to its good biocompatibility and biodegradability properties and has been approved by the US FDA. Previous studies have shown that cells (such as bladder smooth muscle cells, chondrocytes and osteoblasts) respond differently to nano-structured PLGA surfaces compared to traditional smooth surfaces. Therefore, understanding and controlling lung carcinoma cell responses on nanopatterned PLGA are important and necessary before their use to regenerate lung tissue after lung cancer removal. For this reason, the hypothesis of the work described in this chapter was that lung epithelial carcinoma cells might respond differently to various sizes of nanopatterned PLGA surfaces. To test this hypothesis, in the present study, nanopatterned PLGA surfaces with different feature sizes were fabricated by an effective nano cast-mold technology. Atomic force microscopy (AFM) as well as electron spectroscopy for chemical analysis (ESCA) was used for topographical and surface chemistry characterization, respectively. Surface

wettability was characterized with contact angles. Results revealed that the PLGA surface pattern size, surface roughness and wettability can be altered by adjusting the size of polystyrene spherical beads used during the nano cast-mold process. Furthermore, lung epithelial carcinoma cell adhesion, proliferation and morphology results indicated less cell growth and spreading on nano-smooth and 400 nm surface featured PLGA compared to any other substrates (23 nm and 300 nm). Most importantly, results demonstrated decreased lung epithelial carcinoma cell VEGF (a key growth factor secreted for vascularization of tumors) synthesis on the 23 nm surface featured PLGA compared to the nano-smooth substrates for up to 5 days. In summary, these results provided the first insights into understanding the role PLGA nanotopography may play in inhibiting lung carcinoma cell functions for a wide range of applications in regenerative medicine.

2.1. Introduction

Clearly, there is now a plethora of studies [4, 41, 45, 48] to show that nanotopography can regulate cell functions (including adhesion, proliferation and differentiation), probably due to the correlation between surface topography and the adsorption of endogenous proteins (specifically, fibronection and vitronectin) that regulate cell behavior. However, despite this recognition of the importance of substratum topography on promoting tissue growth, relatively little is known concerning the effects of nanometer topographical features on cancer cell behavior [41]. For example, micropillars (1000 nm diameter and 800 nm high) and microlines (750 nm wide) have been shown to strongly modify the dynamics of cancerous (SaI/N) fibroblastic cell

spreading [5], but the effects of nanotopography less than 100 nm on cancer cell functions have been seldomly reported which is the focus of this study.

Lung cancer is the most common cause of cancer-related death in men and women. Surgical removal of a lung tumor is the main method for the treatment of lung cancer. In order to effectively replace the resected lung of these cancer patients, it is necessary to design a lung tissue replacement construct that will decrease interactions with lung carcinoma cells should they have not been completely removed during surgery or if cancer returns to the lung. With this in mind, a key design parameter for the potential regulation of lung cancer cell function is the material surface nanotopography. Synthetic biodegradable polymers (such as poly (lactic acid), poly (glycolic acid), poly (lactic-co-glycolic acid), etc.) with nanotopographies are potential candidates due to its good biocompatibility and biodegradability for a wide range of applications from drug delivery to regenerative medicine in such forms as PLGA nanoparticles and PLGA scaffolds.

For these reasons, the objective of this part of the dissertation was to create uniform nano-spherical topographical surfaces on PLGA by using a polystyrene (PS) bead self assembled process with different diameters and to evaluate lung carcinoma epithelial cell responses on such surfaces. This study investigated lung carcinoma cell interactions (including not just density, but also cell death and viability, and VEGF secretion) with nanopatterned PLGA for up to 5 days. It was an important objective of this *in vitro* study to determine what size of nanopatterned polymer surfaces decreases specific lung cancer cell function without using chemotherapeutics.

2.2. Experimental

2.2.1. Fabrication of nanometer surface PLGA films

PLGA (poly-lactic-co-glycolic acid) films with nanometer spherical surface features were created by improving a method previously described by Carpenter *et al.* [110]. The fabrication conditions of the various nanopatterned PLGA surface are summarized in Table 2.1. Specifically, 18mm diameter borosilicate glass (BG) cover slips (Fisher Scientific, Agawam, MA, USA) were cleaned and degreased by soaking in acetone for 10 minutes, sonicating with a sonicator (B3500A-DTH, VWR, Radnor, PA) in acetone for 10 minutes, washing several times with dH_2O (distilled water), soaking in 70% ethanol for 10 minutes, sonicating in 70% ethanol for 10 minutes, and washing several times with dH_2O. A 10 wt% suspension of polystyrene (PS) beads in water either 23 nm (150 μl), 190 nm (300 μl), 300 nm (300 μl), 400 nm (300 μl), or 530 nm (300 μl) in diameter (Bangs Labs, Fishers, IN, USA) was then dispersed onto the coverslips and allowed to evaporate in ambient air for 48 hours. For smooth PLGA surfaces, no PS beads were used in the process with all the other steps the same to improve the consistency between the smooth and nanopatterned PLGA.

PS monolayers were secured onto a 1 cm high × 18 mm diameter glass pillar using a commercially available glass adhesive (Super glue, The Original, Rancho Cucamonga, CA, USA), which was in turn fixed to the bottom of a borosilicate Petri dish (100 mm diameter × 15 mm height, Fisher Scientific, Agawam, MA, USA) using that same adhesive. These constructs were then used as templates to create inverse PDMS (polydimethylsiloxane) molds, as depicted in Figure 2.1. [110].

PDMS (Sylgard 184 silicone elastomer, Dow Corning, Midland, MI, USA) was then mixed at a curing agent/base volume ratio of 1/10 then exposed to a vacuum oven (1400E, VWR, Radnor, PA) at 25 inches of mercury for 20 minutes to remove bubbles created during the mixing process. The resulting mixture was then poured over the PS bead/glass constructs described above, filling the Petri dishes, and then was allowed to cure for 48 hr at room temperature. PDMS molds were then peeled away from their respective substrates, inverted, and placed in the cover of a borosilicate Petri dish. Additional PDMS was poured around the edge to fix the molds onto the Petri dishes, preventing deformation due to organic solvents, specifically chloroform. All molds were then rinsed several times with chloroform to remove any residual PS beads. This process created a series of 18 mm diameter × 1 cm deep PDMS wells with highly ordered, inverse casts of nanoscale PS beads, which could then be used to create PLGA surfaces with spherical nanoscale surface features.

For this, PLGA (50:50 wt:wt%, mol. wt. 12-16 x 10^3 g, Polysciences, Warrington, PA, USA) was then dissolved by sonicating a 4 % chloroform solution for approximately 10 min, or until fully dissolved. The resultant solution was poured over the PDMS molds described above, then allowed to evaporate for 48 hours at room temperature. PLGA films were then peeled off of their molds, cut into 12 mm diameter discs and put on the top of 12 mm diameter BG cover slips (Fisher Scientific, Agawam, MA, USA). All surfaces were then stored under a vacuum at 20 inches of mercury until use. Prior to cell experiments, all of the PLGA films were cleaned by soaking in 70% ethanol for 20 mins and sterilized by UV light exposure for 4 hours.

12 mm diameter BG cover slips were used as controls. The BG was cleaned and degreased by soaking in acetone for 10 minutes, sonicating in acetone for 10 minutes, washing several times with dH_2O, soaking in 70% ethanol for 10 minutes, sonicating in 70% ethanol for 10 minutes, and washing several times with dH_2O., then etched in 1 M NaOH for 1 hour. The cover slips were then washed in dH_2O and sterilized under UV light for 24 hours.

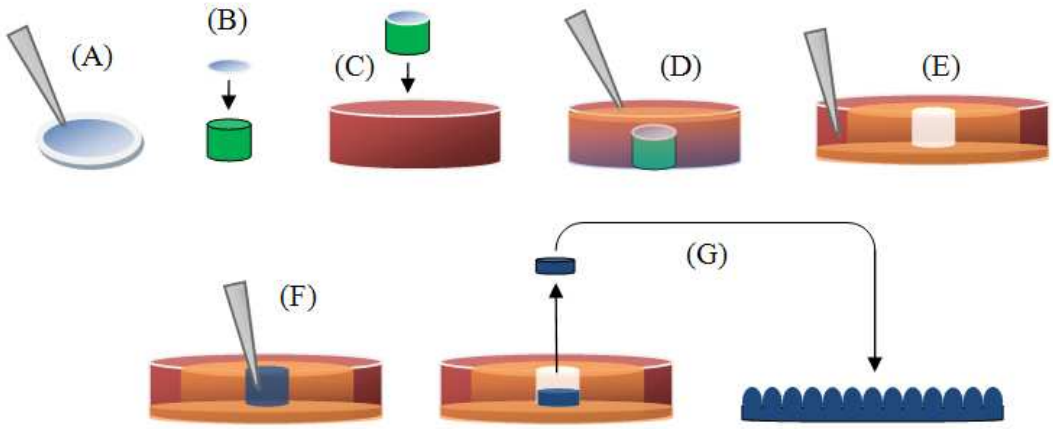

Fig. 2.1. Production of PDMS (polydimethylsiloxane) molds and casting of nano structured PLGA films: (A) 23 nm, 190 nm, 300 nm, 400 nm, and 530 nm PS (polystyrene) beads were dispersion deposited on glass coverslips; (B) Coverslips were fixed to equal diameter glass rods (green); (C) Coverslip / glass rod fixed to petri dish; (D) PDMS (orange) poured to fill the Petri dish; (E) PDMS from the previous step was removed from the Petri dish, inverted, and placed in a larger Petri dish (red), with additional PDMS (orange), leaving a well in PDMS (white) with a nanotextured bottom; (F) PLGA in chloroform (blue) poured into well then allowed to evaporate; and (G) Dried PLGA removed from the well and inverted, leaving PLGA surfaces with spherical nanometer surface features (adapted from [111]).

Table 2.1. Fabrication conditions for the various nanopatterns on PLGA surfaces

Name*	PS diameter (nm)	PS volume for self assembly on glass coverslips (μl)
PLGA0	-	-
PLGA23	23	150
PLGA190	190	300
PLGA300	300	300
PLGA400	400	300
PLGA530	530	300
BG	-	-

* PLGA0: nano-smooth PLGA surfaces without nanopatterns; PLGA23: PLGA surfaces with 23 nm featured nanopatterns; PLGA190: PLGA surfaces with 190 nm featured nanopatterns; PLGA300: PLGA surfaces with 300 nm featured nanopatterns, PLGA400: PLGA surfaces with 400 nm featured nanopatterns. PLGA530: PLGA surfaces with 530 nm featured nanopatterns; BG: borosilicate glass.

2.2.2. Surface characterization (AFM, ESCA and water contact angle analysis)

Atomic force microscopy (AFM) was used to visualize the surface topography of all of the PLGA films created here in ambient air using a PSIA XE150 AFM (Park Systems Inc, Santa Clara, CA). The AFM operated in non-contact mode at a frequency of roughly 300 kHz, a scan rate of 0.8 Hz, and 256 lines/scan. The scan area was 2 μm × 2 μm for all images. The scan rate was chosen depending on the quality of the image. Of course, a lower scan rate leads to a higher quality of the image. However, due to the

drifting effect during the scanning process, that is the tip will drift out of range during a long time scan, the scan rate has to be chosen such that the scan can be finished before the tip drifts out of range. Therefore, 0.8 Hz was chosen as the scan rate in this situation. Finally, the scan size and scan rate determine the time of scan. An XEI image processing program (version 1.7.1; Park Systems) was used to analyze the resulting images. For the analysis of the topographical parameter, root mean square roughness (R_{rms}= $\sqrt{\frac{\sum_{i=1}^{n}(x_i-\bar{x})^2}{n}}$, where x_i is the measured surface height, $\bar{x}$ is the mean height and n is the number of measurements) and the same scan length of 2 μm were used for all the samples and at least three regions on the same sample were scanned and averaged.

Electron spectroscopy for chemical analysis (ESCA) was performed on all samples using a Perkin Elmer 5500 Multitechnique Surface Analyzer. An aluminum $K_{\alpha 1,2}$ monochromatized X-ray source was used to stimulate photoemission of the inner shell electrons of the samples. The energy of the electrons was then recorded and analyzed to identify the surface chemistry.

Contact angles on PLGA surfaces were measured to assess the wettability and energetic states of PLGA. Before measurements, PLGA surfaces were cleaned by soaking 70% ethanol and deionized water. Ethanol used in this procedure is widely applied for biomaterial surface cleaning purposes [112], as such cleaning removes the residual contaminants attached to the material surface by physico-absorption but does not change the chemically bonded molecules on the surface. Contact angles on PLGA surfaces were measured through the sessile drop shape method under ambient conditions. For this, a drop of deionized water (3 μL) was placed on the PLGA surfaces and its

profile was recorded immediately by a drop shape analyzer (Easy Drop FM40, Kruss). Contact angles were then calculated by computer software (DSA1, Kruss) based on the recorded profile of the water drop. At least five different spots on each sample were measured for statistical purposes (N=5).

2.2.3. Cell assays

2.2.3.1. Cells

Lung carcinoma cell A549 (CCL-185, ATCC) and primary small airway normal epithelial cells (PCS-301-010, ATCC) were purchased from ATCC and used without further characterization. Upon arrival, the cell vial was thawed by gentle agitation in a 37°C water bath and removed from the water bath as soon as the contents were thawed. Then, the vial was decontaminated by dipping in or spraying with 70% ethanol. After that, the vial contents were transferred to a centrifuge tube containing 9.0 ml complete culture medium and spun at approximately 125 xg for 5 to7 minutes. Then, cell pellet was resuspended and cultured with the recommended complete medium. Lung carcinoma cells were cultured in Kaighn's Modification of Ham's F-12 Medium (F-12K, ATCC) supplemented with 10% fetal bovine serum (FBS, Hyclone) and 1% penicillin/streptomycin (P/S, Hyclone) under standard cell culture conditions (5% CO_2, humidified air at 37°C). Small airway normal cells were cultured in airway epithelial cell basal media (PCS-300-030, ATCC) supplemented with a small airway epithelial cell growth kit (PCS-301-040, ATCC) under standard cell culture conditions. The cells were cultured until 80 ~ 100% confluence on cell culture polystyrene flasks (75 cm^2 surface

area, Corning Inc.) before conducting the cell tests described below. Cell population numbers between 2 and 7 and were used for following cell assays.

2.2.3.2. Lung carcinoma cell adhesion assay

For the cell adhesion, lung carcinoma cells were lifted from the cell culture polystyrene flask with trypsin-ethylenediaminetetraacetic acid (trypsin-EDTA, Hyclone) after reaching confluence, and were dispersed in F-12K medium supplemented with 10% FBS and 1% P/S. Cell density in the suspension was measured by a hemocytometer (Fisher Scientific) according to standard procedures. Specifically, with a cover slip in place, 10 µl of the cell suspension was transferred to a chamber on the hemocytometer using a pipette. This was done by carefully touching the edge of the cover-slip with the pipette tip and allowing the chamber to fill by capillary action. Then, the cells were counted in the 1 mm center square and the four corner squares. The count was repeated using the other chamber of the hemocytometer. Each square of the hemocytometer (with cover slip in place) represents a total volume of 0.1 mm^3. Since 1 cm^3 is equivalent to 1 ml, the cell concentration per ml would be determined as the average count per square × 10^4 cells/ml. Then, lung carcinoma cells were seeded onto the various PLGA surfaces at a density of 3,500 cells/cm^2 in F-12K medium supplemented with 10% FBS and 1% P/S. After seeding on the PLGA surfaces, cells were cultured under standard cell culture conditions (5% CO_2/95% humidified air and 37°C). After 4 hrs, non-adherent cells were removed by rinsing in phosphate buffer saline (PBS) three times while adherent cells were fixed with 10% formalin (Fisher Scientific) for 10 mins. Then, the formalin was removed and the cells adherent on the substrates were stained with 4’,6-diamidino-2-

phenylindole (DAPI, Sigma Aldrich) for 10 mins. After staining, samples were transferred to a fluorescence microscope (Axiovert 200M, Zeiss) and adherent cells were counted under 10X magnification. For counting, five random areas on each sample were selected or photographed, and cell numbers in all five areas were counted and averaged. The adhesion assay was conducted in triplicate (n=3) and was repeated at least three separate times (N=3).

2.2.3.3. Lung carcinoma cell proliferation assay

For proliferation assays, sample cleaning, the preparation of cells as well as the counting of cells to determine seeding density, was the same as that just described in the adhesion assay. Lung carcinoma cells were seeded onto the various PLGA surfaces at 1,000 cells/cm^2 in F-12K medium supplemented with 10% FBS and 1% P/S. The cells were then cultured under standard cell culture conditions (5% CO_2, 95% humidified air, 37°C) for 1 and 3 days. Cell culture media was changed every other day. After the prescribed time periods, lung carcinoma cells were fixed, stained and counted in a similar way as described above. The proliferation assay was conducted in triplicate (n=3) and was repeated at least three separate times (N=3).

2.2.3.4. Lung carcinoma cell morphology

Lung carcinoma cell morphology on the various PLGA films was observed by fluorescence microscopy. For this, cells were seeded at a density of 5,000 cells/cm^2 and cultured for 12 hrs on the various PLGA substrates in F-12K medium supplemented with 10% FBS and 1% P/S. Adherent cells on the substrates were washed with PBS and fixed

with 4% formaldehyde for 10 mins. After fixation, the cells were stained with fluorescent phalloidin conjugates (Alexa Fluor® 555 phalloidin, Invitrogen). The fluorescent phalloidin conjugates can label F-actin in cells, enabling the fluorescence microscopy observation of cytoskeleton morphology as well as F-actin alignment in cells. For further determining cell density on the substrate, the cell nuclei were stained with DAPI. Fluorescence microscopy images of the stained cells on the substrates were obtained using magnifications of 20X and 40X for quantification and imaging purposes, respectively.

20X fluorescence microscopy images were analyzed by Image J (free resource from http://rsbweb.nih.gov/ij/) for the quantification of unit cell spreading area (area per cell). For each image, total cell spreading area was quantified by threshold processing on the phalloidin stained image and cell density was counted from the DAPI stained image, and then spreading area per cell was calculated. At least three images per sample were analyzed and over 50 cells per sample were averaged.

2.2.3.5. Lung carcinoma cell apoptosis assay

The measurement of phosphatidylserine (apopotosis) expression using fluorescein-labeled (FITC) Annexin V-Programmed cell death (apoptosis) was conducted by flow cytometry using a Sigma-Aldrich apoptosis detection kit (APOAF). In apoptotic cells, the membrane phospholipid phosphatidylserine (PS) is translocated from the inner to the outer leaflet of the plasma membrane, thereby exposing PS to the external cellular environment. Annexin V is a 35-36 kDa Ca^{2+} dependent phospholipid-binding protein that has a high affinity for PS, and binds to cells with exposed PS. FITC Annexin V

staining precedes the loss of membrane integrity which accompanies the latest stage of cell death through apoptosis and necrotic processes. FITC annexin V was used with the vital dye propidium iodide (PI) to separate the late and early apoptotic population of the cells. When apoptosis happens over time, cells can be tracked from FITC Annexin V and PI negative (viable), to FITC Annexin V positive and PI negative (early apoptosis, membrane integrity is present) and finally to FITC Annexin V and PI positive (end stage apoptosis and death). This assay does not distinguish between cells that have undergone apoptotic death versus those that have died as a result of a necrotic pathway since in either case, the dead cells will be both Annexin-FITC and PI positive. The experiment was performed according to the manufacturer's instructions. Briefly, approximately 5×10^5 lung carcinoma cells were seeded onto the various substrates in 24 well plates with 1 ml of media. Then, cells were cultured in a similar manner to that described in the cell proliferation section. After 1, 3 and 5 days, cells were washed with PBS. The cells were then lifted from the substrates with trypsin-EDTA, centrifuged and resuspended in 1× binding buffer. 5 µl of FITC-Annexin V and PI were added to the cell suspension and incubated at room temperature for 10 minutes. The cells were analyzed with flow cytometry (BDBiosciences FACSAria) and the results analyzed by BDBiosciences DiVa 5.0 software. The apoptosis assay was conducted in triplicate (n=3) and was repeated at least three separate times (N=3).

2.2.3.6. Lung carcinoma VEGF cellular assays

The quantikine human VEGF (vascular endothelial growth factor) immunoassay kit (R&D systems) was used for determining VEGF concentration. The medium for the

VEGF measurements were collected after 1, 3 and 5 days of the culture process for the apoptosis assay. The experiment was performed according to the manufacturer's instruction. Briefly, 200 µl standards (prepared from the kit) and sample medium were pipetted into the 96-well plate (from the kit) and incubated for 2 hrs at room temperature. After washing with a binding buffer, an enzyme-linked polyclonal antibody specific for VEGF (from the kit) was added to the wells. Following a wash to remove any unbound antibody-enzyme reagent, a substrate solution (from the kit) was added to the wells and a color developed in proportion to the amount of VEGF bound in the initial step. Color development was stopped by adding a stop solution from the kit and the intensity of the color was measured by a micro plate reader (Molecular Devices). The VEGF concentration was determined from a standard curve of absorbance versus known concentrations of VEGF solutions (prepared from the kit) run in parallel with the experimental samples. The VEGF assay was conducted in triplicate (n=3) and was repeated at least three separate times (N=3).

2.2.3.7. Primary small airway epithelial cell MTT assay

Primary small airway epithelial cells were used as a contrast to lung carcinoma cells. The method of culturing cells and counting cell density for seeding purposes were the same as described above. For the MTT assay, small airway epithelial cells were seeded on the PLGA surfaces at a density of 150,000 cells/cm^2. After seeding, the cells were cultured under standard cell culture conditions (5% CO_2, humidified air at 37°C). After one-, three- and five days, the viable cell number was determined using the Celltiter 96 Non-radioactive Cell Proliferation Assay (G4100, Promega) that measures the

reduction, by living cells only, of the 3-(4,5-Dimethylthiazol-2-yl)-2,5-diphenyltetrazolium compound (MTT). Shortly, after one-, three- and five days, medium was removed from the wells and the cells were washed with PBS twice. Then, all the samples were transferred to new unused 24 well tissue culture plates and 1 ml of fresh growth medium was added to each well. 150 µl of the dye solution (from the cell proliferation assay kit) was added to each well and the plates were incubated at 37°C in a humidified, 5% CO_2 atmosphere. After 4 hrs, 1 ml of the Solubilization Solution/Stop Mix was added to each well and the plates were allowed to stand overnight in a humidified atmosphere to completely solubilize the formazan crystals. After overnight culture, the contents of the wells were mixed to get a uniformly colored solution and transferred to 96 well plates (215 µl per well). The absorbance at 570 nm was recorded by using a microplate reader (Molecule Devices, $340PC^{384}$).The value of the background absorbance at 570 nm without cells run in parallel with the experimental samples was subtracted to yield a corrected absorbance. The live cell number was determined from a standard curve of absorbance versus known concentrations of live small airway epithelial cell solutions run in parallel with the MTT assay. All the experiments were performed in triplicate (n=3) and repeated three times (N=3).

2.2.3.8. Statistical analysis

All experimental results are presented as the mean ± standard error of the mean (SEM) and analysis of variance (ANOVA) was used to check statistical significance between means.

2.3. Results

2.3.1. Topographical evaluation of nanopatterned PLGA surfaces

AFM images of the various PLGA surfaces demonstrated different nanometer roughness, which provided evidence of the intended spherical surface topography on the PLGA surfaces using the methods described above (Fig. 2.2). The PLGA nano-spherical particle size corresponds to the PS spherical particle size used. Quantitative roughness values (R_{rms}) and local geometric area (A_{geo}) surface areas of the various PLGA surfaces are listed in Table 2.2. Specifically, PLGA surfaces with RMS values of 3.73 nm, 10.78 nm and 24.11 nm were obtained using PS beads with diameters of 23 nm, 300 nm and 400 nm, respectively. Nano-smooth PLGA surfaces had lower roughness value (RMS ~ 0.54 nm) than nanopatterned PLGA surfaces. PLGA23, PLGA300 and PLGA400 had much higher surface roughness as a result of the surface nanopatterns compared to nano-smooth PLGA.

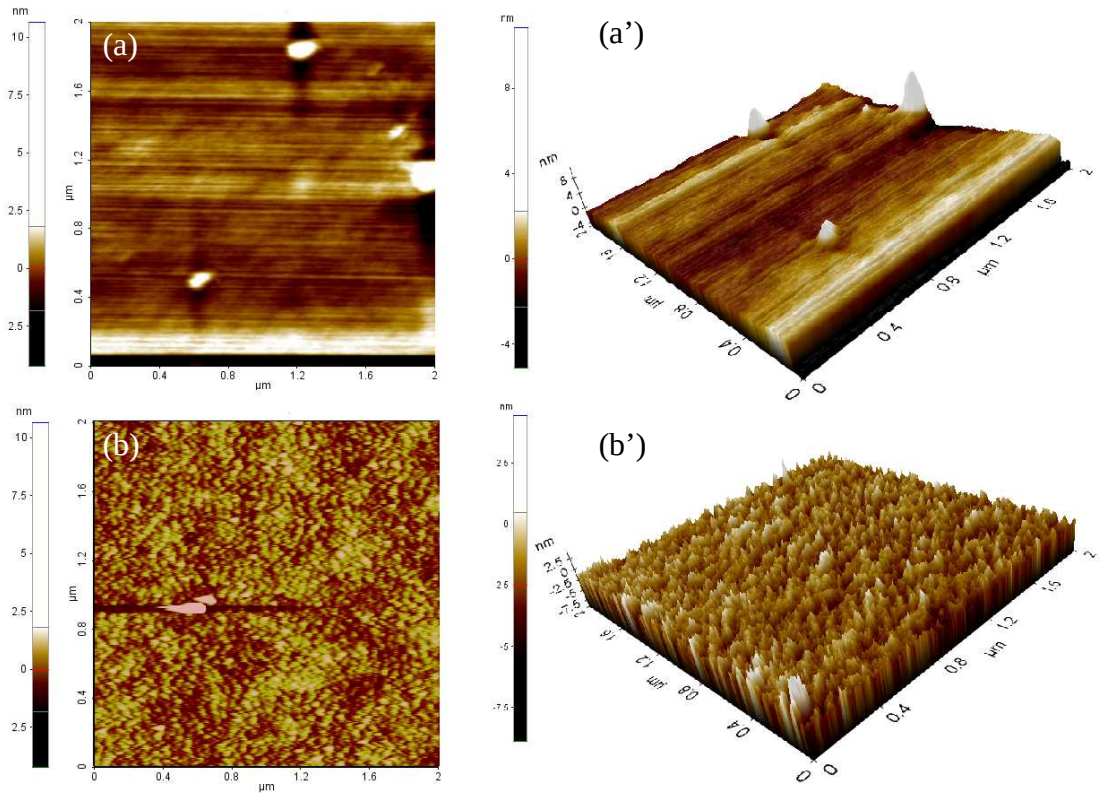

(continued on next page)

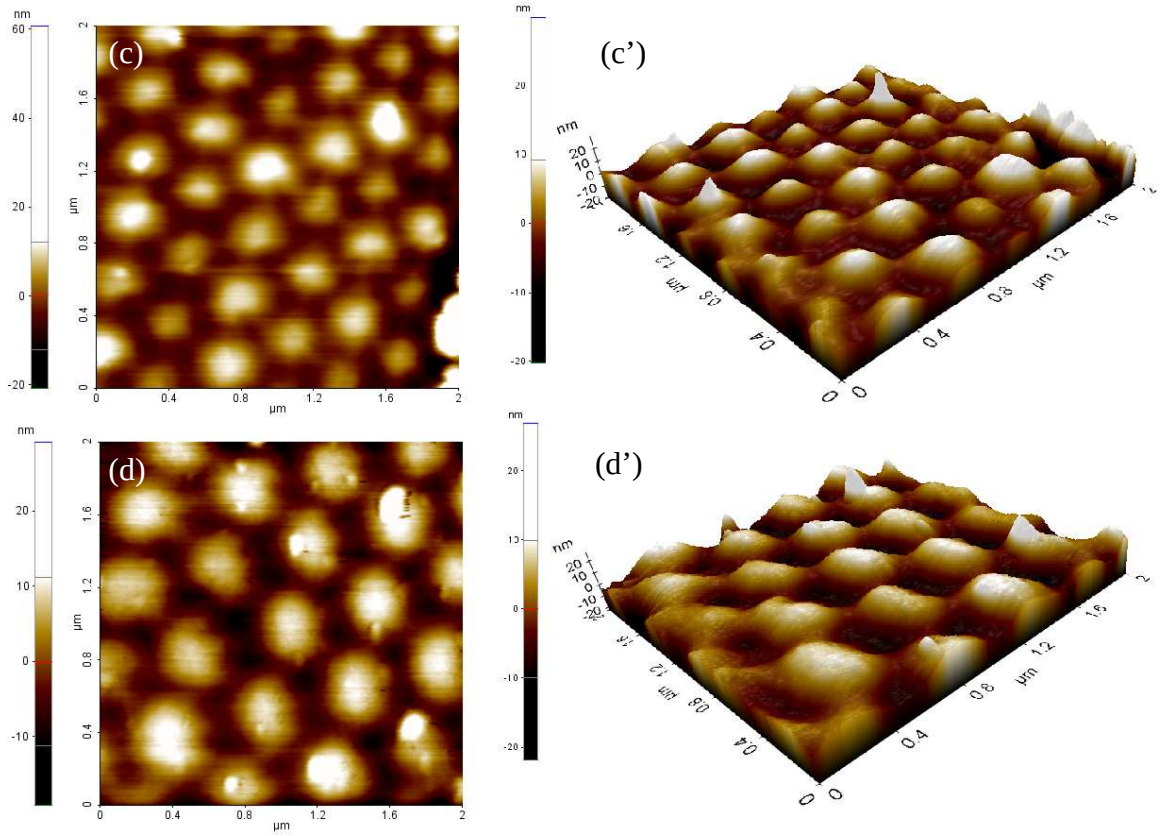

Fig. 2.2. 2D and 3D AFM images of PLGA0 (a and a'), PLGA23 (b and b'), PLGA300 (c and c') and PLGA400 (d and d').

Table 2.2. Surface roughness (R_{rms}), local geometric area (S_{geo}) and static water contact angles $\theta(H_2O)$ on the various PLGA films

Substrate	R_{rms} (nm)	S_{geo} (μm^2)	$\theta(H_2O)$ (^{0})
PLGA0	0.54	4.0	98.1 ± 0.4
PLGA23	3.73	4.0	93.8 ± 1.8
PLGA300	10.78	4.1	91.6 ± 1.6
PLGA400	24.11	4.1	96.6 ± 0.5

2.3.2. Surface chemistry of nanopatterned PLGA films

Surface chemistry of the various PLGA films was analyzed by ESCA and the spectra are shown in Fig. 2.3. Clearly, the spectra of nano-smooth PLGA and nano surface featured PLGA (created by PS beads) showed the same chemistry. This result indicated that there was no silicon contamination on the PLGA cast surfaces through the use of the PDMS mold process. The two peaks with binding energies at ~285 and ~532 eV were assigned to carbon atoms of saturated hydrocarbons, carbon atoms with a single bond to oxygen (O–C–C=O or –C–O–C=O) and carbon atoms in carbonyl groups (–C=O) [113]. The two very weak Si peaks were attributed to the borosilicate glass substrate used in the ESCA experiment since the PLGA samples were very thin or the borosilicate glass substrates weren't totally covered by the PLGA samples. The same chemistry permitted a focused exploration of the effects of the PLGA surface nanotopography alone in regulating cell functions, especially important cancer cell functions such as apoptosis and VEGF secretion.

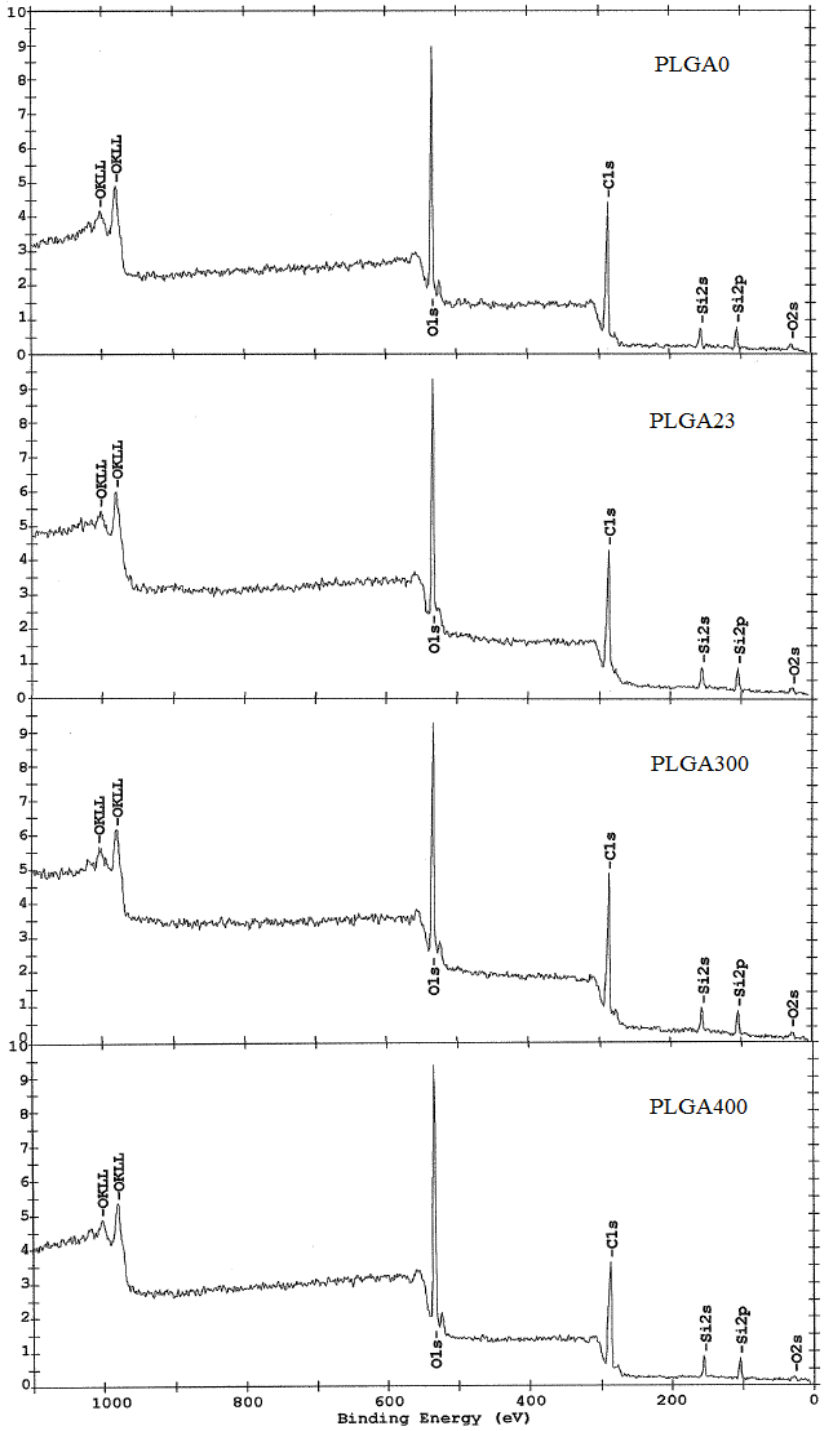

Fig. 2.3. ESCA spectra for nano-smooth (PLGA0) and nanopatterned PLGA (PLGA23, PLGA300, and PLGA400) surfaces. These four spetra showed the same peaks, indicating the same surface chemistry.

2.3.3. Wettability of nanopatterned PLGA surfaces

Static water contact angle measurements indicated similar results on the various PLGA surfaces, as shown in Table 2.2. All of the PLGA films were hydrophobic ($\theta > 90^0$), with water contact angles 98.1^0, 93.8^0, 91.6^0, 96.6^0 corresponding to the nano-smooth, 23 nm, 300 nm and 400 nm nano-featured PLGA substrates, respectively. The similar hydrophobility on nano-smooth and nanopatterned PLGA surfaces may be due to the same surface chemistry described above, which plays an important role in affecting surface wettbility. However, surface free energy, which can be calculated utilizing the results of the contact angle measurements, could be substantially influenced by surface topography and will be discussed in Chapter 5.

2.3.4. Lung carcinoma cell adhesion and proliferation

Four-hour lung carcinoma cell adhesion results (Fig. 2.4.) showed that lung carcinoma cells responded differently to the various nanopatterned PLGA surfaces, indicating the possibility of nanotopography to direct cancer cell behaviors. Specifically, PLGA0 showed the least number of adherent lung carcinoma cells than that on any other PLGA surface. Comparing PLGA surfaces with nanopatterns, PLGA400 had significantly lower cell adhesion density than PLGA300 and PLGA530. The highest adhesion density was observed on PLGA530 with the largest size surface pattern in this study. When comparing nano-smooth and nanopatterned PLGA surfaces, four-hour lung carcinoma cell adhesion results demonstrated that nanopatterned surfaces increased the initial lung cancer cell adhesion and the size scale of the nanopattern could have specific effects on cell adhesion. In addition, compared to BG, various PLGA substrates except

PLGA530, showed lower lung cancer cell adhesion density, suggesting that lung cancer cells may be prone to decrease cell interactions with PLGA.

Here, PLGA23 had the smallest pattern size (less than 100 nm) in the nano scale and more pronounced effects on cell functions were found on topographical surfaces with decreasing nanometer size. PLGA400 both showed lower adhesion density compared to other nano scale patterns, indicating the possibility of decreasing cancer cell functions. Moreover, a transition in lung cancer cell adhesion density happened between PLGA300 and PLGA400. Therefore, in the following study, PLGA23, PLGA300 and PLGA400 were chosen from the various nanopatterned PLGA surfaces and a complete study of cancer cell functions (including proliferarion, viability, apoptosis and VEGF secretion) were conducted on these nanopatterned PLGA surfaces.

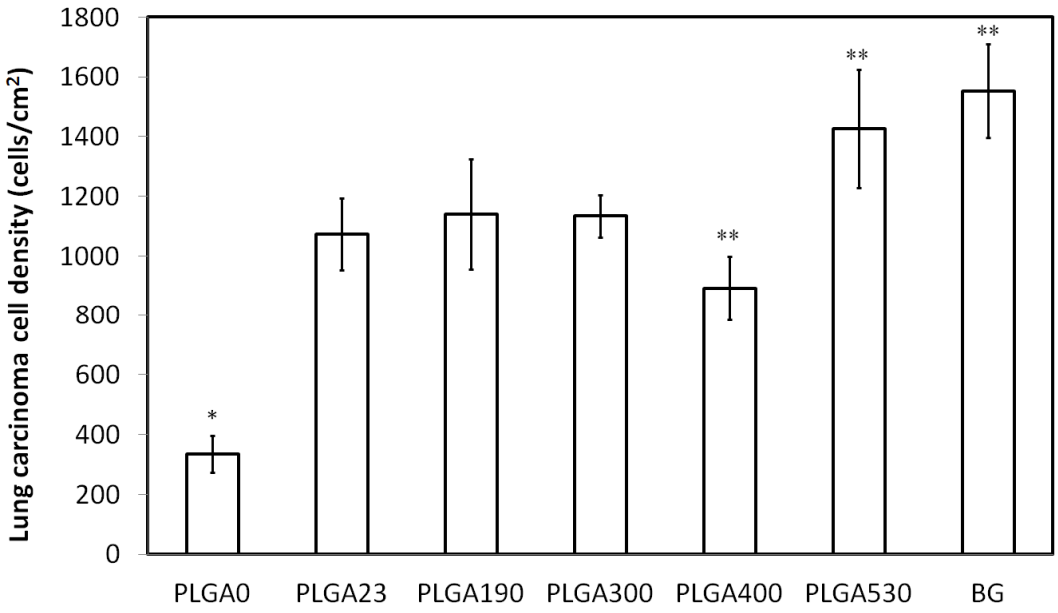

Fig. 2.4. Four-hour lung carcinoma cell adhesion on various PLGA surfaces and BG controls. The seeding density was 3500 cells/cm^2. Data=mean±SEM; N=3; * $p<0.01$ compared to PLGA23, PLGA190, PLGA300, PLGA400, PLGA530 and BG; ** $p<0.05$ compared to PLGA300 and PLGA530.

One- and three day cell proliferation results on the different nanopatterned PLGA surfaces are shown in Fig.2.5. After one day, PLGA400 had less cell density than PLGA0, PLGA23 and PLGA400, while no significant difference existed between PLGA0 and PLGA23. Among the nanopatterned PLGA surfaces, PLGA300 had greater lung carcinoma cell proliferation density than PLGA23. One day cell proliferation results indicated that the PLGA400 inhibited lung carcinoma cell proliferation compared to any other PLGA surface. After three days, PLGA400 again had significantly lower cell density than PLGA23 and PLGA300. PLGA300 showed the highest cell density among all the PLGA substrates. These cell density results indicated that PLGA400 decreased

lung carcinoma cell proliferation compared to nano-smooth and other nanopatterned PLGA surfaces, while PLGA300 promoted lung carcinoma cell proliferation.

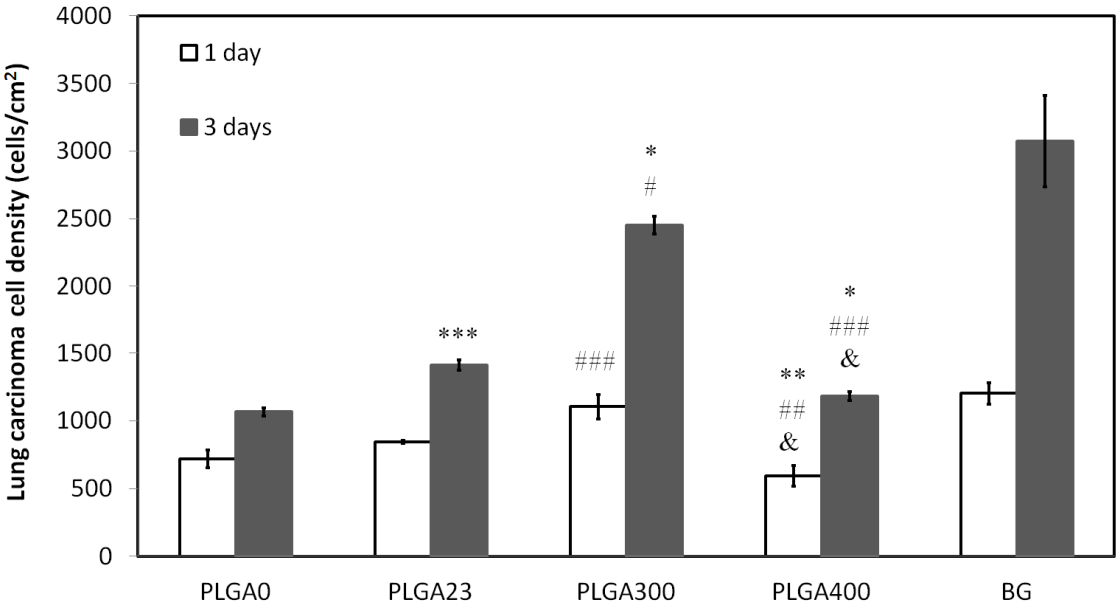

Fig. 2.5. One- and three-day lung carcinoma cell proliferation on various PLGA surfaces and BG controls. Data=mean±SEM; N=3; *$p < 0.01$, **$p < 0.05$ and ***$p < 0.1$ compared to PLGA0 at the same time point; $^{\#}p < 0.01$, $^{\#\#}p < 0.05$ and $^{\#\#\#}p < 0.1$ compared to PLGA23 at the same time point; $^{\&}p < 0.01$ compared to PLGA300 at the same time point. For all the samples, all time points are statistically different from each other.

2.3.5. Lung carcinoma cell morphology

Cell spreading morphologies on the various substrates observed by fluorescent microscopy are shown in Fig. 2.6. Spreading area per cell was quantified on each substrate and the results are shown in Fig. 2.7. Cells on PLGA300 spread out more than

those on the nano-smooth and 400 nm surface featured PLGA. Cells spread 33% more on the 300 nm surface featured PLGA than on the nano-smooth PLGA, and cell spreading on PLGA0, PLGA23 and PLGA400 showed no significant difference. Thus, cell proliferation on the PLGA substrates had a significant relationship with the cell spreading, as more spreading may result in higher proliferation. The morphology of phalloidin-stained F-actin networks in cells on the 300 nm surface featured PLGA exhibited more and thicker contractile filaments and more cell-cell connections than on any other substrates, indicating stronger cell-substrate interactions or active cell movements on this substrate. The morphology of F-actin networks on other PLGA substrates (PLGA0, PLGA23 and PLGA400) showed similar filament spreading and not many cell-cell connections were observed.

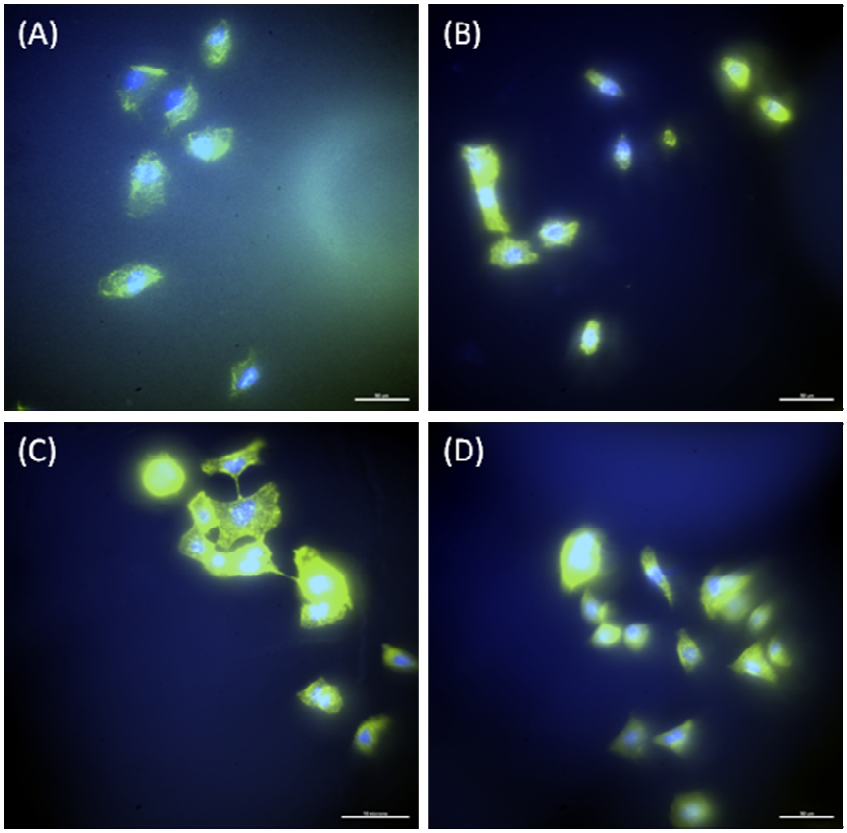

Fig. 2.6. Fluorescent microscopy images (40X) showing lung cancer epithelial cell morphology on the various PLGA substrates after 12 hrs at a seeding density of 5,000 cells/cm^2: (A) PLGA0, (B) PLGA23, (C) PLGA300 and (D) PLGA400. The scale bar is 50 micrometers.

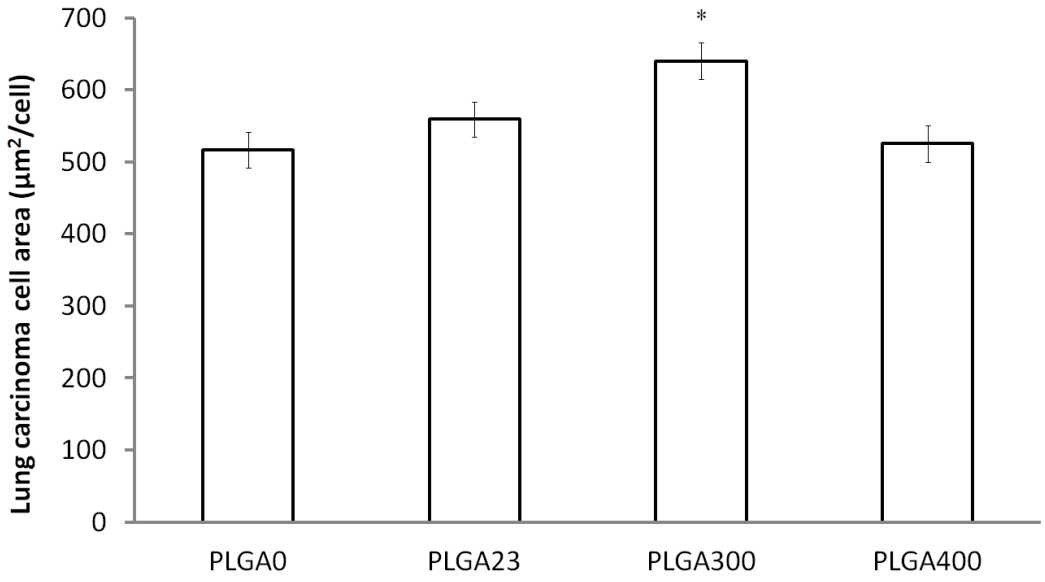

Fig. 2.7. Lung carcinoma cell area on the various PLGA substrates after 12 hrs at a seeding density of 5,000 cells/cm^2. Data were expressed as mean ± SEM, N=3. * $p < 0.01$ compared to PLGA23, PLGA300 and PLGA400.

2.3.6. Lung carcinoma cell apoptosis

Cell numbers alone are not accurate to determine cell activity since some cells may be dead. Therefore, cell apoptosis was investigated to determine apoptotic/dead/live cell percentages. Three day cell apoptosis results are shown in Fig. 2.8. After three days, the 23 nm and 300 nm surface featured PLGA showed significantly higher apoptotic cell percentages compared to the nano-smooth PLGA, 252% and 206%, respectively. However, there was no significant difference between the nano-smooth and the 400 nm surface featured PLGA substrates. For dead cell percentages, the 23 nm surface featured PLGA had significantly higher dead cell percentages compared to the PLGA0, PLGA300 and PLGA400 substrates: 209%, 172% and 168% more, respectively. These results indicated that after three days, PLGA23 exhibited significantly higher apoptotic and dead

cell percentages than any other PLGA substrate, suggesting that cell apoptosis was induced by 23 nm surface patterns, resulting in lower cell viability.

Furthermore, the trend in five day cell apoptosis results was consistent with the three day results but the difference became smaller among the various PLGA surfaces. Specifically, compared to the nano-smooth PLGA, PLGA23, PLGA300 and PLGA400 all had significantly higher apoptotic cell percentages, 202%, 180% and 127% more, respectively, as shown in Fig. 2.9. Among the nanopatterned PLGA surfaces, the 23 nm and 300 nm surface featured PLGA had higher apoptotic cell percentages than the 400 nm surface featured PLGA, 159% and 142% more, respectively. For dead cell percentages, only PLGA23 showed significantly 15% higher dead cell percentage compared to PLGA0. In summary, the five day cell apoptosis results further confirmed that the 23 nm surface featured PLGA substrates induced the largest percentage of lung cancer cell apoptosis, decreasing lung carcinoma cell viability.

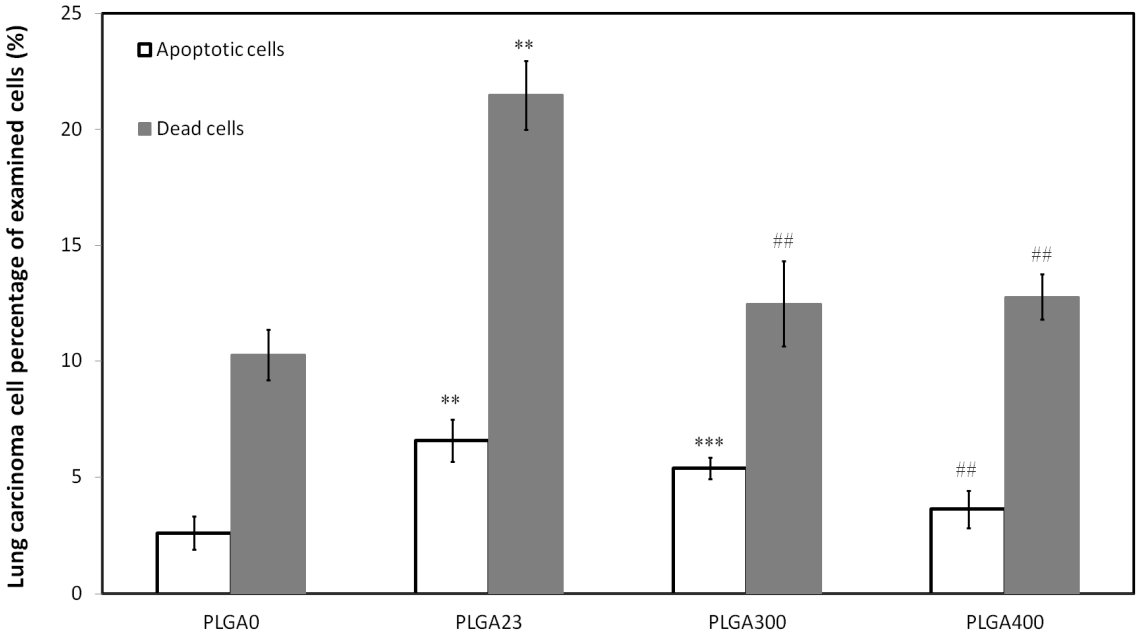

Fig. 2.8. Three day apoptotic/dead cell percentages of lung carcinoma cell populations cultured on the various PLGA substrates. The percentage stands for the ratio of apoptotic/dead cells to the total cells examined by flow cytometry. Data are expressed as the mean ± SEM; N=3. ** $p < 0.05$ and *** $p < 0.1$ compared to PLGA0; $^{\#\#}$ $p < 0.05$ compared to PLGA23.

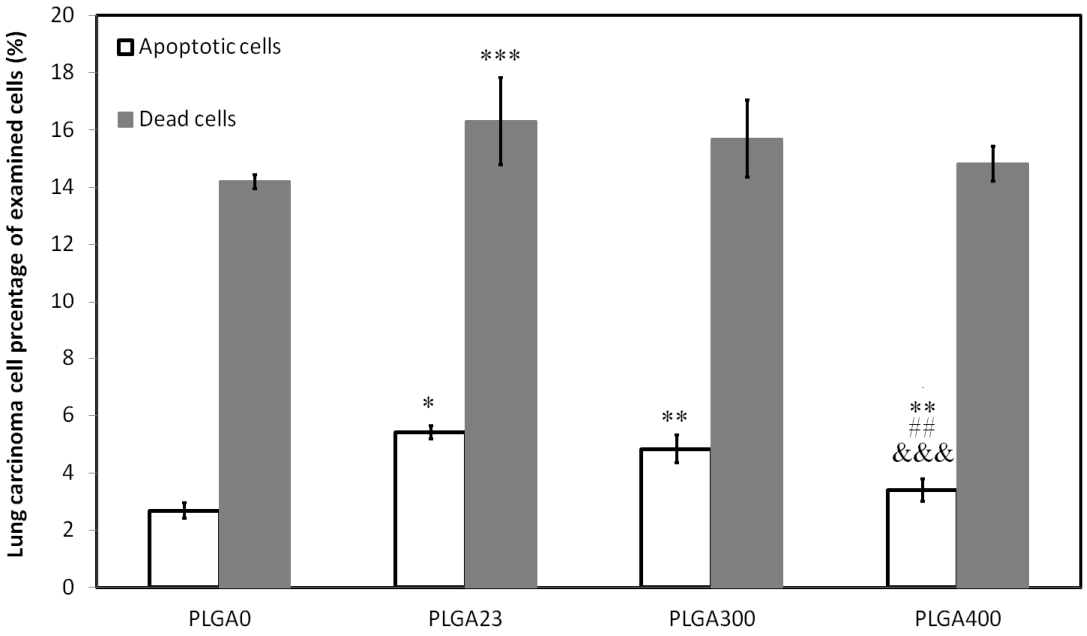

Fig. 2.9. Five day apoptotic/dead cell percentages of lung carcinoma cell populations cultured on the various PLGA substrates. The percentage stands for the ratio of apoptotic/dead cells to the total cells examined by flow cytometry. Data are expressed as the mean ± SEM; N=3. * $p < 0.01$, ** $p < 0.05$ and *** $p < 0.1$ compared to PLGA0; $^{\#\#}$ $p < 0.05$ compared to PLGA23; $^{\&\&\&}$ $p < 0.1$ compared to PLGA300.

As for the live cell percentages after getting rid of apoptotic and dead cells, all nanopatterned PLGA substrates showed significantly lower live cell percentages compared to the nano-smooth PLGA substrates after three days (Fig. 2.10.). Moreover, consistent with the dead and late apoptotic cell results, the 23 nm surface featured PLGA showed significantly lower live cell percentages compared with PLGA300 and PLGA400 after three days. However, after five days, only PLGA23 revealed significantly lower live cell percentages compared to nano-smooth PLGA substrates.

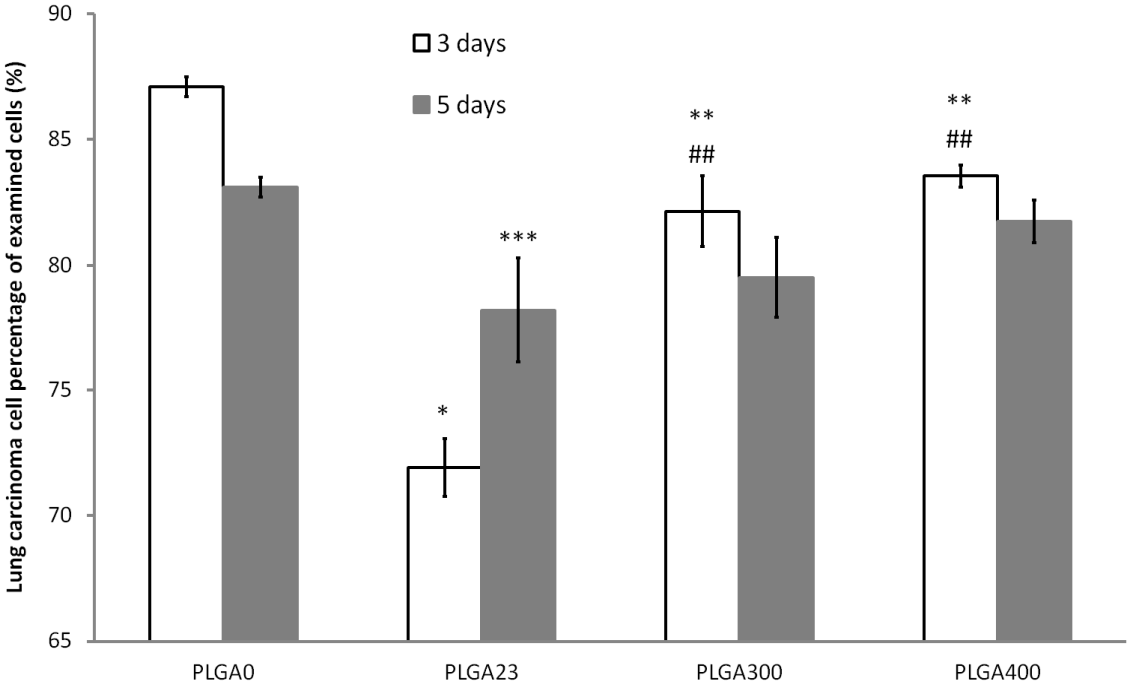

Fig. 2.10. Three- and five day live cell percentages of lung carcinoma cell populations cultured on the various PLGA substrates. The percentage stands for the ratio of live cells to the total cells examined by flow cytometry. Data are expressed as the mean ± SEM; N=3. * $p < 0.01$, ** $p < 0.05$ and *** $p < 0.1$ compared to PLGA0; $^{\#\#}$ $p < 0.05$ compared to PLGA23.

2.3.7. Lung carcinoma cell VEGF secretion

VEGF is secreted by lung carcinoma cells driving tumor angiogenesis (the formation of new blood vessels) and controls tumor growth. VEGF secretion after one-, three- and five days of cultured lung epithelial carcinoma cells is shown in Fig. 2.11. The same trend was revealed at each time point. Specifically, after one day, lung carcinoma cells on the 23 nm surface featured PLGA secreted significantly less VEGF than PLGA0, PLGA300 and PLGA400: 40%, 46% and 38% less, respectively. However, no significant difference was observed among other PLGA substrates. Three day results also showed the lowest VEGF concentration on the 23 nm surface featured PLGA compared to any other PLGA substrates. Moreover, the 400 nm surface featured PLGA had significantly lower VEGF synthesis from lung epithelial carcinoma cells than the 300 nm surface featured PLGA. Five day results further showed the same trend as one- and three-day concentrations and PLGA23 again had significantly lower VEGF concentration than PLGA0, PLGA300 and PLGA400: 30%, 34% and 24% less, respectively. VEGF results indicated that cells on the 23 nm featured PLGA substrates secreted the least amount of VEGF, suggesting decreased lung carcinoma cell activity on such nanopatterned PLGA surfaces. Therefore, the 23 nm surface featured PLGA may have potential applications for inhibiting lung cancer cell function.

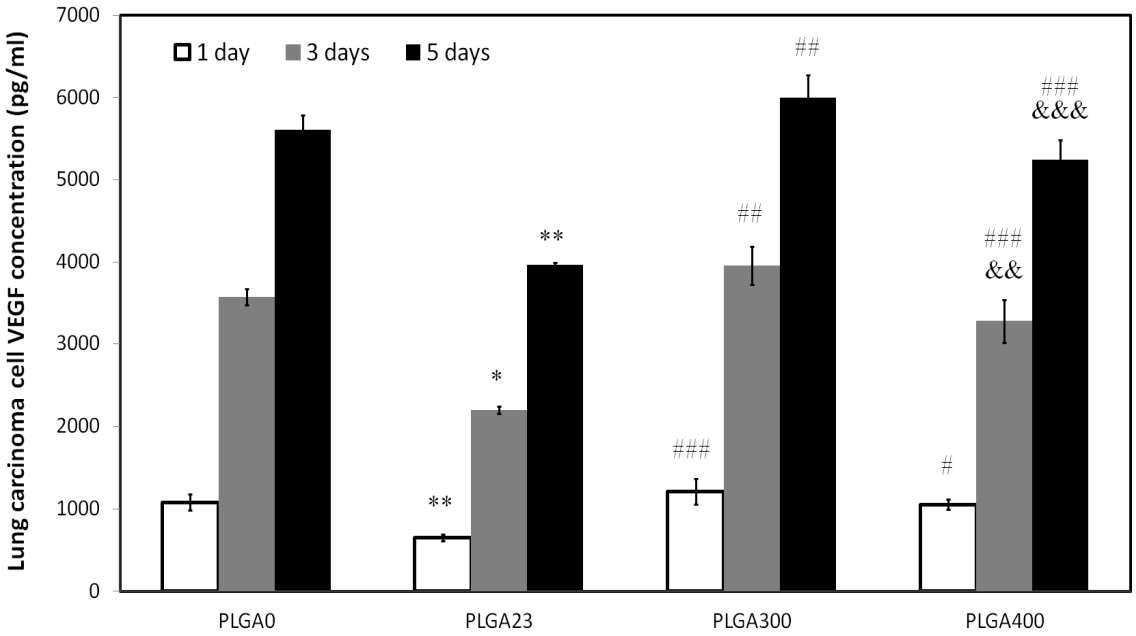

Fig. 2.11. One-, three- and five day VEGF secretion by lung carcinoma cells cultured on the various PLGA substrates. Data are expressed as the mean ± SEM; N=3. * $p < 0.01$ and ** $p < 0.05$ compared to PLGA0 at the same time point; $^{\#}$ $p < 0.01$, $^{\#\#}$ $p < 0.05$ and $^{\#\#\#}$ $p < 0.1$ compared to PLGA23 at the same time point; $^{\&\&}$ $p < 0.05$ and $^{\&\&\&}$ $p < 0.1$ compared to PLGA300 at the same time point. For all the samples, all time points are statistically different from each other.

Furthermore, after normalizing VEGF concentration and cell density on PLGA0, nominal VEGF per cell were obtained on the various PLGA surfaces and results are shown in Table 2.3. After one- and three-day, cells on PLGA23 had the lowest nominal VEGF per cell and had only 0.52 and 0.38 nominal VEGF per cell compared to nano-smooth PLGA. This result indicated that cells on 23 nm surface featured PLGA were significantly less bioactive and secreted much less VEGF compared to PLGA0.

Table 2.3. One- and three-day nominal VEGF per lung cancer cell on the various PLGA films

Sample	PLGA0	PLGA23	PLGA300	PLGA400
Normalized VEGF concentration (one day)*	1.00	0.61	1.12	0.98
Normalized total cell density (one day)**	1.00	1.17	1.54	0.82
Nominal VEGF per cell (one day)***	**1.00**	**0.52**	**0.73**	**1.18**
Normalized VEGF concentration (three day)	1.00	0.61	1.11	0.92
Normalized total cell density (three day)	1.00	1.61	2.80	1.12
Nominal VEGF per cell (three day)	**1.00**	**0.38**	**0.39**	**0.82**

*Normalized VEGF concentration obtained by normalizing all the VEGF concentration on PLGA0, PLGA23, PLGA300 and PLGA400 to the concentration on PLGA0; **normalized cell density obtained by normalizing all the total (live and dead) cell density on PLGA0, PLGA23, PLGA300 and PLGA400 to the total cell density on PLGA0; ***nominal VEGF per cell obtained by dividing the normalized VEGF concentration by normalized cell density.

2.3.8. Primary small airway lung epithelial cell MTT assay

Prior results concerning lung carcinoma cells showed that the nanopatterned PLGA surfaces could inhibit cancer cell functions compared to nanosmooth PLGA surfaces. Cancer cell functions including adhesion, proliferation, apoptosis, morphology and VEGF synthesis have been thoroughly investigated and the results indicated the anticancer function of the nanopatterns without the use of chemotherapeutics. When biomaterials are in contact with human tissue to regenerate healthy tissue where cancer tissue once was, they might interact with both cancer cells and healthy cells. Thus, it is necessary to investigate healthy cell growth on the proposed nanopatterned PLGA surfaces.

The cell viability of small airway lung epithelial cells after one- and three-days was investigated by an MTT assay and the results are shown in Fig. 2.12. Importantly, the total live cell numbers on the nanopatterned PLGA surfaces were significantly larger than that on the nanosmooth surfaces. Specifically, after one day, the total live cell numbers on PLGA23 and PLGA300 were significantly larger than that on PLGA0. Moreover, the PLGA23 had significantly more healthy live cells compared to PLGA400. On average, small airway epithelial cell growth on PLGA23, PLGA300 and PLGA400 resulted in 81%, 65% and 27% more live cells than that on PLGA0 after one day, suggesting that nanopatterned PLGA surfaces could improve healthy cell growth. After three days, live cell numbers on PLGA23, PLGA300 and PLGA400 were significantly larger than that on PLGA0, separately, with 23%, 21% and 19% more live cells compared to PLGA0. The increased healthy cell viability and resultant total live cell numbers indicated that the nanopatterned PLGA surfaces could be ideal candidates for

anticancer implants, since it possesses a novel double function of inhibiting cancer cell function while improving healthy cell growth without the use of pharmaceutical agents.

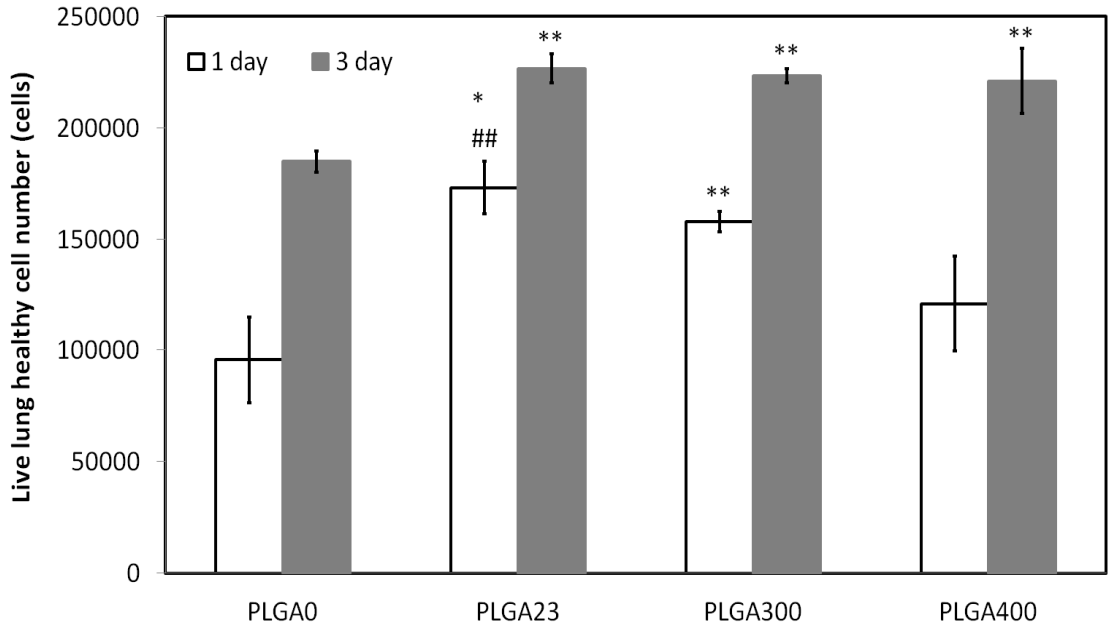

Fig. 2.12. One- and three-day total live cell numbers of primary small airway lung epithelial cells cultured on the various PLGA substrates. Data are expressed as the mean ± SEM; N=3. * $p<0.01$ and ** $p<0.05$ compared to PLGA0 at the same time point. $^{\#\#}$ $p<0.05$ compared to PLGA400 at the same time point. For all the samples, all time points are statistically different from each other.

2.4. Discussion

2.4.1. Control of PLGA surface properties (topography, wettability and chemistry)

Surface characterization studies on the various PLGA surfaces exhibited the successful fabrication of nanopatterned PLGA surfaces with pattern sizes as small as ~ 20 nm. AFM images demonstrated that the intended spherical nanotopographical surfaces had highly orderly arrays with extended surface areas. Moreover, the gradually increased pattern sizes also explained the trend that R_{rms} values gradually increased as the use of self assembly PS sphere diameter increased (from 23 nm to 400 nm), the patterns on the surface became larger and consequently made the surface more rough (from 3.73 nm to 24.11 nm). On the other hand, a comparatively smooth PLGA surface was fabricated without the use of PS beads, but still with some degree of nanoroughness (R_{rms}=0.54 nm) and, thus, these surfaces were termed nano-smooth PLGA surfaces.

Many methods have also been used to create nanopatterned surfaces, but some problems exist with the various approaches. For example, one problem with optical lithography is the limited resolution of optical lithography (mostly in micro scale), e-beam lithography involves high cost and is very time-consuming, while the polymer demixing technique is limited to the copolymer with phase separation ability. In this study, the method used to fabricate nanopatterned PLGA surfaces is extremely easy and inexpensive and does not alter the molecular weight or functional chemistry of the cast polymer. A further advantage of this technique is that it can be expanded to polymers beyond PLGA (considering only if the solvent used does not adversely affect the PDMS mold) [110]. In this manner, many different polymeric materials can be created to have diverse nanopattern features to investigate a wide range of cancerous cell responses. For

example, silicone substrates, photopolymers, and polycaprolactone, etc., with order nanopattern arrays have been produced by this approach [114-116]. Importantly, this method implies the possibility that topographical features of nanopatterned PLGA surfaces (including, but not limited to, pattern size and surface roughness) can be simply controlled by altering the self assembly monolayer described here.

In addition, ESCA results showed the same chemistry between all PLGA surfaces created in this study (including nano-smooth and nanopatterned PLGA surfaces). ESCA spectra showed the same peaks on various PLGA surfaces, indicating that there was no silicon contamination on the various PLGA cast surfaces through the use of the PDMS mold process. Thus, the only difference between these materials was the surface topography as created by the different sizes of the spherical features. Therefore, this study fabricated two types of PLGA films (nano-smooth and nanopattern) with different surface topographies but same chemistry. This allowed for a focused investigation concerning the effect of PLGA topography alone on regulating lung carcinoma cell functions, suggesting that the differences in cell responses can be attributed to the surface topography and surface roughness.

Furthermore, static water contact angle results showed slightly different hydrophobicity as all the PLGA samples were hydrophobic ($\theta > 90^0$). Considering all the PLGA surfaces had same chemistry but different surface topography, similar wettability can be contributed to the same surface chemistry. However, surface topography may still interfere with wetting of hydrophobic surfaces, but the effects of topography on surface wettability may not be as significant as surface chemistry.

Again, the results above suggest that surface topography can be precisely controlled by the method proposed in this study. Other surface properties can be de-convoluted, making surface topography an independent parameter on mediating cancer cell responses. In this sense, a more complete and thorough understanding of the effects of nanotopography on cancer cell functions can be expected.

2.4.2. Lung carcinoma cell adhesion and proliferation

Lung carcinoma cell adhesion results indicated that all the nanopatterned PLGA surfaces increased lung carcinoma cell adhesion. However, among all the nanopatterned PLGA surfaces prepared in this study, lung cancer cells showed least adhesion density on PLGA400 than any other nano pattern size, suggesting that the topographical pattern can regulate cell responses and the topographical scale can affect the degree to which the cell behavior is regulated. In addition to pattern size differences, it is important to emphasize that PLGA0, PLGA23, PLGA300 and PLGA400 had very different pattern features that also influenced surface roughness, surface area and surface free energy. As pattern size increased and the resultant surface roughness, it is not surprising that more cancer cell adhesive proteins (such as fibronectin) may have adsorbed on nanopatterned PLGA surfaces to induce better lung carcinoma cell adhesion. Importantly, many studies have been conducted to determine why tissue growth (such as bone, bladder, and neural tissue) is enhanced on nanostructured surfaces whether composed of polymers, metals, ceramics, or composites [117]. Such studies have focused on altered initial protein adsorption and bioactivity when adsorbing on nanostructured compared to microstructured or smooth

surfaces. Since the A549 cell has been found to express a fibronectin receptor, but not vitronectin receptor αvβ3 [118], fibronectin adsorption is important for A549 cell adhesion. Although the greater cell adhesion could be attributed to the increased surface area on nanopatterned surfaces, in this study, surface area showed no significant difference, only PLGA300 and PLGA400 had slightly higher surface areas. However, the adherent cell density was still lower on PLGA400 which had slightly higher surface area. Therefore, in addition to protein adsorption, other properties influenced by nanotopography (such as protein patterning, surface geometry features, etc.) may further affect initial cell adhesion. Moreover, although cell adhesion is important in subsequent cell development, cell adhesion alone can't predict future cell responses and functions.

Nanotopography has also been shown here to affect lung carcinoma cell proliferation. After one- and three-days, lung carcinoma cells grew less on PLGA400, while the highest cell proliferation was observed on the 300 nm surface featured substrates. Obviously, the proliferation difference between nano-smooth and nanopatterned PLGA surfaces was much smaller than the adhesion difference and again, PLGA400 exhibited lower cell proliferation than any other PLGA surface. This decrease can be in part attributed to the lower cell adhesion on PLGA400, but the lowest cell adhesion on PLGA0 did not lead to largely decreased cell proliferation. Inversely, PLGA23 did not show dramatically different cell proliferation compared to PLGA0 although they had much higher cell adhesion density, indicating the decreased cell proliferation rate on PLGA23. Some other surface properties related to lung cancer cell proliferation (such as protein adsorption, surface free energy, and surface topography) will be discussed in Chapter 5.

2.4.3. Lung carcinoma cell functions

Cellular interactions with biomaterial surfaces are regulated by surface properties which play an important role in mediating cell behaviors. Some studies have shown that nano-features can affect cancer cell behaviors, such as adhesion, proliferation, morphology, orientation and migration [79, 119-122]. For example, El-Said *et al.* [121] found that Hela cancer cells exhibited better cell adhesion and proliferation on nanoporous alumina coated with polypyrrole nanowires than traditional flat substrates. Moreover, the focal contacts of cells indicated that cell migration on the polypyrrole nanowires/nanoporous alumina surface may be easier and have higher motility than the cells on smooth surfaces. Another study indicated that the number of adherent lung carcinoma and Hela cells and their proliferation rates exhibited a maximum on moderately rough (Ra ~ 10-45 nm) electrochemically etched silicon substrates [119]. However, no general trend was found concerning cancer cell functions on topographical surfaces. In yet another example, human hepatoblastoma cells spread and grew confluently with elongated and aligned morphology along nano-grooves/ridges with various widths (from 100 to 500 nm) and depths (from 100 to 380 nm), while albumin synthesis and urea conversion decreased with increasing groove depths [120]. Andersson *et al.* [79] found that human bladder carcinoma cells cultured on hemispherically (167 ± 6 nm average diameter) nano-structured surfaces showed a decrease in IL-6 and IL-8 production and were less spread, less round and more stellate (larger dispersion). All these studies suggest that cancer cell functions can be up or down regulated by nano-features. In this study, increased lung cancer cell apoptosis and decreased VEGF secretion has been found on 23 nm topographical surfaces.

Cell morphology was investigated by fluorescent microscope to further elucidate the PLGA topographical effects on lung cancer cells. From fluorescent images, cells on PLGA0, PLGA23, and PLGA400 demonstrated less spreading than those on 300 nm surface featured PLGA, indicating that cell expansion was related to surface topography. This observation also supports the findings of enhanced bioactivity including cell adhesion, proliferation, apoptosis and VEGF secretion than any other substrates. Filopodia sensing of the topographical features has been proposed as a cell adaptation mechanism to surface topography [123]. It is possible that cell filopodia extension and cell spreading can be affected by the lateral dimensions or height of nanometer surface features. In the present study, the alteration of cell spreading on nanotopographical surfaces exhibited dependence on the pattern sizes.

Furthermore, apoptosis assays were conducted and results indicated that after three and five days, lung cancer cells on the 23 nm surface featured PLGA substrates had higher apoptotic and dead cell percentages than all the others, therefore resulting in a lower live cell percentage among all the substrates. Apoptosis is the process of programmed cell death and can be induced by biochemical and biophysical events. Topography could provide an extracellular physical stimulation and lead to cellular apoptosis. For example, Park *et al.* [124] found that mesenchymal stem cell adhesion and spreading were severely impaired on nanotube layers with a tube diameter larger than 50 nm, resulting in dramatically reduced cellular activity and a high extent of programmed cell death. Another study also reported that human foreskin fibroblasts exhibited significantly smaller cell size and lower proliferation on needle-like nanoposts [67]. In this study, the 23 nm PLGA surface topography was such a cell-stimulating cue that it

induced more lung carcinoma cell apoptosis compared to the nano-smooth PLGA surface. The possible mechanism may be that 23 nm surface topography doesn't support cell focal contact formation (including integrin assembly and actin filament assembly) and cell signaling to nucleus, thus leading to apoptosis [124].

Lastly, lung cancer cells on the 23 nm surface featured PLGA substrates secreted less VEGF than all the other samples, representing a possible critical detrimental step in tumor development through which the tumor establishes an independent blood supply, consequently facilitating tumor growth [125, 126]. This result can be attributed to the aforementioned higher apoptotic and dead cell percentages on the 23 nm surface featured PLGA substrates. Furthermore, after normalizing VEGF concentration and cell density on PLGA0, cells on PLGA23 had the lowest nominal VEGF per cell. This result indicated that cells on 23 nm surface featured PLGA were significantly less bioactive and secreted much less VEGF which could largely limit the growth of tumors, considering the essential role of VEGF on tumor growth. Importantly, although the relatively little higher cell adhesion and cell proliferation on PLGA23 than that on PLGA0, PLGA23 showed a pronounced potential towards inhibiting cancer cell functions as lung carcinoma cells on PLGA23 showed a higher percentage of apoptosis and death and decreased ability to secrete VEGF.

2.4.4. Primary small airway epithelial cell viability

Primary small airway epithelial cell represents lung healthy cells in contrast to the previously tested lung cancer cells. Lung carcinoma cell responses on nano-smooth and

nanopatterned PLGA surfaces (including adhesion, proliferation, morphology, apoptosis and VEGF secretion) have been thoroughly investigated and PLGA23 showed the highest potential anticancer property. However, lung healthy cell responses on the various PLGA surfaces are also important since the positive effects of nanopatterns on healthy cell are expected at the same time of inhibiting cancer cell functions. Therefore, the viability of primary small airway cells was studied on the various PLGA surfaces by MTT tests. One- and three-day results indicated that PLGA23 and PLGA300 both enhanced lung healthy cell viability and had more live cells compared to nano-smooth PLGA. Collectively, this result revealed that PLGA23 enhanced lung healthy cell proliferation and viability but inhibited lung cancer cell functions. The reasons for the enhanced lung healthy cell proliferation may relate to various surface properties and will be discussed in Chapter 5. Therefore, the 23 nm PLGA surface pattern could be an ideal biomaterial topography compared to nano-smooth and other larger nanopatterned (PLGA300 and PLGA400) surfaces.

In this manner, without changing the chemistry of materials, cancer cell functions may be selectively minimized on 23 nm topographical PLGA surface features which could contribute to the design of better materials for a wide range of cancer applications.

2.5. Conclusions

A simple and effective method was developed and used here to create various nanopatterned PLGA surfaces with the same surface chemistry and similar wettability. For the first time, these fabricated PLGA surfaces were systematically tested for lung carcinoma and primary small airway epithelial cell responses. The results of cell adhesion

and proliferation showed that total (live and dead) less lung carcinoma cells grew on the 400 nm surface featured PLGA compared to the other substrates, while the highest total cell density was observed on the 300 nm surface featured substrates. However, cell apoptosis assays indicated that after three and five days, cells on the 23 nm surface featured PLGA substrates had higher apoptotic and dead cell percentages than all the others, therefore possessing a lower live cell percentage among all the substrates. VEGF assays also showed decreased lung carcinoma cell bioactivity on PLGA23. In addition, the investigation of lung normal cell growth on the various PLGA surfaces showed increased healthy cell proliferation and viability on nanopatterned PLGA surfaces, which can be fundamental and critical information for the further investigation of nanotopographies for ideal anti-cancer implant applications. Obviously, different cell lines could have different responses to the same biomaterials. Thus, to investigate the universality of nanopatterned PLGA substrates to inhibit numerous cancer cell functions, breast adenocarcinoma epithelial cell (MCF-7) functions on the various PLGA surface will be described in the next chapter.

Chapter 3 Breast Adenocarcinoma Cell Functions on Polymer Nanometer Surface Features

3.0. Preface

In Chapter 2, the effects of PLGA surface properties (specifically, pattern size, surface topography and wettability) on lung carcinoma and lung normal cell functions (including adhesion, proliferation, morphology, apoptosis and VEGF secretion) were systematically identified. Results demonstrated, for the first time, decreased lung carcinoma epithelial cell functions on 23 nm surface featured PLGA compared to traditional nano-smooth PLGA. However, clearly, different cell lines could have different responses to the same biomaterials. Thus, to investigate the universality of nanopatterned PLGA substrates to inhibit numerous cancer cell functions, here, breast adenocarcinoma epithelial cell (MCF-7) adhesion, proliferation, apoptosis and VEGF secretion were determined on the same PLGA nanometer surface topographies created and tested in Chapter 2. To isolate surface nanotopographical effects from all other surface properties, PLGA surfaces with various nanotopographies but similar chemistry and hydrophobicity were fabricated here. Atomic force microscopy (AFM) verified the varied nanotopographies on the PLGA surfaces prepared in this study. Importantly, results

demonstrated for the first time significantly decreased breast adenocarcinoma cell functions (including decreased proliferation rate, increased apoptosis and decreased VEGF synthesis) on 23 nm featured PLGA surfaces compared to all other PLGA surface topographies fabricated (specifically, nano-smooth, 300 nm and 400 nm surface featured PLGA surfaces). In contrast, healthy breast epithelial cells proliferated more on the 23 nm featured PLGA surfaces compared to all other PLGA samples. In summary, these results provided further insights into understanding the roles PLGA surface nanotopographies can play on cancer cell functions and more importantly, opens the possibility of using polymer nanotopographies for a wide range of anticancer applications (without chemotherapeutics) from drug delivery to tissue engineering after breast cancer removal.

3.1. Introduction

According to ACS, it is estimated that about 1 in 8 women in the US (12%) will develop invasive breast cancer (cancer that spreads outside the membrane of the lobule or duct into the breast tissue) over the course of her lifetime. For women in the United States, breast cancer is the second leading cause of cancer death after lung cancer. An estimated 226,870 new cases of invasive breast cancer are expected to occur among women in the US during 2012; about 2,190 new cases are expected in men (ACS, 2012). Most patients with breast cancer have surgery to remove the cancer from the breast, such as lumpectomy and mastectomy. If a patient has a mastectomy, breast reconstruction (surgery to rebuild the breast's shape after a mastectomy and lumpectomy) may be used. At present, most of the reconstructed breast is made from an implant, such as a saline

implant, silicone gel, or polyurethane foam coating [127-129]. Thus, it is important to have cytocompatable biomaterials to avoid cancer recurrence and implant failure. Clearly, even if all the breast cancer is removed at the time of the surgery, there is still a possibility that the cancer will return, called breast cancer recurrence. According to the ACS, 11% of women will suffer breast cancer recurrence within five years and 20% in 10 years following the initial treatment. In this manner, biomaterials with anti-cancer properties would be an ideal implant after breast cancer resection. It is clear that the current plethora of materials used for breast reconstruction, were not originally designed to inhibit the return of cancer. For example, breast implants with polyurethane foam covers can leak toluene diamine, a demonstrated carcinogen in animals [38] and silicone implants can release platinum into tissues adjacent to silicone breast implants [130].

It is now known that cancer cells respond differently to nano structured (albeit large nanofeatures) compared to nano smooth topographies. For example, Keon *et al.* [131] constructed flat or nanostructured polymer surfaces (400 nm pillars, 400 nm perpendicular and 400 nm parallel lines with respect to the direction of flow) on the bottom of PDMS microfluidic channels to exploit the adhesion differences between normal breast epithelial cells (MCF-10A) and breast carcinoma cells (MCF-7). It was found that MCF-10A cells adhered in higher amounts than MCF7 cells regardless of culture time and surface nanotopography at all flow rates (from 10 ml/min to 1200 ml/min). Another study conducted by this group prepared smaller nanostructures (50 nm pillars, 50 nm perpendicular and 50 nm parallel lines with respect to the direction of flow) out of PDMS microfluidic channels and showed that healthy cells adhered in greater forces than cancer cells [132]. In this way, the nanopatterned PLGA surfaces could be an

ideal biomaterial interface which has a weak interaction with breast cancer cells and strong interaction with breast healthy cells. Although at the micron scale, Barr *et al.* [133] fabricated numerous well-defined micron-sized silicone topographies (100 μm lines, 10 μm wide and 20 μm spaced pits, and 5 μm wide and 15 μm spaced pillars) to examine breast tissue-derived fibroblast interactions. It was found that these micron topographies were capable of inducing differences in fibroblast adhesion and directional control of cell growth with alterations in cell shape and phenotype, illustrating that fibroblast adhesion and functions on silicone can be manipulated by microtopographies to enhance biointegration between the implant and the breast tissue. Lastly, Matthew *et al.* [134] presented the first data of an intracellular signaling molecule RACK1 (a multi-functional signaling adaptor protein) involved in the regulation of cell contact guidance on large scale nanometric growth polycaprolactone surfaces (12.5 μm line patterns, 353 nm deep). It was found that on nanometric grooves, over-expression of RACK1 in human breast cancer cells (MCF-7) led to a pro-adherent morphology and limited responses of cells to contact guidance. RACK1 therefore exerts a tonic inhibitory effect on cell contact guidance, while positively promoting a cell adhesive phenotype.

These studies collectively indicated that the substrate topography (both large nanometer and micrometer) can induce various cancer cell and healthy cell behaviors. The topographically patterned substrates could open opportunities for understanding and tailoring various cell growth, and further controlling cell functions. However, relatively little attention has been paid in terms of designing tissue engineering materials (specifically, PLGA) with true nanometer features to inhibit breast cancer function and promote healthy breast cell functions, criteria critical for regenerating healthy breast

tissue after breast cancer tissue removal. In addition, examining cancer cell functions beyond density (such as VEGF synthesis) on various nanotopographies are necessary, and currently missing.

For the above reasons, in this study, breast adenocarcinoma cell functions (such as adhesion, proliferation, apoptosis and VEGF synthesis) on various nanopatterned PLGA surfaces were investigated and compared to nano-smooth PLGA surfaces without nanopatterns. All the PLGA surfaces were prepared by the same procedure to allow for identical surface chemistry and similar wettability comparisons but with different topographies, enabling the exclusion of other surface properties (such as surface chemistry and surface wettability) from the surface nanotopographical effect.

3.2. Experimental

3.2.1. Fabrication of nanopatterned PLGA surfaces

PLGA surfaces with various nanotopographies were fabricated using the same method described in Chapter 2 Section 2.2.1. All PLGA surfaces were stored under a vacuum at a pressure of 20 inches of mercury until use. Prior to cell experiments, all of the PLGA films were cleaned by soaking in 70% ethanol for 20 mins and sterilized by UV light exposure for 4 hours.

3.2.2. Cells

A breast epithelial adenocarcinoma cell line MCF-7 (HTB-22, ATCC) was purchased from the ATCC and used without further characterization. Cells were cultured

in Dulbecco's Modified Eagle's Medium (DMEM, Hyclone) supplemented with 10% fetal bovine serum (FBS, Hyclone) and 1% penicillin/streptomycin (P/S, Hyclone) under standard cell culture conditions (5% CO_2, humidified air at 37°C). Human mammary epithelial cells (HEMpiC, ScienceCell, 7610) representing healthy breast epithelial cells at population numbers less than 5 were used for the MTT assay. HEMpiC from ScienceCell were isolated from normal human breast tissue. Mammary Epithelial Cell Medium (MEpiCM) consisting of basal medium (ScienceCell, 7611), mammary epithelial cell growth supplement (MEpiCGS, ScienceCell, 7652) and penicillin/streptomycin (P/S, ScienceCell, 0503) was used to culture HEMpiC cells. The cells were cultured until 80 ~ 100% confluence on cell culture polystyrene flasks before conducting the cell tests described below. Cell population numbers between 2 and 7 and were used for following cell assays.

3.2.3. Breast adenocarcinoma cell adhesion assay

After reaching confluence, MCF-7 cells were lifted from the tissue culture polystyrene flask with trypsin-EDTA and were dispersed in DMEM supplemented with 10% FBS and 1% P/S. Cell density in the suspension was measured by a hemocytometer (Fisher Scientific) according to standard procedures. For adhesion assays, MCF-7 cells were seeded onto the various PLGA surfaces and BG substrates (controls) at a density of 3,500 cells/cm^2 in DMEM supplemented with 10% FBS and 1% P/S. After seeding on the PLGA surfaces, cells were cultured under standard cell culture conditions (5% CO_2/95% humidified air and 37°C) for 4 hrs. After the prescribed time period, non-adherent cells were removed by rinsing in phosphate buffer saline (PBS) three times

while adherent cells were fixed with 10% formalin (Fisher Scientific) for 10 mins. Then, the formalin was removed and the cells adherent on the PLGA surfaces were stained in 4', 6-diamidino-2-phenylindole (DAPI, Sigma Aldrich) for 10 mins. After staining, samples were transferred to a fluorescence microscope (FM, Axiovert 200M, Zeiss) and adherent cells were counted under 10X magnification. For counting, five random areas on each sample were selected or photographed, and cell numbers in all five areas were counted and averaged. The adhesion assay was conducted in triplicate (n=3) and was repeated at least three separate times (N=3).

3.2.4. Breast adenocarcinoma cell proliferation assay

For the breast adenocarcinoma cell proliferation assay, cells were seeded onto the various PLGA surfaces at a density of 5×10^5 cells/well in 24 well tissue culture plates (treated by vacuum gas plasma, FALCON) in DMEM supplemented with 10% FBS and 1% P/S. The breast adenocarcinoma cells were cultured for four-hours, as well as one-, three- and five-days under the standard cell culture conditions described above. After the prescribed time period, MCF-7 cells were lifted from the substrates with trypsin-EDTA and dispersed in DMEM supplemented with 10% FBS and 1% P/S. The PLGA substrates were examined under fluorescence microscopy after trypsinization to determine that all cells were lifted. Cell density in the suspension was measured by a hemocytometer according to standard procedures. The proliferation assay was conducted in triplicate (n=3) and was repeated at least three separate times (N=3).

Furthermore, the cell growth equation was obtained by plotting the cell density over time to generate an exponential equation as follows [135]:

$$N(t)=N_0e^{rt} \quad \text{(Equ. 3.1.)}$$

where N(t) is the number of cells present at time t, N_0 is the population cell number at time 0, *r* determines the rate at which the population grows, and e (or Euler's number) is a transcendental number where e = 2.7182. Cell doubling time can be obtained by using equation 3.2:

$$T_h=(\ln 2)/r \quad \text{(Equ. 3.2)}$$

where T_h is the doubling time (hours) and r is the rate at which the population grows obtained by Equ. 3.1.

3.2.5. Breast adenocarcinoma cell apoptosis assay

Measurements of phosphatidylserine (apopotosis) expression using fluorescein-labeled (FITC) Annexin V-Programmed cell death (apoptosis) was conducted by flow cytometry using a Sigma-Aldrich apoptosis detection kit (APOAF). FITC Annexin V staining precedes the loss of membrane integrity which accompanies the latest stage of the cell death through the apoptosis and necrotic processes. FITC annexin V was used with the vital dye propidium iodide (PI) to separate the late and early apoptotic population of the cells. The experiment was performed according to the manufacturer's instruction. Specifically, 5×10^5 breast adenocarcinoma cells were seeded onto the various substrates in 24 well plates with 1 ml media. Then, cells were cultured in a similar manner to that described in the cell proliferation section. After three- and five-days, cells were washed with PBS. The cells were pelleted and resuspended in 1× binding buffer contained in the kit. 5 µl of FITC-Annexin V and PI were added to the cell

suspension and incubated at room temperature for 10 minutes. The cells were analyzed with flow cytometry (BDBiosciences FACSAria) and the results analyzed by BDBiosciences DiVa 5.0 software. The apoptosis assay was conducted in triplicate (n=3) and was repeated at least three separate times (N=3).

3.2.6. Breast adenocarcinoma cell VEGF immunoassay

For the breast adenocarcinoma cell VEGF assay, cells were seeded onto the various PLGA surfaces and polystyrene well plate surfaces at a density of 5×10^5 cells/well in 24 well tissue culture plates in DMEM supplemented with 10% FBS and 1% P/S. The breast adenocarcinoma cells were cultured for one-, three- and five-days under standard cell culture conditions. The media for the VEGF measurements were collected after 1 day. The quantikine human VEGF (vascular endothelial growth factor) immunoassay kit (R&D systems) was used for determining VEGF concentration. The experiment was performed according to the manufacturer's instruction. Briefly, 200 µl standards (prepared from the kit) and sample medium were pipetted into the 96-well plate (from the kit) and incubated for 2 hrs at room temperature. After washing with a binding buffer, an enzyme-linked polyclonal antibody specific for VEGF (from the kit) was added to the wells. Following a wash to remove any unbound antibody-enzyme reagent, a substrate solution (from the kit) was added to the wells and a color developed in proportion to the amount of VEGF bound in the initial step. Color development was stopped and the intensity of the color was measured by a micro plate reader (Molecular Devices). The VEGF concentration was determined from a standard curve of absorbance versus known concentrations of VEGF run in parallel with the experimental samples. The

VEGF immunoassay was conducted in triplicate (n=3) and was repeated at least three separate times (N=3).

3.2.7. Breast healthy epithelial cell MTT assay

Human mammary epithelial cells (HEMpiC, ScienceCell, 7610) representing healthy breast epithelial cells at population numbers less than 5 were used for the MTT assay. HEMpiC from ScienceCell were isolated from normal human breast tissue. Mammary Epithelial Cell Medium (MEpiCM) consisting of basal medium (ScienceCell, 7611), mammary epithelial cell growth supplement (MEpiCGS, ScienceCell, 7652) and penicillin/streptomycin (P/S, ScienceCell, 0503) was used to culture HEMpiC cells. For the MTT assay, HEMpiC were seeded on the PLGA surfaces at a density of 100,000 cells/cm^2. After seeding, the cells were cultured under standard cell culture conditions (5% CO_2, humidified air at 37°C). After one-, three- and five-days, viable cell numbers were determined using the Celltiter 96 Non-radioactive Cell Proliferation Assay (G4100, Promega) the same as described in Section 2.2.3.7. The live cell number was determined from a standard curve of absorbance versus known concentrations of live small airway epithelial cell solutions run in parallel with the MTT assay. All the experiments were performed in triplicate (n=3) and repeated three times (N=3).

3.2.8. Statistical analysis

Results were analyzed using one-way analysis of variance (ANOVA) and data were expressed as the mean ± standard error of the mean (SEM).

3.3. Results

3.3.1. Breast adenocarcinoma cell adhesion

Four-hour breast adenocarcinoma cell adhesion results (Fig. 3.1.) showed different breast cancer cell adhesion on various PLGA surfaces compared to lung carcinoma cells. Specifically, PLGA0 did not show significantly different cell adhesion density compared to the nanopatterned PLGA surfaces including PLGA190, PLGA300, PLGA400 and PLGA530. They all had similar cell adhesion densities after four hours although distinctly altered surface topographies. However, when the pattern size decreased to the nano scale, the effect of surface nanotopography on breast adenocarcinoma cell adhesion was observed. PLGA23 had the highest breast cancer cell adhesion density than that on any other PLGA surfaces (including PLGA0, PLGA190, PLGA300, PLGA400 and PLGA530). As the size of surface topography increased, PLGA400 had significantly lower adhesion density compared to PLGA300. This transition concerning cell adhesion density also happened to lung carcinoma cells. These results demonstrated that surface topography could play an important role in breast cancer cell adhesion as nano scale patterns had a more pronounced effect than 300 nm and 400 nm patterns. In addition, compared to the lung carcinoma cell adhesion results, although they are both cancer cells, the responses to specific nanotopographied PLGA surfaces were distinctly different, indicating that it is necessary to separately study the behaviors of lung cancer and breast cancer cells on the nanotopographied PLGA surfaces in this dissertation.

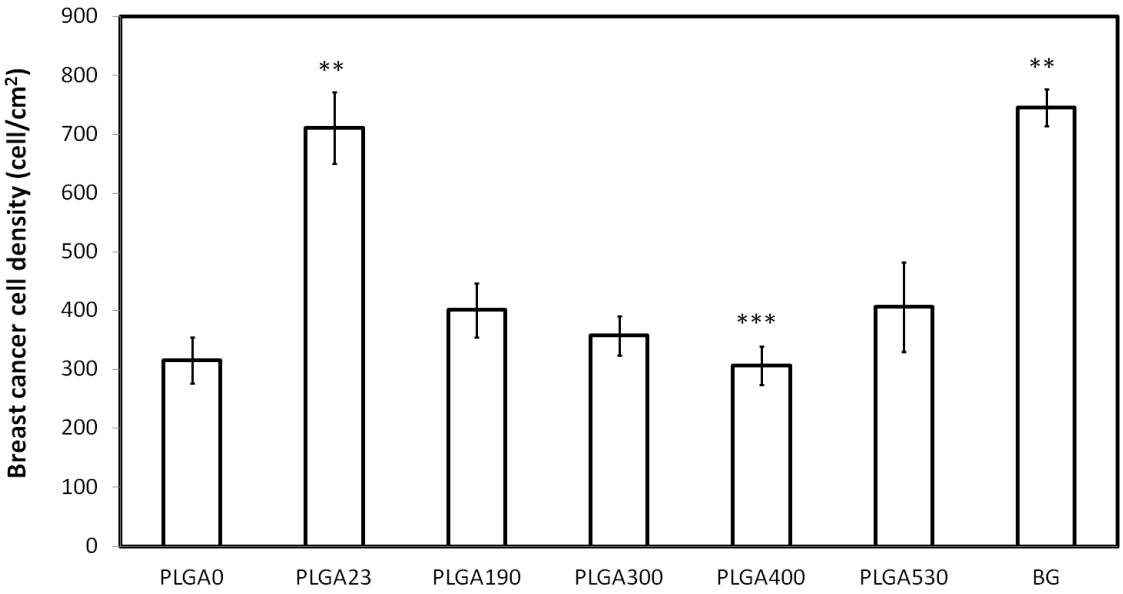

Fig. 3.1. Four-hour breast adenocarcinoma cell adhesion on various PLGA surfaces and BG controls. Data=mean±SEM; N=3; ** $p<0.05$ PLGA23 and BG compared to PLGA0, PLGA190, PLGA300, PLGA400 and PLGA530; *** $p<0.1$ PLGA400 compared to PLGA300.

3.3.2. Breast adenocarcinoma cell proliferation

Breast cancer cell proliferation on the various PLGA surfaces is shown in Fig. 3.2. After one day, breast cancer cell proliferation on PLGA0 and PLGA23 substrates were significantly higher compared to that on PLGA300 and PLGA400. As a result, both of the PLGA0 and PLGA23 had higher breast cancer cell densities than PLGA300 and PLGA400 after one day. Specifically, PLGA23 had 25% and 23% more cells compared to PLGA300 and PLGA400. For PLGA0, results indicated 15% and 13% more cells than that on PLGA300 and PLGA400. However, there was no significant difference between PLGA0 and PLGA23 after one day of proliferation. However, after three days, the breast

cancer cell proliferation results showed no significant difference among the various PLGA surfaces. Interestingly, the cell densities after three-days of culture on the various PLGA surfaces were similar as that after one-day of culture and the reasons for this abnormality will be further discussed later. After five days, the breast cancer cell density on PLGA0 was significantly smaller than that on PLGA23. However, no significant difference existed among all the nano-patterned PLGA surfaces. Considering that the various PLGA surfaces had identical surface chemistry and hydrophobicity properties but their topographies were different, these changes in short-term breast cancer cell interactions (adhesion and proliferation) can be correlated to the variations in surface topography only.

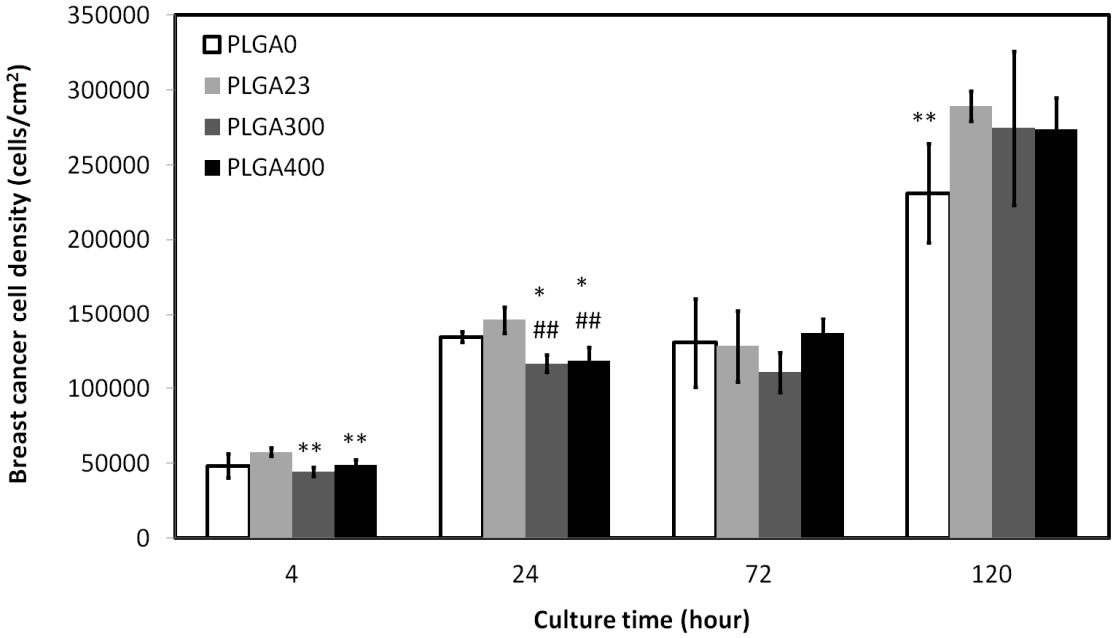

Fig. 3.2. MCF-7 four-hour adhesion and one-, three- and five-day proliferation on PLGA0, PLGA23, PLGA300 and PLGA400. Data are expressed as mean±standard deviation of the mean (SEM); N=3. * $p<0.01$ and ** $p<0.05$ compared to PLGA23 at the same time point; $^{\#\#}$ $p<0.05$ compared to PLGA0 at the same time point.

Fig. 3.3. shows the relative proliferation density of breast cancer cells (normalized to four-hour breast cancer cell adhesion density) on PLGA0, PLGA23, PLGA300 and PLGA400. The breast cancer cell doubling time on PLGA0, PLGA23, PGA300 and PLGA400 was 64.2 hrs, 62.5 hrs, 53.7 hrs and 55.0 hrs, respectively. The proliferation rate of breast cancer cells on each substrate (indicated by the slope of the best-fit line) demonstrated the smaller breast cancer cell proliferation rate on PLGA0 and PLGA23. PLGA300 showed the highest proliferation rate (20% higher than PLGA0) although it had relatively low cell densities at all the time points. In summary, PLGA300 and PLGA400 had a higher breast cancer cell proliferation rate than PLGA0 and PLGA23, suggesting that smaller nanotopographical surfaces (PLGA0 and PLGA23) could inhibit breast cancer cell proliferation compared to a larger size scale of nanotopographies (PLGA300 and PLGA400).

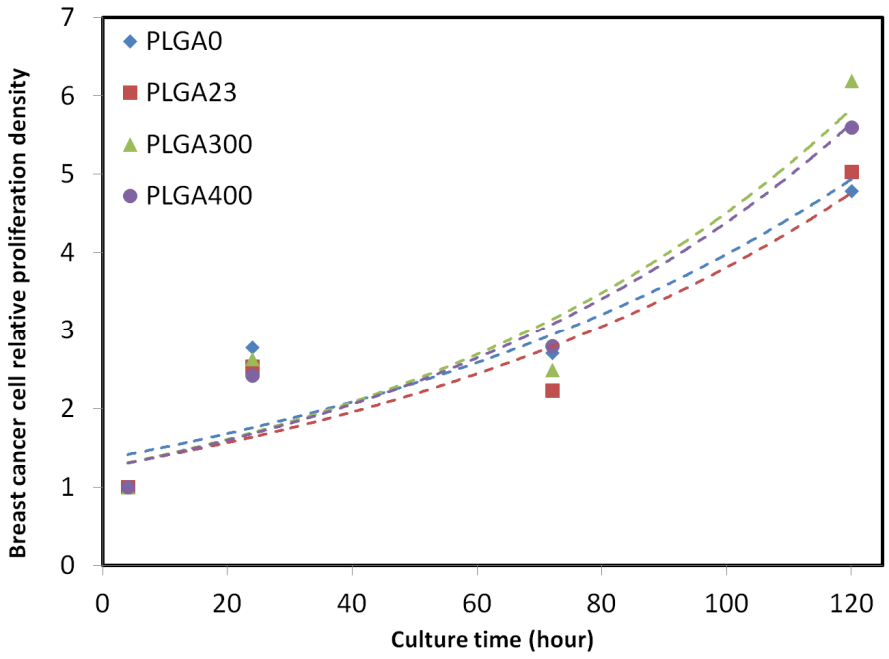

Fig. 3.3. Relative proliferation density of breast cancer cells (normalized to 4-hr breast cancer cell adhesion density) on PLGA0, PLGA23, PLGA300 and PLGA400.

3.3.3. Breast adenocarcinoma cell apoptosis

Although the previous section demonstrated higher total numbers of breast cancer cells on PLGA23, results of this part of the study demonstrated that of those numbers, a higher number of breast cancer cells on PLGA23 were dead or apoptotic, resulting in a lower number of live cells compared to PLGA300 and PLGA400. Specifically, PLGA23 had 96% more apoptotic cells than PLGA300 after three days (Fig. 3.4.). As for PLGA400, results showed almost no apoptotic cells after three days. For PLGA0, results also showed higher percentages of apoptotic cells than PLGA400, and thus a lower percentage of live cells on PLGA0. These results indicated that the nanotopographies on PLGA23 induced cancer cell apoptosis more easily than on PLGA300 and PLGA400. In addition, since apoptosis is an expected cell death process, the larger percentages of apoptotic cancer cells indicated that on PLGA23, breast cancer cell growth was inhibited and weakened by a 23 nm PLGA surface nanotopography after three days.

In addition, the five-day apoptotic and dead cell percentage results were shown in Fig. 3.5. For dead cells, nano-patterned PLGA (PLGA23, PLGA300 and PLGA400) showed average higher percentages compared to nano-smooth surfaces (PLGA0). When comparing apoptotic cells, PLGA0, PLGA23 and PLGA300 exhibited significantly higher apoptotic cell percentages than that on PLGA400. This result was consistent to the three-day results that cells on PLGA400 showed almost no early apoptotic trend.

The difference among dead and apoptotic cell percentages on the various PLGA surfaces led to the different live cell percentages (Fig. 3.6.). PLGA23 had significantly lower live cell percentages compared to PLA300 and PLGA400 after three days. This difference largely resulted from the higher dead and apoptotic cell percentages on

PLGA23. PLGA0 also showed lower percentages of live cells compared to PLGA400. The high live cell percentages on PLGA400 could be attributed to low apoptotic cell percentages. In addition, after five days, all the PLGA surfaces had lower live cell percentages compared to three-day results, indicating that as the culture time increased, more breast cancer cells were induced to die.

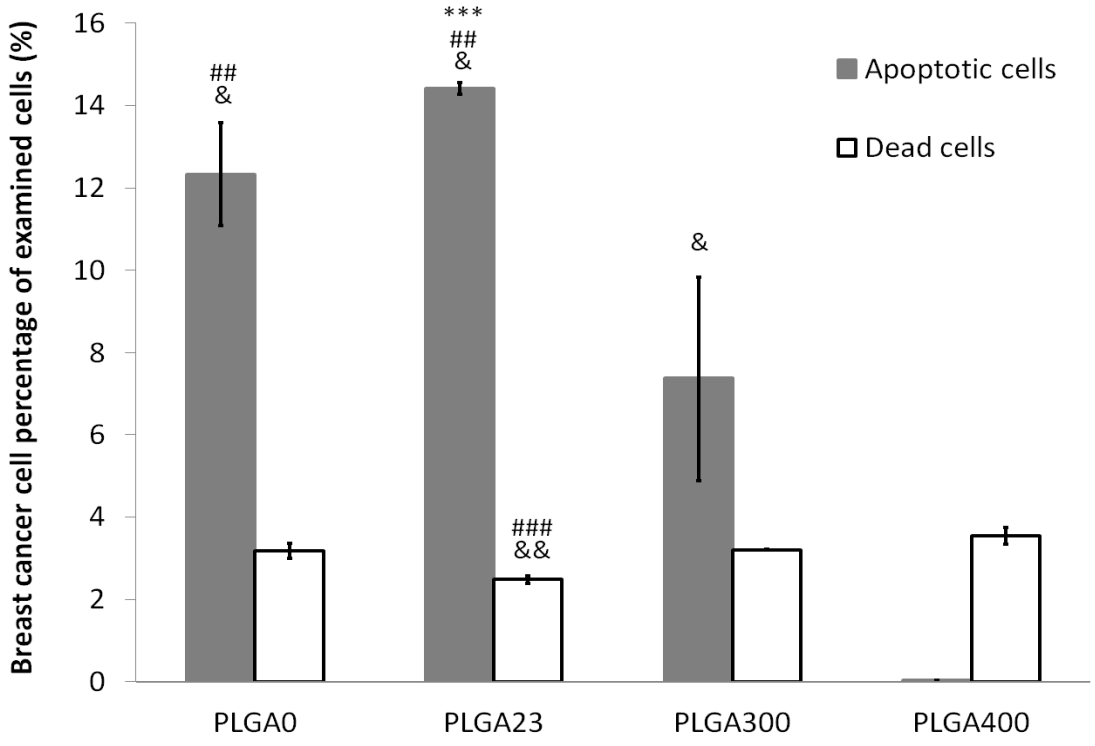

Fig. 3.4. Three-day apoptotic/dead cell percentages of MCF-7 (breast adenocarcinoma cells) populations cultured on the various PLGA substrates. The percentage is the ratio of apoptotic/dead cells to the total cells examined by flow cytometry. Data are expressed as the mean ± SEM; N=3. *** $p<0.1$ compared to same cell value on PLGA300; ## $p<0.05$ and ### $p<0.1$ compared to the same cell value on PLGA300; & $p<0.01$ and && $p<0.05$ compared to the same cell value on PLGA400.

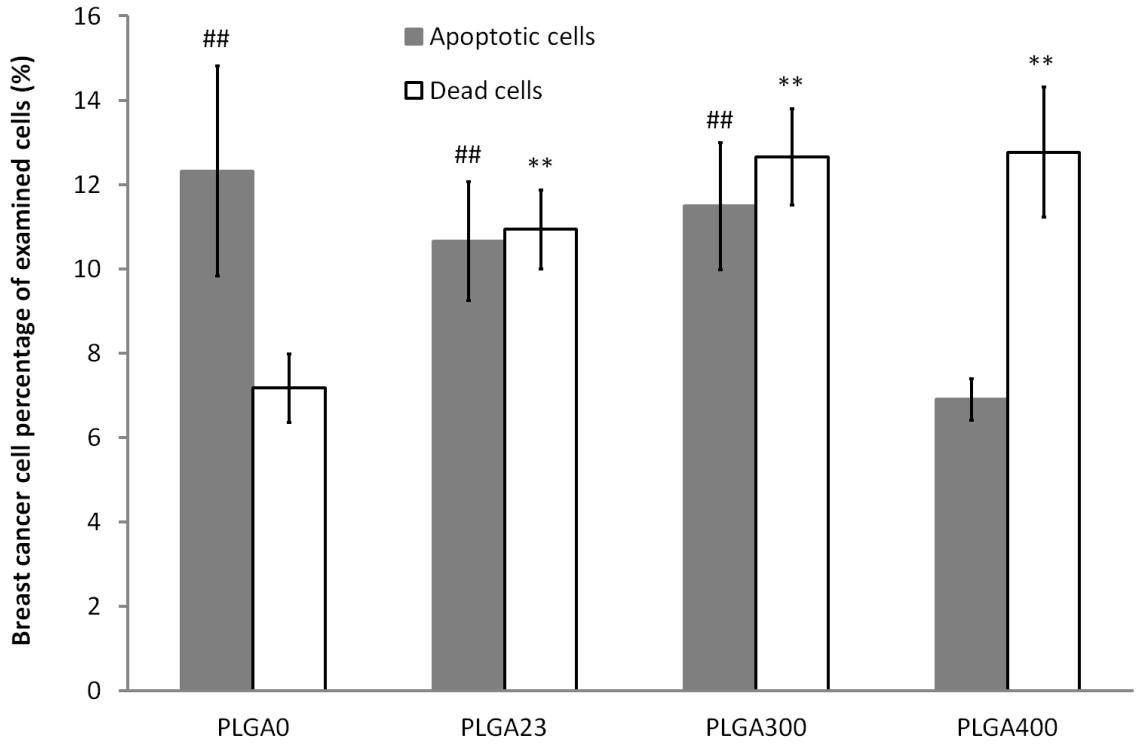

Fig. 3.5. Five-day apoptotic/dead cell percentages of MCF-7 (breast adenocarcinoma cells) populations cultured on the various PLGA substrates. The percentage is the ratio of apoptotic/dead cells to the total cells examined by flow cytometry. Data are expressed as the mean ± SEM; N=3. ** $p<0.05$ compared to the same cell value on PLGA0; ## $p<0.05$ compared to the same cell value on PLGA400.

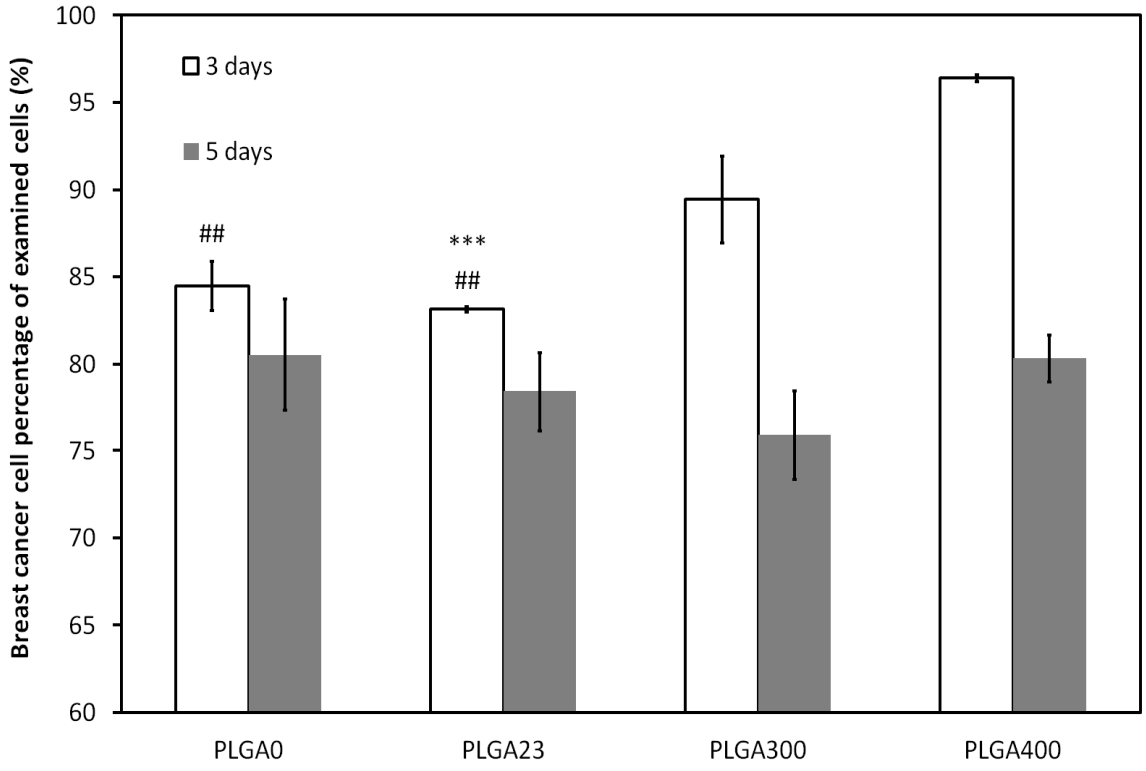

Fig. 3.6. Three- and five-day live cell percentages of MCF-7 (breast adenocarcinoma cells) populations cultured on the various PLGA substrates. The percentage is the ratio of live cells to the total cells examined by flow cytometry. Data are expressed as the mean ± SEM; N=3. ***$p<0.1$ compared to the same cell value on PLGA300; ## $p<0.05$ compared to the same cell value on PLGA400.

3.3.4. Breast adenocarcinoma cell VEGF immunoassay

VEGF is produced by cancer cells to stimulate angiogenesis and it is critical in cancer growth and metastasis. After one day, VEGF secretion by breast adenocarcinoma cells on PLGA23 was about 10% significantly lower than that on PLGA0 and PLGA400 (Fig. 3.7.). Comparing nanopatterned PLGA surfaces, PLGA23 stimulated less VEGF synthesis than that on PLGA400. However, there were no significant difference between PLGA23 and PLGA300. In contrast, PLGA0 showed significantly higher VEGF concentrations (specifically, 10%, 11% and 4%) than that on PLGA23, PLGA300 and PLGA400, respectively, indicating that nanotopographies on PLGA surfaces inhibited VEGF synthesis by breast adenocarcinoma cells. Comparing the different surface topography sizes among PLGA23, PLGA300 and PLGA400 substrates, a smaller nanotopographical surface feature size (PLGA23) had a stronger ability to inhibit breast adenocarcinoma cell VEGF synthesis than larger sizes (PLGA300 and PLGA400). After three days, PLGA300 had significantly lower VEGF concentrations than that on PLGA400. On the average, PLGA23 showed a slightly lower VEGF concentration than PLGA0, PLGA300 and PLGA400, although the differences were not statistically significant. Furthermore, five-day VEGF results revealed no statistically significant difference among all the PLGA surfaces, but, on the average, PLGA23 and PLGA300 again showed lower VEGF concentrations than PLGA0 and PLGA400. The possible reasons for the slight difference between three- and five- days will be discussed in Section 3.4.4.

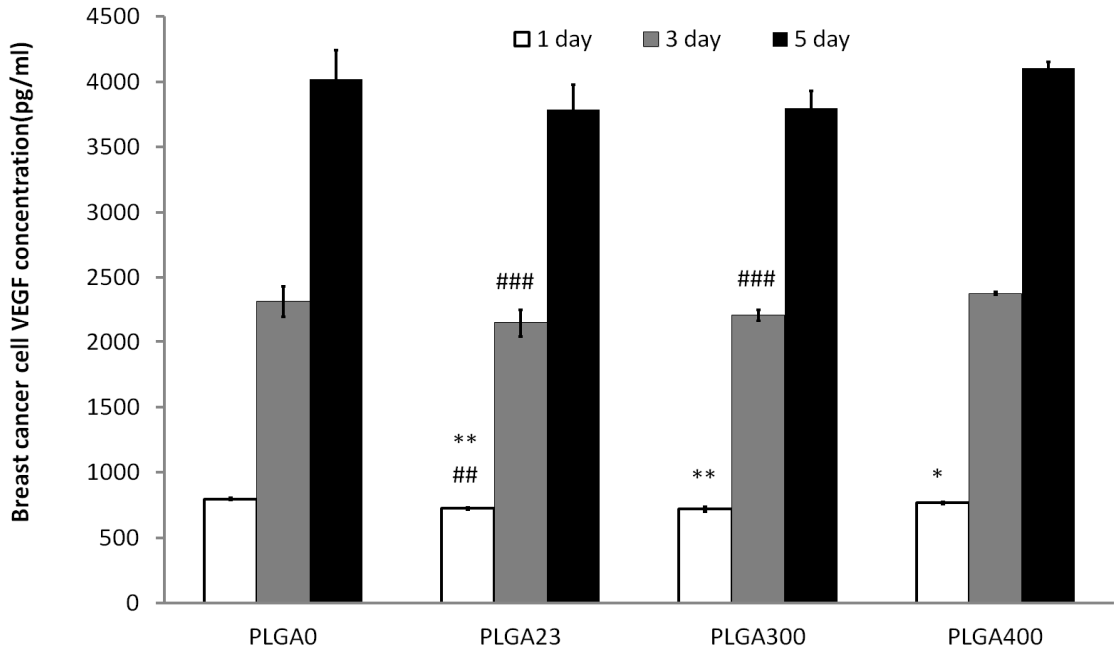

Fig. 3.7. VEGF secreted by MCF-7 (breast adenocarcinoma cells) cultured on the various PLGA substrates after one-, three- and five-days. Data are expressed as the mean ± SEM; N=3. *$p < 0.01$ and **$p < 0.05$ compared to PLGA0 at the same time point; ## $p < 0.05$ and ### $p<0.1$ compared to PLGA400 at the same time point. For all the samples, all time points are statistically different from each other.

Furthermore, after normalizing one- and five-day VEGF concentration and cell density on PLGA0, nominal VEGF per cell values were obtained on the various PLGA surfaces and are shown in table 3.1. After one- and five-day, groups of cells on PLGA23 had the lowest nominal VEGF per cell at 0.84 and 0.75 nominal VEGF per cell compared to nano-smooth PLGA, respectively. This result indicated that the group of cells on 23 nm surface featured PLGA had significantly decreased bioactivity to secret much less VEGF and thus could largely limit the growth of tumors considering the essential role of VEGF on tumor growth.

Table 3.1. One- and five-day nominal VEGF per breast cancer cell on the various PLGA films

Sample	PLGA0	PLGA23	PLGA300	PLGA400
Normalized VEGF concentration (one day)*	1.00	0.91	0.90	0.96
Normalized total cell density (one day)**	1.00	1.08	0.87	0.88
Nominal VEGF per cell (one day)***	**1.00**	**0.84**	**1.04**	**1.09**
Normalized VEGF concentration (five day)	1.00	0.94	0.94	1.02
Normalized total cell density (five day)	1.00	1.25	1.19	1.18
Nominal VEGF per cell (five day)	**1.00**	**0.75**	**0.80**	**0.86**

*Normalized VEGF concentration obtained by normalizing all the VEGF concentration on PLGA0, PLGA23, PLGA300 and PLGA400 to the concentration on PLGA0;

**normalized cell density obtained by normalizing all the total (dead and live) cell density on PLGA0, PLGA23, PLGA300 and PLGA400 to the density on PLGA0;

***nominal VEGF per cell obtained by dividing normalized VEGF concentration by normalized cell density.

3.3.5. Breast healthy epithelial cell MTT assay

Prior results from this study indicated that the various sizes of nanotopographies on PLGA surfaces can affect cancer cell functions (including cell adhesion, proliferation, apoptosis and VEGF synthesis). However, for cancer tissue replacement by healthy tissue, it is also important to investigate the interactions of healthy breast cells on nanopatterned PLGA surfaces. For this, live HEMpiC cell numbers were determined using the CellTiter 96 Non-Radioactive Cell Proliferation Assay (MTT) kit following protocols by the manufacturer (Promega). Results of total live cell numbers on the various PLGA surfaces are presented in Fig. 3.8. After one day, more live HEMpiC cells were measured on PLGA23 and PLGA300 than on PLGA0 and PLGA400. Specifically, after one day, PLGA23 and PLGA300 had 24% and 25% more live healthy breast cells than that on PLGA0. Compared to PLGA400, PLGA23 and PLGA300 also had significantly higher live cell numbers. However, there was no significant difference in living breast healthy cells after one day of culture between PLGA0 and PLGA400. After three days, the number of live cells on PLGA0 was significantly less than that on PLGA23 and PLGA300, but no significant difference was observed between PLGA0 and PLGA400. As for five-day results, PLGA23 had significantly higher breast healthy cell numbers compared to PLGA0 and PLGA400. The results suggested that PLGA23 enhanced live healthy cell growth compared to any other nano-smooth and nanopatterned PLGA surfaces up to five days. This finding further confirmed the large potential PLGA23 has for anticancer breast implants, since such materials can inhibit cancer cell functions and at the same time, improve healthy cell growth.

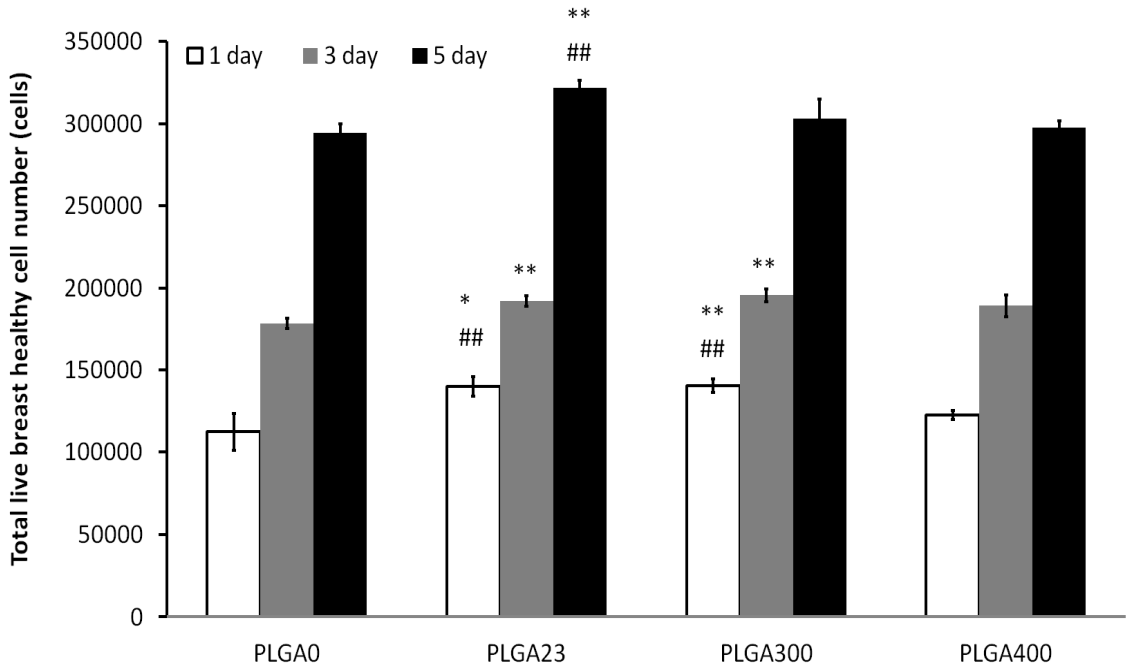

Fig. 3.8. One-, three- and five-day total live cell numbers of HEMpiC (normal breast epithelial cells) cultured on the various PLGA substrates. Data are expressed as mean ± SEM; N=3. * $p<0.05$ and ** $p<0.1$ compared to PLGA0 at the same time point; ## $p<0.1$ compared to PLGA400 at the same time point. For all the samples, all time points are statistically different from each other.

3.4. Discussion

A previous study in Chapter 2 on biomaterial-cell interactions between nanopatterned PLGA surfaces and lung epithelial carcinoma cells demonstrated the inhibition of lung cancer cell functions on 23 nm PLGA surface features. Here, in order to investigate the anticancer properties of PLGA nanotopographies on other cells, cell functions of another cell line, breast cancer cells (MCF-7) (including short-term

adhesion, proliferation, apoptosis and VEGF synthesis) were systematically investigated. Similarly, this study fabricated two types of PLGA surfaces (nano-smooth and nanopatterned) with different surface topographies but almost identical chemistries. This permitted a focused exploration of the impact of the PLGA surface topographies alone in mediating cancer cell behaviors, especially important cell functions including apoptosis and VEGF secretion. On Chapter 2, ESCA results provided evidence that the method used here to fabricate nano-smooth and nanopatterned PLGA surfaces did not influence surface chemistry.

3.4.1. Impact of nanotopography on breast cancer cell adhesion and proliferation

Obviously, breast adenocarcinoma cells showed different responses to various nano feature PLGA surfaces compared to lung cancer cells, although they are both cancer cell lines. Complicated cell responses based on altered topographic size, shape, uniformity and cell lines largely increase the difficulty of investigating the mechanisms behind topographically regulated cell behaviors and responses. In this dissertation, our study focused on orderly arrayed semispherical pattern with different sphere diameters but several different cell lines (including cancer cells and healthy cells) were extensively studied.

Breast cancer cell adhesion results demonstrated that 23 nm surface features improved cell adhesion compared to PLGA0, PLGA300 and PLGA400. However, after one day of proliferation, cancer cell densities were not significantly different between PLGA0 and PLGA23, whereas cancer cell densities on PLGA300 and PLGA400 were still significantly smaller than that on PLGA0 and PLGA23. This study showed that a

nanotopography with pattern sizes less than 100 nm (specifically 23 nm) promoted selective breast cancer cell adhesion compared to larger pattern sizes (300 nm and 400 nm). Due to pattern size differences, it is important to emphasize that PLGA0, PLGA23, PLGA300 and PLGA400 have very different topographical features that also influence surface area, surface wettability, surface energy, etc. However, based on the water contact angle and surface area measurements presented in Chapter 2, there was no significant difference between the various PLGA surfaces. Thus, better cancer cell adhesion on the PLGA23 could be attributed to the surface nanotopography, which may have influenced protein adsorption and conformation (such as fibronectin, vitronectin, etc.). Topographical surface features whose size and shape corresponds to the size and shape of the protein can lead to increased adsorption as the protein finds suitable "dock-in" sites [136]. Normally, most protein size dimensions are in the nanometer scale and fold into nano-structured globalular domains [137]. This size and shape significantly corresponds to the size and shape of the 23 nm featured PLGA surfaces. Thus, increased select protein adsorption and subsequent breast cancer cell adhesion were observed on PLGA23 surfaces.

This study also showed that PLGA23 enhanced breast cancer cell proliferation compared to PLGA300 and PLGA400 after one day. This enhancement may be attributed to more breast cancer cell adhesion on PLGA23. However, the proliferation difference after one day was largely smaller than the adhesion difference between PLGA0 and PLGA23. After three days, surprisingly, cell densities on the various PLGA surfaces showed no distinct change compared to one-day results. The possible reason for this may be that cells cultured for this time point had low activity or cell culture condition was

changed compared to other time points. Further experiments will be needed to identify accurate reasons. Five-day cell proliferation results revealed that PLGA23 promoted breast cancer cell proliferation compared to nano-smooth PLGA. Furthermore, proliferation rate results suggested that cells on PLGA23 had relatively lower proliferation rates (doubling time 62.5 hrs) than that on PLGA300 and PLGA400 (doubling time 53.7 hrs and 55.0 hrs, respectively), and, thus, although the initial cell adhesion was large on PLGA23, cells proliferated slow, resulting in similar cell densities on PLGA23, PLGA300 and PLGA400 after five days. Therefore, it is the cell adhesion density as well as proliferation rate together that determined subsequent cell densities.

In summary, breast adhesion and proliferation results indicated that PLGA300 and PLGA400 decreased breast adenocarcinoma cell proliferation compared to PLGA0 and PLGA23. But PLGA23 showed a relatively low proliferation rate, although it had a high initial cell adhesion density.

3.4.2. Impact of nanotopography on breast cancer cell functions

Importantly, upon further investigation, it was found that a significant number of breast cancer cells on the 23 nm PLGA surfaces were dead or apoptotic after three days. Apoptosis is an active, inherently programmed phenomenon, which has been shown to be initiated or inhibited by a variety of environmental stimuli, both physiological and pathological [138]. Apoptosis is programmed cell death and, thus, is expected for cancer cells. Three-day apoptosis results showed that PLGA23 induced more cells to enter the apoptosis process compared to PLGA300 and PLGA400, resulting in an overall lower

live cell percentage compared to any other nano-modified substrate in this study. However, after five days, PLGA23 and PLGA300 on the average showed lower live cell percentages than any other substrate. After further investigating the origins of this low live cell percentage on PLGA23 and PLGA300, it was found that this decrease on PLGA23 and PLGA300 resulted from a higher percentage of total apoptotic and dead cells after five days. According to the principles of the apoptosis assay, cells in the dead phase have experienced the loss of membrane integrity which accompanies the latest stages of cell death resulting from either apoptotic or necrotic processes. Therefore, a single observation indicating that cells are in a dead phase, in of itself, reveals little information about the process by which the cells underwent their demise. Thus, it is reasonable to put more emphasis on apoptotic cell percentages, which indicated that cells were undergoing programmed cell death. In addition, results demonstrated that after five days, the dead and apoptotic cell percentages increased on nano-patterned PLGA surfaces compared to the three-day results. These results revealed that PLGA nanotopography was a continuous external stimulus to induce breast cancer cell apoptosis. This apoptosis study also highlights the importance of not just relying on cell numbers, but also examining cell viability to determine cell responses which was not done in many other cell research.

Moreover, tumors cannot grow beyond a few millimeters without an adequate blood supply. For this, cancer cells secrete VEGF to drive tumor angiogenesis (the formation of new blood vessels), growth and metastasis [139]. Results of the present VEGF assay further demonstrated that nanotopographies (specifically, 23 nm) may have anticancer properties as breast cancer cells on PLGA23, PLGA300 and PLGA400

synthesized significantly less VEGF than PLGA0. Furthermore, after one- and five days, group of cells on PLGA23 had the lowest nominal VEGF per cell (0.84 and 0.75, respectively) compared to nano-smooth PLGA. This result indicated that the group of cells on the 23 nm surface featured PLGA had significantly decreased bioactivity to secret much less VEGF and, thus, could largely limit the growth of tumors considering the essential role of VEGF on tumor growth. It seems that although breast adenocarcinoma cells were prone to adhere on PLGA23, subsequent cell functions (such as viability and VEGF synthesis) were significantly inhibited by this nanotopography. There are a number of reasons for this that require further investigation which will be discussed in Chapter 5.

3.4.3. Impact of nanotopography on breast healthy cell growth

This study also investigated healthy cell growth on the various PLGA surfaces. Results showed significantly more live healthy breast cells on PLGA23 compared to PLGA0 and PLGA400 up to five days. As a result, PLGA23 up-regulated breast healthy cell response and promoted healthy cell growth. Again, this effect was highly related to the nano pattern size since PLGA400 did not increase healthy cell viability compared to PLGA23 and PLGA300. Importantly, combining the results already mentioned from breast cancer cells, PLGA23 and PLGA300 both decreased breast cancer cell functions and increased breast healthy cell growth. The different interaction of cancer cells and healthy cells deserves some explanation and may be related to cancer versus healthy cell stiffness, organization of the cytoskeleton, interactions with the extracellular matrix,

initial protein interactions, cell protein secretion, and cell adhesion forces [140]. These differences result in the significantly different or even opposite cell responses to the same nanotopographical substrates. For example, studies by Keon *et al.* [131] have shown that healthy, non-cancerous, breast cells (MCF-10A) adhered in higher amounts than breast cancer cells (MCF7) on nanostructured polyurethane acrylate (PUA) surfaces (400 nm pillars, 400 nm perpendicular, or 400 nm parallel lines). Here, in this study, this specific nanometer surface feature size (23 nm) was delineated which inhibited cancer cell functions and enhanced healthy cell viability. The mechanism involved in the increased breast healthy cell response on PLGA23 will be examined in Chapter 5.

3.4.4. Impact of seeding density on long-term cell behaviors

In this study, various cell behaviors (including adhesion, proliferation, apoptosis and VEGF secretion) up to five days were examined with the same experimental methods at all time points. However, statistically significant differences decreased among various PLGA surfaces for longer term (three- and five days) cell functions. Here, a possible reason is proposed that seeding density may influence the degree of cell-biomaterial interactions. In order to test the effects of nanotopographies on cancer cell functions in an extreme situation with limited resources and space as well as to increase statistical accuracy, the seeding density was designed to be very high for proliferation, apoptosis, VEGF, and MTT assays. Thus, after a longer time, cells grew into multilayers and the cells may not have directly contacted the material surfaces which mean they would not be significantly affected by the surface nanotopographies. Also, they would secrete their

own ECM to potentially mask nanotopographies. Fortunately, longer term cell functions did show some degree of significant difference, even though these differences were not as distinct as the short term ones. This result indicated that nanotopography could exert a durative influence on cell functions. It is also important to mention that short term effects could play an important role on subsequent cell protein secretion and result in cell function increases or decreases.

In summary, this study provides exciting results for the potential applications of nanopatterned biomaterials in cancer regenerative medicine, especially small PLGA nanometer scale size features such as 23 nm. These nanopatterned tissue engineering materials may be applied on implants inserted to regenerate tissue after tumor removal since they can potentially inhibit the return of cancer cells yet positively interact with healthy cells. This study recognized for the first time that 23 nm and 300 nm PLGA topographies could be one of those ideal implant surfaces.

3.5. Conclusions

In this part of the study, various nanopatterned PLGA surfaces with similar surface chemistry but different topographies were prepared. Breast cancer cell adhesion and proliferation results indicated higher cell densities on PLGA0 and PLGA23 than that on PLGA300 and PLGA400. VEGF immunoassay results showed significantly lower VEGF synthesis on PLGA23 and PLGA300 compared to any other PLGA surface, suggesting inhibited cancer cell functions on 23 nm and 300 nm surface featured PLGA. More importantly, healthy breast cell results indicated that the same PLGA23 and

PLGA300 improved healthy breast cell viability and proliferation. Thus, PLGA23 and PLGA300 may be ideal surface topographies for anticancer implants because they inhibited cancer cell functions and enhanced healthy cell growth. In summary, these results provided further insights into understanding the role surface nanotopographies can have on cancer cell interactions and more importantly, may open the possibility of using such polymer nanotopographies for a wide range of anticancer applications without chemotherapeutics.

Chapter 4 Impact of Surface Chemistry Modification of Nanostructured PLGA on Cancer and Healthy Cell Functions

4.0. Preface

In the last two chapters, the effects of nanotopography on cell functions (including adhesion, proliferation, apoptosis and VEGF secretion) were studied on both cancer and healthy cell lines. In this chapter, other important surface properties (specifically, surface chemistry as well as associated surface charges) were studied to comprehensively understand the effects of surface chemistry and surface charge on cancer cell functions with a goal of developing PLGA to further inhibit cancer cell functions. This study utilized an effective method, layer-by-layer (LBL) self assembly, to alter PLGA surface chemistry and surface charge by self assembling monolayers of biocompatible alginate and chitosan which have antifouling properties in the hope to control protein adsorption so that cancer cell functions will be further decreased without affecting healthy cell responses. Surface terminations on PLGA after coating with self assembly monolayers were confirmed by fourier transform infrared spectroscopy (FTIR). To further understand the influence of these surface properties on cell functions, cell responses (including proliferation and VEGF synthesis) were determined on the

chemically modified nano-smooth and nanopatterned PLGA surfaces using lung cancer cells, lung healthy cells, breast cancer cells and breast healthy cells. A strong dependence of cell proliferation and VEGF secretion on surface chemistry was observed for lung cancer cells, breast cancer cells and breast healthy cells. PLGA surfaces which were modified with an alginate self assembled monolayer exhibited an anti-cancer property, significantly decreasing lung carcinoma cell and breast cancer cell VEGF synthesis. Furthermore, alginate modified PLGA inhibited breast cancer cell proliferation, while promoted lung cancer cell proliferation. However, the 23 nm patterned PLGA substrates (regardless of surface chemistry and self-assembled monolayer) promoted lung healthy cell proliferation. Decreased breast healthy cell proliferation was observed on alginate- and chitosan-terminated PLGA substrates. The results of this part of the dissertation provided an important understanding of cell functions mediated by surface chemistry in addition to surface topography. Alginate-terminated PLGA substrates with 23 nm surface patterns were found to be the best anti-cancer material overall for lung and breast applications. An effective surface chemistry (alginate) coating on PLGA was discovered to inhibit cancer cell functions, which expands insights into designing and fabricating anti-cancer implants for the lung and breast.

4.1. Introduction

In addition to physical nanotopography, nanoscale chemistry and electrical signaling through surface changes can also regulate cell functions by modulating the extracellular milieu of the cell-biomaterial interface. Surface chemistry is highly related

to other associated surface properties (such as surface wettability, surface free energy and surface charge) and thus cell functions can be significantly affected. Altered surface chemistry can produce various defined biological surfaces (including protein adsorption, protein repellent, biofouling, etc.) and in turn affect cell behaviors. Surface charge is another important factor affecting protein adsorption and cell functions by inducing attraction or repulsion of proteins or cells depending on their isoelectric point and charges. For instance, thin polystyrene films irradiated by an electron beam to create trapped charges were able to immobilize the positively-charged protein, avidin-fluorescein through electrostatic attraction [141]. Another study revealed that chitosan nanoparticles with a high degree of deacetylation had extended conformation because of charge repulsion, which allowed them to bind more readily to cell membranes than coiled chitosan of a lower degree of deacetylation. As a result, the uptake of chitosan nanoparticles by A549 cells increased with increasing degree of deacetylation [142]. Therefore, it is desirable to control protein adsorption and cell functions by altering surface chemistry and surface charge.

Surface modification of PLGA substrates (PLGA0 and PLGA23) was developed here to change surface chemistry and surface charge but take advantage of the anti-cancer properties from the aforementioned 23 nm PLGA compared to nano-smooth PLGA. Specifically, an effort was made to identify proteins that can be coated on such surfaces to further inhibit cancer cell functions. Polyelectrolyte layer-by-layer deposition provides a facile and effective technique for the modification of various surfaces. In this method, a polyelectrolyte is deposited from an aqueous solution onto a surface of opposite charges resulting in a reversal of the net surface charge. A second, oppositely charged

polyelectrolyte, can be further deposited due to electrostatic interactions [143]. A biodegradable pair of polyelectrolytes, alginate (Alg) and chitosan (Chi) (Fig. 4.1.), has been used to coat PLGA surfaces because of the following two considerations [103, 143]: (1) an Alg or Chi multilayer coating has antifouling properties resistant to protein adsorption and, thus, may lead to decreased cancer cell adhesion and proliferation. For example, bovine serum albumin deposition could not be observed on an Alg or Chi multilayer formed on PLGA nanoparticles, for both Alg and Chi used as top layers. Moreover, HepG2 cellular uptake of Chi/Alg coated PLGA nanoparticles was significantly less compared to the bare nanoparticles [103]; and (2) an Alg or Chi multilayer provide many functional groups that can allow the covalent attachment of other functional sequences (such as collagen and folic acid) to achieve specific cell responses of interest, such as increasing healthy cell adhesion and proliferation by binding specific adhesion proteins for healthy cells on Alg- or Chi-terminated surfaces.

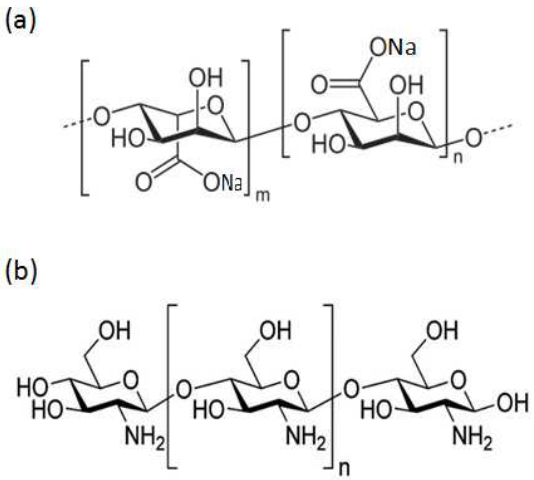

Fig. 4.1. Chemical formulas of the biological polyelectrolytes employed here to modify PLGA substrates: (a) sodium alginate and (b) chitosan.

Therefore, identifying appropriate surface chemistry in conjugation with surface topography on PLGA surfaces and understanding relevant cellular responses and behaviors are important for a wide range of biomedical applications. Specifically, for anti-cancer implant applications, the protein-resistant ability is expected to improve on nanopatterned PLGA substrates which are desirable for decreasing the initial protein adsorption on the nanopatterns and subsequent cancer cell adhesion and proliferation. The *in vitro* experiments of Chapter 2 and Chapter 3 revealed that the 23 nm featured PLGA surfaces showed higher cancer cell adhesion and proliferation but decreased cancer cell functions in terms of apoptosis and VEGF secretion compared to other PLGA substrates. This increased cancer cell adhesion and proliferation may be attributed to the higher nonspecific protein adsorption (such as fibronectin and vitronectin).
For example, Meng *et al.* [144] found that fibronectin induced A549 cell migration and invasion and A549 cells stimulated by fibronectin showed increased phosphorylation of focal adhesion kinase.

In addition, alginates of various forms have attracted much attention due to a wide range of their pharmacological properties, such as hemostatic agents, antiulcer drug and acidity-reducing drug [145]. More importantly, alginates have been observed to inhibit metastasizing of Lewis pulmonary carcinoma and exhibited antimetastatic effect in combination with cyclophosphamide [145]. Fujihara *et al.* [146, 147] also reported that sodium alginate showed a considerable antitumor activity against various murine tumors and revealed that the alginate had the ability to enhance cytostatic and cytolytic activities of macrophages, and thus the antitumor effect may partly be caused by the activation of macrophages. Moreover, another study by Otterlei *et al.* [148] found that alginates

stimulated human monocytes to produce high levels of three cytokines (tumor necrosis factor-alpha, interleukin-6, and interleukin-1) and further demonstrated that the mannuronic acid residues are the active cytokine inducers in alginates. These results suggest that alginate may exhibit antitumor activities to lung cancer and breast cancer. In addition, chitosan has also exhibited toxicity to various types of malignant cells. For instance, Qi *et al.* [149] found that chitosan nanoparticles (CNP) showed high antitumor activities to human hepatocellular carcinoma cells and induced cell necrosis *in vitro*, which was mediated by neutralization of cell surface charge, decrease of mitochondrial membrane potential and induction of lipid peroxidation. Further *in vivo* study in mice treated with chitosan and CNP found typical necrotic morphological changes of tumor tissues but no liver abnormalities. Another study by Lin *et al.* [150] demonstrated that mice fed with a diet containing chitosan had significant fewer aberrant crypt foci (one of the earliest changes seen in the colon that may lead to cancer) formation than those fed with control diet (cellulose). Also, the anti-tumorigenesis effect of water-soluble chitosan oligomer was observed as it significantly suppressed human colon adenocarcinoma cell and human gastric cancer cell proliferation, most probably through the p21/Cip and p27/Kip (cell cycle-related genes) pathways. Moreover, the conjugates of some kinds of anticancer agents with chitosan and its derivatives display good anticancer effects with a decrease in the adverse effects of the original drug due to a predominant distribution into the cancer and a gradual release of free drug from the conjugates in cancer chemotherapy [151]. These results imply the anti-cancer properties of alginate and chitosan and suggest their potential in inhibiting lung cancer and breast cancer cell functions.

Therefore, in this chapter, surface chemical modification was achieved using a LBL self assembly method (alginate or chitosan monolayer) and its influence on cell functions (including proliferation and VEGF secretion) of lung cancer cells, lung healthy cells, breast cancer cells and breast healthy cells were investigated. Furthermore, surface chemistry modification was conducted on both nano-smooth and 23 nm surface featured PLGA surfaces to create a combined effect of surface chemistry and surface topography on cell behavior. The surface chemistry modification altered surface wettability and surface free energy which could be related to observed differences in cell responses. As a result, a strong correlation between surface chemistry and cell responses was demonstrated in this chapter, although PLGA surface topography also played an important role in mediating cell behaviors previously emphasized in Chapter 2 and Chapter 3. Moreover, the mechanism(s) of surface property (surface topography, surface chemistry and surface free energy) mediated cancer cell functions will be reported in Chapter 5.

4.2. Experimental

4.2.1. LBL deposition onto PLGA surfaces

PLGA0 and PLGA23 were prepared according to Fig. 2.1. described in Chapter 2. Then, the PLGA films were soaked in 70% ethanol for 20 mins to sterilize and remove the residual contaminants attached to the material surfaces and were placed into individual wells of sterile 24 well tissue culture plates. All further treatment steps took place within a biological safety cabinet using sterilized solutions. The preparation

conditions for the various LBL deposited substrates are listed in Table 4.1. First, the surfaces were aminolyzed using 1 ml per well of a 20mg/ml solution of polyethylenimine (PEI, Mw ~ 2000 Da, Sigma-Aldrich) in water for 60 mins and rinsed thoroughly with 0.5 M NaCl three times. Sodium alginate (Alg, ACROS) and chitosan (Chi, Mw ~ 100-300 kDa, ACROS) were assembled separately at a concentration of 1 mg/ml in 0.5 M NaCl. The pH value of the Alg and Chi solution was adjusted to 5 by the addition of either 1 M HCl or NaOH and was sterized by filtration (pore size 0.22 μm, Corning). Then, the Alg solution was added to the wells (1 ml/well). After 15 mins, the Alg solution was removed and replaced with 0.5 M NaCl and rinsed for three times, followed by replacement with 1 ml of Chi solution for 15 mins and rinsed again with 0.5 M NaCl for three times. This process produced PLGA substrates with surface monolayers of Alg or Chi.

Table 4.1. Preparation conditions for Alg/Chi chemistry modified PLGA surfaces

Name*	Assembly layers	Layer composition	Surface chemistry
PLGA0	-	-	PLGA
PLGA0/Alg	2	PEI/Alg	Alg
PLGA0/Alg/Chi	3	PEI/Alg/Chi	Chi
PLGA23	-	-	PLGA
PLGA23/Alg	2	PEI/Alg	Alg
PLGA23/Alg/Chi	3	PEI/Alg/Chi	Chi

* PLGA0: PLGA surfaces with nano-smooth features, PLGA0/Alg: PLGA surfaces with nano-smooth features and alginate surface chemistry, PLGA0/Alg/Chi: PLGA surfaces with nano-smooth features and chitosan surface chemistry, PLGA23: PGLA surfaces with 23 nm featured nanopatterns, PLGA23/Alg: PLGA surfaces with 23 nm featured nanopatterns and alginate surface chemistry, PLGA23/Alg/Chi: PLGA surfaces with 23 nm featured nanopatterns and chitosan surface chemistry.

4.2.2. Surface characterization

4.2.2.1. Atomic force microscopy (AFM)

Atomic force microscopy (AFM) images of all the PLGA films created here were obtained in ambient air using AFM-MFP3D (Asylum Research, Santa Babara, CA) and sharp topped cantilevers with a K value, stiffness value, of 0.06 N/M. The AFM operated

in contact mode at a scan rate of 256 lines/scan. Root mean square roughness (R_{rms}) values of various substrates were calculated from the scanning data.

4.2.2.2. Fourier transform infrared (FTIR) spectroscopy

Fourier transform infrared spectroscopy (FTIR) spectra were measured on a Nicolet Nexus 670 FTIR spectrometer equipped with a MCT/A detector and a Smart Aperture Grazing Angle accessory. FTIR spectra were background corrected by subtraction of a spectrum of the clean silicon wafer, and recorded by integrating 300 scans with a resolution of 4 cm^{-1}.

4.2.2.3. Electron spectroscopy for chemical analysis (ESCA)

ESCA was performed on all samples using a Perkin Elmer 5500 Multitechnique Surface Analyzer. An aluminum $K_{\alpha 1,2}$ monochromatized X-ray source was used to stimulate photoemission of the inner shell electrons of the samples. The energy of the electrons was then recorded and analyzed to identify the surface chemistry.

4.2.2.4. Water contact angle measurements

Water contact angles on the various PLGA surfaces of interest to this part of the study were measured through the sessile drop shape method under ambient conditions. For this, a drop of deionized water (3 μL) was placed on the PLGA surfaces and its profile was recorded immediately by a drop shape analyzer (Easy Drop FM40, Kruss). Contact angles were then calculated by computer software (DSA1, Kruss) based on the

recorded profile of the water drop. At least five different spots on each sample were measured for statistical purposes (N=5).

4.2.3. Lung cancer and lung healthy cell assays

4.2.3.1. Lung carcinoma epithelial cell (A549) MTT assay

Lung carcinoma epithelial cell A549 (CCL-185, ATCC) at population numbers less than 7 were used in this study. The method of culturing cells and counting cells for seeding purposes were described in Section 2.2.3.2. For the MTT assay, lung carcinoma cells were seeded onto the PLGA surfaces at a density of 50,000 cells/cm^2. After seeding, the cells were cultured in F-12K medium supplemented with 10% fetal bovine serum (FBS, Hyclone) and 1% penicillin/streptomycin (P/S, Hyclone) under standard cell culture conditions (5% CO_2, humidified air at 37°C). After one day, the viable cell number was determined using a Celltiter 96 Non-radioactive Cell Proliferation Assay (G4100, Promega) that measures the reduction, by living cells only, of MTT. Shortly, after one day, medium was removed from the wells and the cells were washed with PBS twice. Then, all the samples were transferred to new unused 24 well tissue culture plates and 1 ml of fresh growth medium was added to each well. 150 µl of the dye solution (from the cell proliferation assay kit) was added to each well and the plates are incubated at 37°C in a humidified, 5% CO_2 atmosphere. After 4 hrs, 1 ml of the Solubilization Solution/Stop Mix was added to each well and the plates were allowed to stand overnight with a humidified atmosphere to completely solubilize the formazan crystals. Then, contents of the wells were mixed to obtain a uniformly colored solution and the solution was transfered to 96 well plates (215 µl per well). The absorbance at 570 nm was

recorded using a microplate reader (Molecule Devices). The value of the background absorbance at 570 nm without cells run in parallel with the experimental samples was subtracted to yield corrected absorbance. The viable cell number was determined from a standard curve of absorbance versus known concentrations of lung carcinoma epithelial cell solutions run in parallel with the MTT assay. All the experiments were performed in triplicate (n=3) and repeated three times (N=3).

4.2.3.2. Lung carcinoma epithelial cell (A549) VEGF immunoassay

The quantikine human VEGF (vascular endothelial growth factor) immunoassay kit (R&D systems) was used for determining VEGF secretion from cells. The medium for the VEGF measurements were collected after one day of culture for the MTT assay in Section 4.2.3.1. The immunoassay was performed according to the manufacturer's instruction. Briefly, 200 µl standards (prepared from the kit) and sample medium were pipetted into the 96-well plate (from the kit) and incubated for 2 hrs at room temperature. After washing with a binding buffer, an enzyme-linked polyclonal antibody specific for VEGF (from the kit) was added to the wells. Following a wash to remove any unbound antibody-enzyme reagent, a substrate solution (from the kit) was added to the wells and a color developed in proportion to the amount of VEGF bound in the initial step. Color development was stopped and the intensity of the color was measured at 450 nm by a micro plate reader (Molecular Devices). The VEGF concentration was determined from a standard curve of absorbance versus known concentrations of VEGF run in parallel with the experimental samples. The VEGF assay was conducted in triplicate (n=3) and was repeated at least three separate times (N=3).

4.2.3.3. Primary small airway epithelial cell (lung normal cell) MTT assay

Primary small airway normal epithelial cells (PCS-301-010, ATCC) at population numbers less than 5 were also used here. Primary small airway cells were seeded on the various PLGA surfaces at a density of 85,000 cells/cm^2. After seeding, the cells were cultured in airway epithelial cell basal media (PCS-300-030, ATCC) supplemented with small airway epithelial cell growth kit components (PCS-301-040, ATCC) under standard cell culture conditions (5% CO_2, humidified air at 37°C), the same as in Section 2.2.3.1. After one day, the viable cell number was determined using the Celltiter 96 Non-radioactive Cell Proliferation Assay (G4100, Promega), the same as described in Section 4.2.3.1. The viable cell number was determined from a standard curve of absorbance versus known concentrations of live small airway epithelial cell solutions run in parallel with the MTT assay. All the experiments were performed in triplicate (n=3) and repeated three times (N=3).

4.2.4. Breast cancer and breast healthy cell assays

4.2.4.1. Breast adenocarcinoma epithelial cell (MCF-7) MTT assay

Breast adenocarcinoma epithelial cells (HTB-22, ATCC) at population numbers less than 7 were used for MTT assay. Breast cancer cells were seeded on the various PLGA surfaces at a density of 50,000 cells/cm^2. After seeding, the cells were cultured in DMEM supplemented with 10% fetal bovine serum (FBS, Hyclone) and 1% penicillin/streptomycin (P/S, Hyclone) under standard cell culture conditions (5% CO_2, humidified air at 37°C). After one day, the viable cell number was determined using the

Celltiter 96 Non-radioactive Cell Proliferation Assay (G4100, Promega), the same as described in Section 4.2.3.1. The viable cell number was determined from a standard curve of absorbance versus known concentrations of live breast cancer epithelial cell solution run in parallel with the MTT assay. All the experiments were performed in triplicate (n=3) and repeated three times (N=3).

4.2.4.2. Breast carcinoma epithelial cell (MCF-7) VEGF immunoassay

The medium for the VEGF measurements was collected after one day of culture for the MTT assay in Section 4.2.4.1. The quantikine human VEGF immunoassay kit (R&D systems) was used for determining VEGF concentration, the same as described in Section 4.2.3.2. The VEGF assay was conducted in triplicate (n=3) and was repeated at least three separate times (N=3).

4.2.4.3. Breast healthy cell (human mammary epithelial cell) MTT assay

Human mammary epithelial cells (HEMpiC, 7610, ScienceCell) representing healthy breast epithelial cells at population numbers less than 5 were also used in this study. HEMpiC from ScienceCell were isolated from normal human breast tissue. Mammary Epithelial Cell Medium (MEpiCM) consisting of basal medium (ScienceCell, 7611), mammary epithelial cell growth supplement (MEpiCGS, ScienceCell, 7652) and penicillin/streptomycin (P/S, ScienceCell, 0503) was used to culture HEMpiC cells. For the MTT assay, HEMpiC were seeded on the PLGA surfaces at a density of 35,000 cells/cm^2 and were cultured under standard cell culture conditions (5% CO_2, humidified air at 37°C). After three days, the viable cell number was determined using the Celltiter

96 Non-radioactive Cell Proliferation Assay (G4100, Promega), the same as described in Section 4.2.3.1. The viable cell number was determined from a standard curve of absorbance versus known concentrations of live human mammary epithelial cell solutions run in parallel with the MTT assay. All the experiments were performed in triplicate (n=3) and repeated three times (N=3).

4.2.5. Statistical analysis

Statistical results were analyzed using one-way analysis of variance (ANOVA) and the data are expressed as the mean ± standard deviation of the mean.

4.3. Results

4.3.1. Impact of LBL deposition on PLGA surface morphology and chemistry

The chemistry treatments using LBL self assembly monolayers (alginate and chitosan) revealed a significant effect on altering the surface topography of PLGA surfaces as shown in Fig. 4.2. Clearly, after the deposition of LBL monolayers, the nano surface pattern of PLGA23 remained, but a noticeable change in surface topography and surface roughness of PLGA0, PLGA0/Alg and PLGA0/Alg/Chi was revealed. In addition, the results of R_{rms} values also confirmed that there were significant variations in PLGA surface nanotopography (Table 4.2.). The surface roughness increased after the first layer deposition of alginate (R_{rms}(PLGA0/Alg)>R_{rms}(PLGA0), R_{rms}(PLGA23/Alg>R_{rms}(PLGA23)), but the R_{rms} values decreased as the further deposition of a chitosan monolayer. It is possible that the adding of another self assembly

monolayer may partly go into the space created by the first deposition and, thus, decrease surface roughness values. These results revealed that the LBL self assembly treatment changed surface topography and surface roughness at the same time as changing surface chemistry. This is an important point in the study of the effect of surface chemistry on cell behavior, since the impact of surface roughness was not ruled out here but the combined influence of surface roughness and surface chemistry were presented by the LBL self assembly treatment.

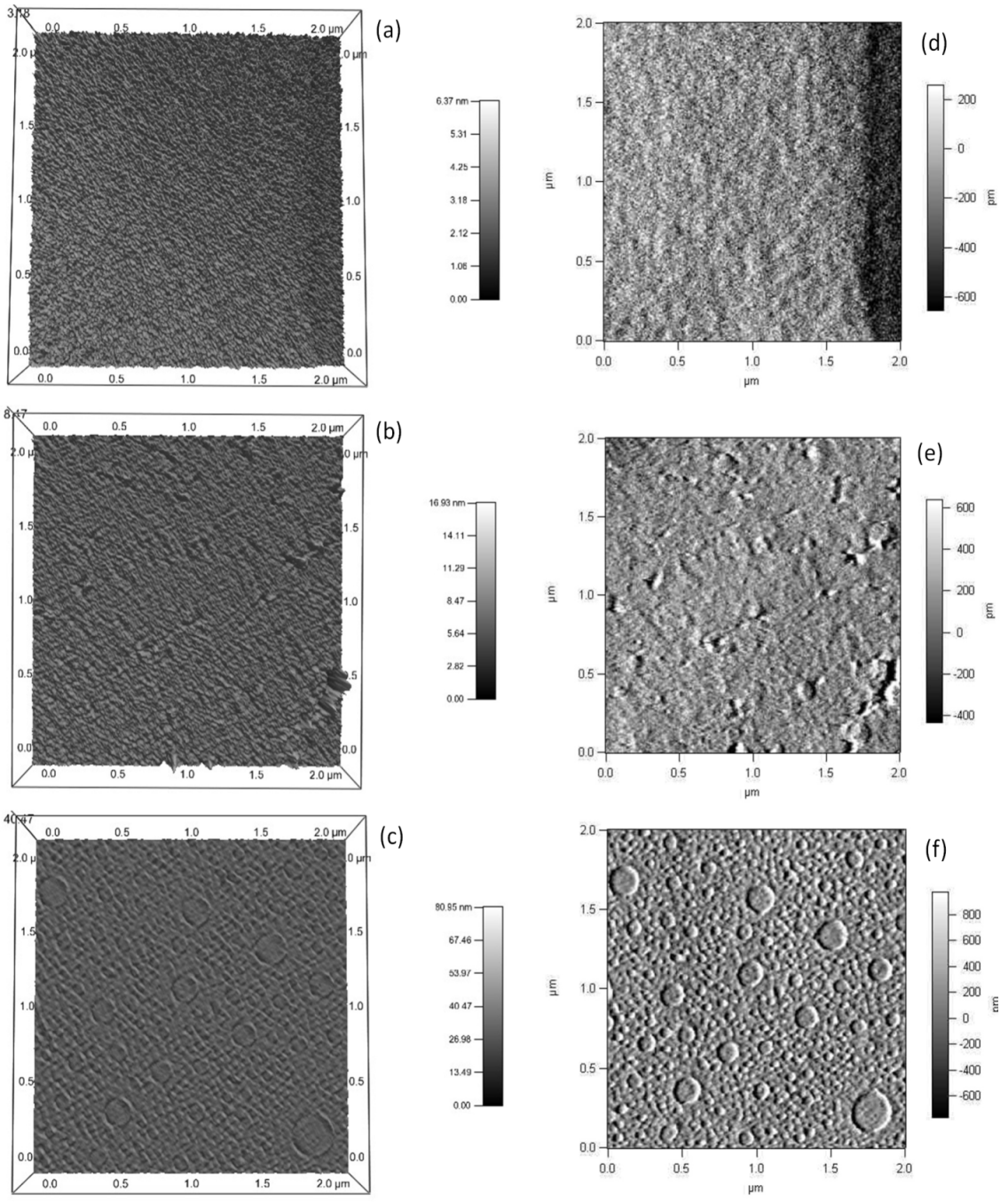

(Continued on next page)

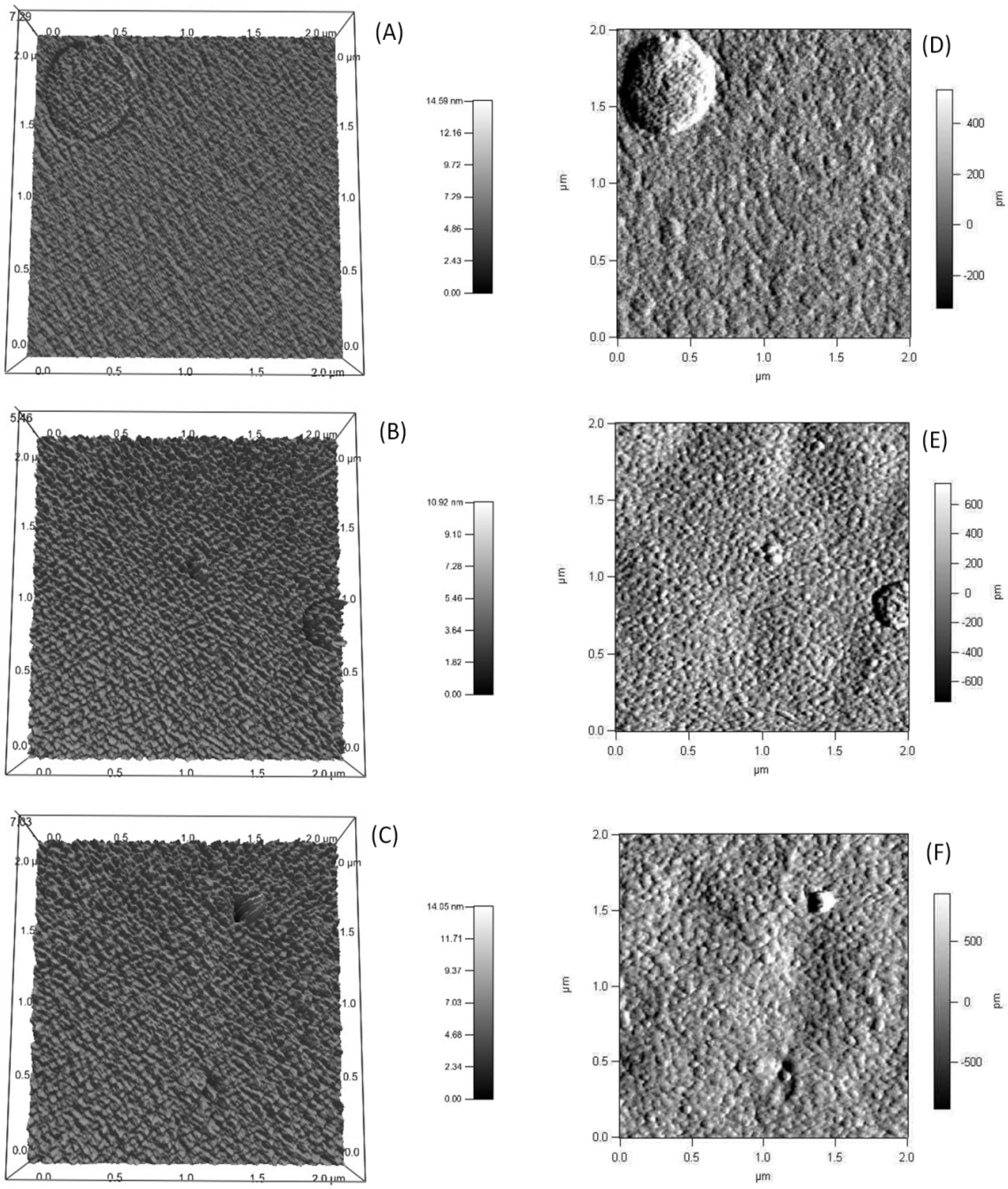

Fig. 4.2. 3D and 2D AFM images of PLGA0 (a and d), PLGA0/Alg (b and e), PLGA0/Alg/Chi (c and f), PLGA23 (A and D), PLGA23/Alg (B and E) and PLGA23/Alg/Chi (C and F).

4.3.2. FTIR spectra

The FTIR spectra for various substrates after deposition of monolayers are shown in Fig. 4.3. For PLGA, the peak at 1775 cm^{-1} was assigned to the PLGA ester -C=O stretching. As the PEI aminolyzed PLGA surface, the peak at 1775 cm^{-1} was observed to lessen in intensity and a second peak at 1630 cm^{-1} appeared, which was a characteristic absorbance peak for the -C=O stretching of amide bonds. In addition, another two new peaks at about 1590 cm^{-1} and 1550 cm^{-1} were observed which were assigned to the primary amine N-H and secondary amine N-H bend in PEI. These results indicated that PLGA surface was activated by PEI through aminolysis. Furthermore, the FTIR spectra of PLGA/PEI/Alg showed characteristic peaks at around 1614 cm^{-1} of alginate from symmetric $-COO^-$ stretching vibrations. In addition, the band at 1520 cm^{-1} from the symmetric $-NH_3^+$ deformation was observed after the deposition of alginate and chitosan. However, after LBL assembly, the bands corresponded to the species $-COO^-$ and $-NH_3^+$ was observed in the FTIR, but their position is retained as the separate species. Thus, FTIR cannot be used directly to identify the interaction of $-COO^-$ with $-NH_3^+$ and the presence of polyelectrolyte complexes.

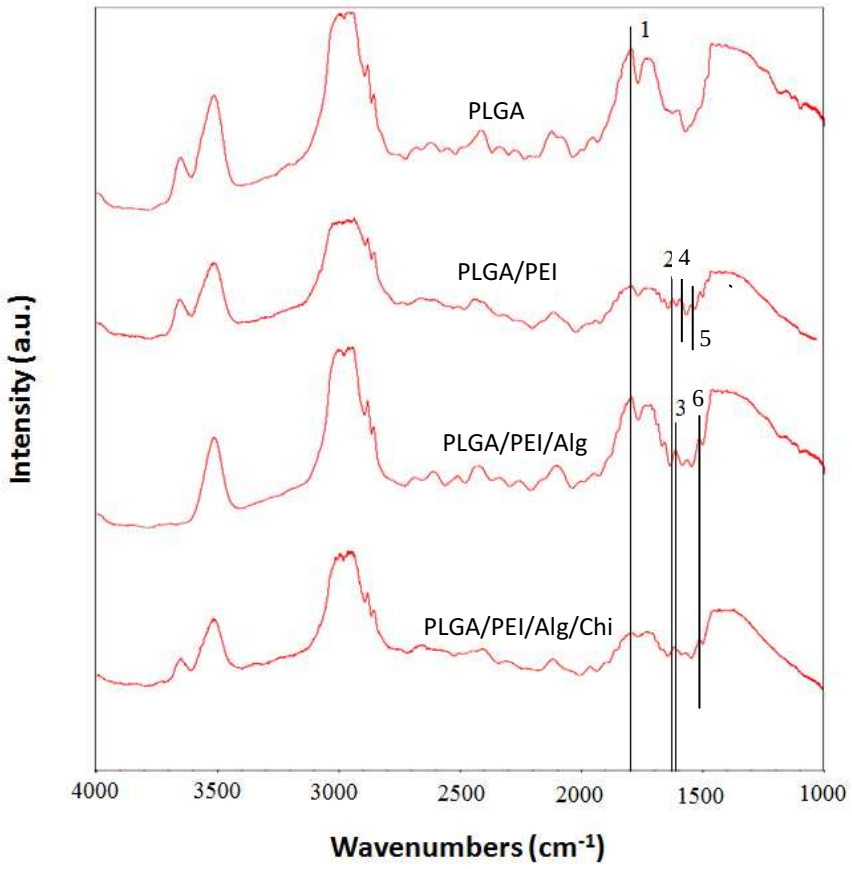

Fig. 4.3. FTIR spectra of PLGA, PLGA/PEI, PLGA/PEI/Alg and PLGA/PEI/Alg/Chi from 1000 to 4000 cm^{-1}. Peak 1, 2, 3, 4, 5 and 6 correspond to 1775 cm^{-1}, 1630 cm^{-1}, 1614 cm^{-1}, 1590 cm^{-1}, 1550 cm^{-1} and 1520 cm^{-1}, respectively.

4.3.3. ESCA spectra

Surface chemistry of the various PLGA films was analyzed by ESCA and the spectra are shown in Fig. 4.4. After the aminolysis of PLGA by PEI, a new element, nitrogen was added to the surface, and, thus, a new peak at ~400 eV corresponded to N1s was observed in the ESCA of PLGA/PEI. After deposition of alginate, a new peak of Na1s was observed, but the nitrogen peak disappeared, indicating that the alginate

(containing Na) monolayer covered the PLGA/PEI surfaces. Furthermore, the deposition of chitosan was confirmed by the N1s peak in the spectra of PLGA/PEI/Alg/Chi since chitosan contains nitrogen. Clearly, ESCA results confirmed the aminolysis of PLGA by PEI and the deposition of alginate and chitosan.

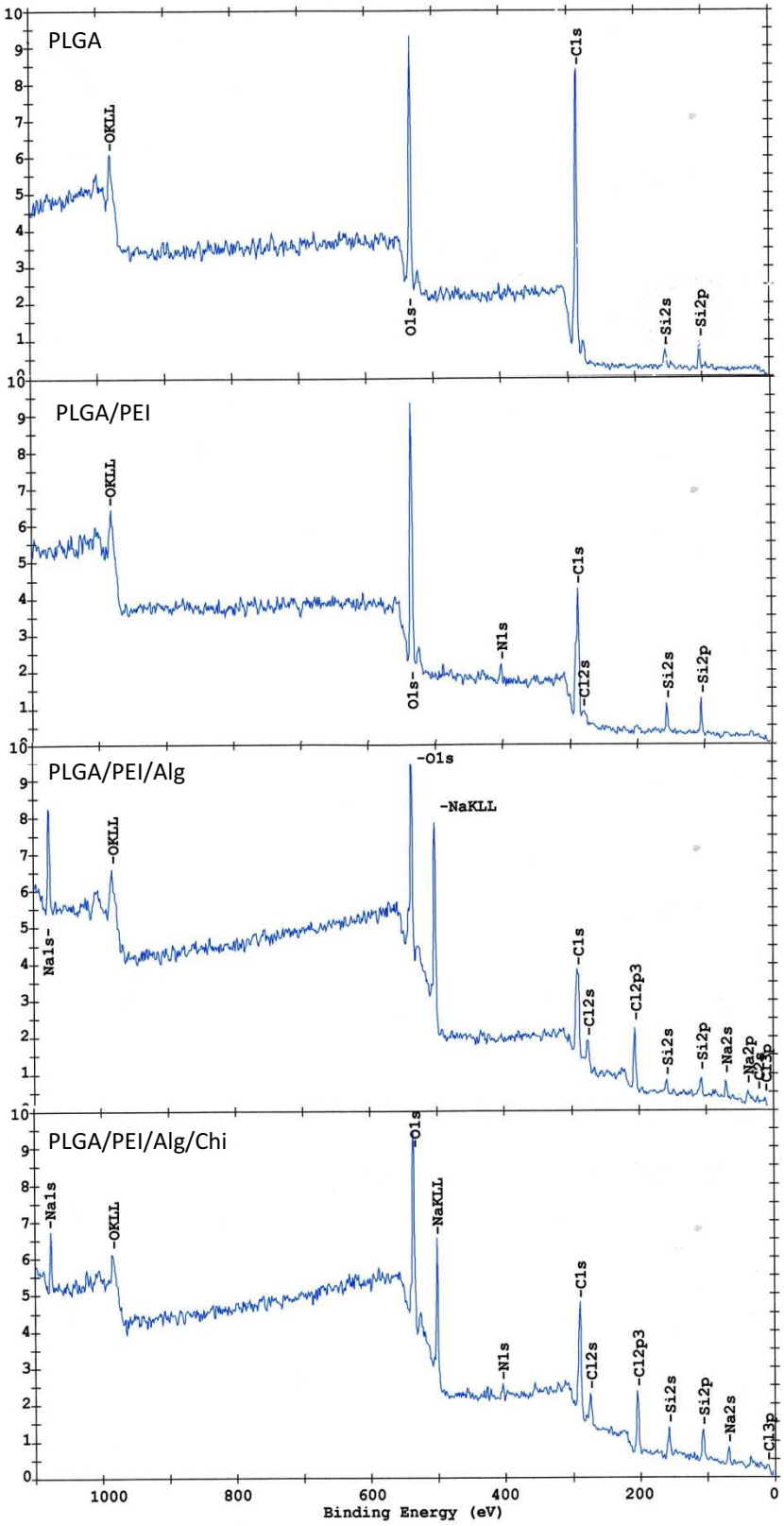

Fig. 4.4. ESCA spectra of PLGA, PLGA/PEI, PLGA/PEI/Alg and PLGA/PEI/Alg/Chi.

4.3.4. Surface wettability of LBL deposited PLGA

Water contact angle measurements are listed in Table 4.2. Surface wettability (i.e., hydrophilic or hydrophobic surfaces) has been traditionally determined by water contact angles (θ) according to the definition of hydrophilic surfaces having a water contact angle (θ) less than 65° by Vogler [152]. Thus, all the PLGA surfaces of present study were hydrophobic according to that definition and the chemistry modification increased the hydrophilicity of PLGA surfaces. Water contact angle results indicated the following trend with hydrophobicity: PLGA0>PLGA0/Alg>PLGA0/Alg/Chi, PLGA23>PLGA23/Alg>PLGA23/Alg/Chi. These two groups of results revealed that the change of surface chemistry had a significant influence on surface wettability and alginate and chitosan made the substrates more hydrophilic. The water contact angle for PLGA0 was higher than that of PLGA23, PLGA0/Alg higher than PLGA23/Alg, and PLGA0/Alg/Chi higher than PLGA23/Alg/Chi. Since PLGA0 and PLGA23 (PLGA0/Alg and PLGA23/Alg, PLGA0/Alg/Chi and PLGA23/Alg/Chi) had the same chemistry, this difference could be attributed to the altered surface topography and surface roughness. With the same surface chemistry, increased roughness on nanopatterned surfaces (PLGA23, PLGA23/Alg and PLGA23/Alg/Chi) demonstrated increased hydrophilicity. The water contact angle of various PLGA substrates was found to have a strong correlation with both surface chemistry and surface topography.

Table 4.2. Surface roughness (R_{rms}), local geometric areas (S_{geo}) (2 µm × 2 µm) and static water contact angles on the various PLGA films

Substrate	R_{rms} (nm)	S_{geo} (μm^2)	Contact angles $\theta(H_2O)$
PLGA0	0.54	4.0	98.1 ± 0.4
PLGA0/Alg	5.38	4.0	90.8 ± 0.9
PLGA0/Alg/Chi	3.31	4.1	87.4 ± 0.6
PLGA23	3.73	4.0	93.8 ± 1.8
PLGA23/Alg	7.41	4.0	76.3 ± 2.2
PLGA23/Alg/Chi	5.01	4.0	68.5 ± 1.4

4.3.5. Lung carcinoma cell (A549) responses

4.3.5.1. Lung carcinoma cell proliferation

Viable lung carcinoma epithelial cell results on the various PLGA surfaces after one-day are shown in Fig 4.5. Compared to the pure uncoated PLGA surfaces, the chemistry modified surfaces with self assembled monolayers of alginate or chitosan had significantly more live lung carcinoma cells. Specifically, after one-day, the total live cell numbers on PLGA0/Alg and PLGA0/Alg/Chi were 35% and 30% significantly higher than that on PLGA0, respectively. Similarly, PLGA23/Alg and PLGA23/Alg/Chi both showed more live cells than PLGA23, 31% and 17% more, respectively. However, no significant difference was observed between PLGA0/Alg and PLGA0/Alg/Chi or between PLGA23/Alg and PLGA23/Alg/Chi. Moreover, on the average, substrates with

nanopatterns (i.e., PLGA23, PLGA23/Alg and PLGA23/Alg/Chi) demonstrated significantly higher viable cell numbers compared to nano-smooth substrates (i.e., PLGA0, PLGA0/Alg and PLGA0/Alg/Chi). Thus, both surface chemistry and surface topography influenced lung cancer cell growth but the competitive interactions of the two factors need to be further investigated.

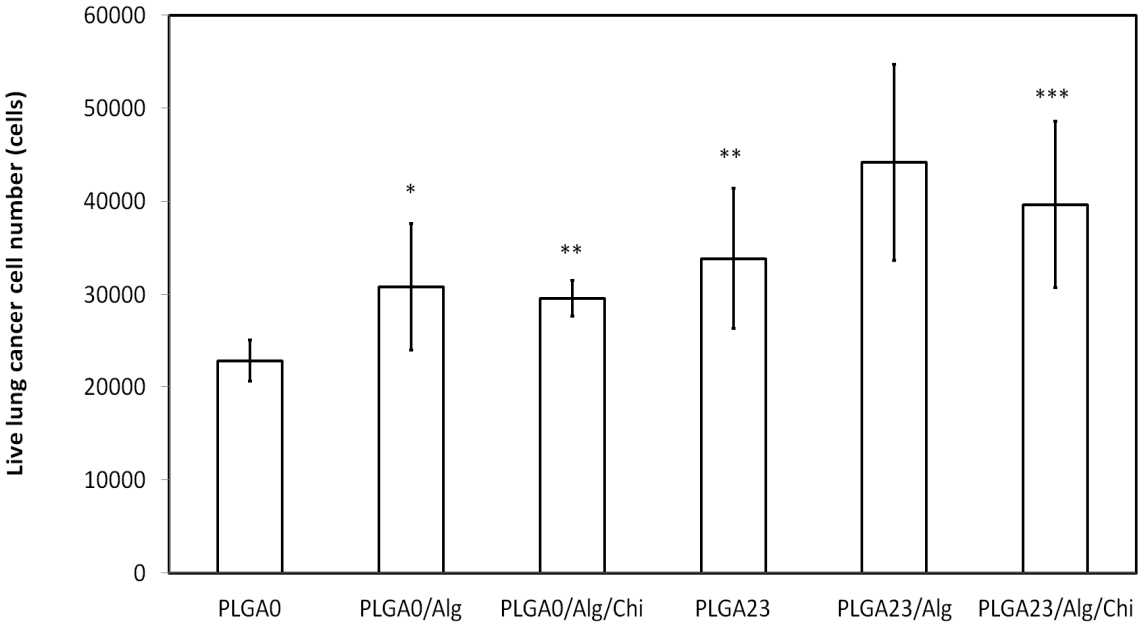

Fig 4.5. One-day total live cell numbers of lung carcinoma epithelial cells cultured on the various PLGA substrates. Data are expressed as the mean ± SEM; N=3. *p<0.01 and **p<0.05 compared to PLGA0; ***p<0.1 compared to PLGA0/Alg/Chi.

4.3.5.2. Lung carcinoma cell VEGF synthesis

Although chemistry (alginate and chitosan) modified PLGA surfaces demonstrated more live lung carcinoma cells than the pure uncoated PLGA surfaces, VEGF secretion by lung carcinoma cells showed an impressive opposite result. Specially, VEGF secretion results after one-day of culturing lung epithelial carcinoma cells on the

various substrates are shown in Fig 4.6. Clearly, alginate modified surfaces showed significantly lower VEGF concentration compared to the unmodified PLGA surfaces. Specifically, on the average, cells on PLGA0/Alg secreted 12% less VEGF than cells on PLGA0. Moreover, cells on PLGA23 secreted 8% less VEGF than PLGA0 and PLGA23/Alg showed 10% lower VEGF concentration compared to PLGA23. Furthermore, cells on PLGA23/Alg exhibited 18% less VEGF secretion compared to PLGA0. These results revealed that cells on alginate modified PLGA surfaces (no matter whether nano-smooth or 23 nm surface nanopattern) secreted less amounts of VEGF, suggesting decreased lung carcinoma cell bioactivity. Moreover, it is safe to conclude that a collective effect of surface nanopattern and chemistry was achieved on PLGA23/Alg to obtain significant decrease in VEGF secretion.

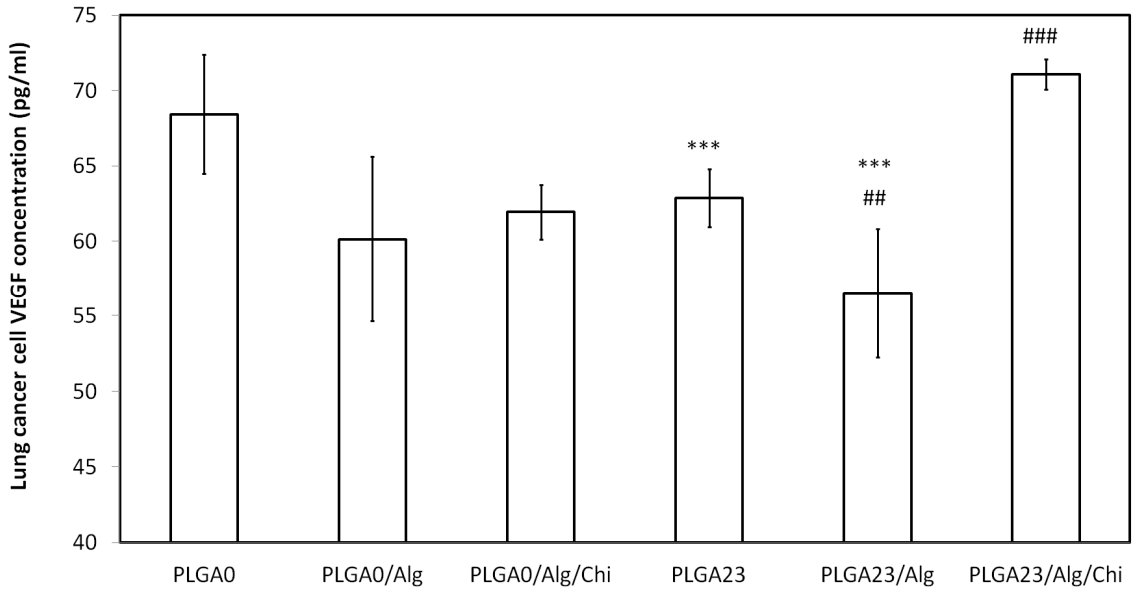

Fig. 4.6. One-day VEGF secretion by lung carcinoma cells cultured on the various PLGA substrates. Data are expressed as the mean ± SEM; N=3. *** $p < 0.1$ compared to PLGA0; ## $p < 0.05$ compared to PLGA23; ### $p < 0.05$ compared to PLGA23, PLGA23/Alg and PLGA0/Alg/Chi.

4.3.6. Lung healthy epithelial cell proliferation

One-day total live cell number results of healthy lung epithelial cells, primary small airway cells, are shown in Fig. 4.7. Interestingly, surface chemistry (no matter whether alginate and chitosan) did not show any statistically significant influence on lung healthy cell proliferation. There was no significant difference between PLGA0, PLGA0/Alg and PLGA0/Alg/Chi. Also, no significant difference was observed between PLGA23, PLGA23/Alg and PLGA23/Alg/Chi. However, on the average, PLGA23 had 33% more viable lung healthy cells than PLGA0, similar to the result in Section 2.3.8 of Chapter 2. Moreover, PLGA23/Alg and PLGA23/Alg/Chi both showed significantly

more viable cells, 37% and 25% than PLGA0/Alg and PLGA0/Alg/Chi, respectively. The results revealed that nanotopography can play a more pronounced role on healthy lung epithelial cell proliferation, whereas the surface chemistries of interest to this study showed no significant influence.

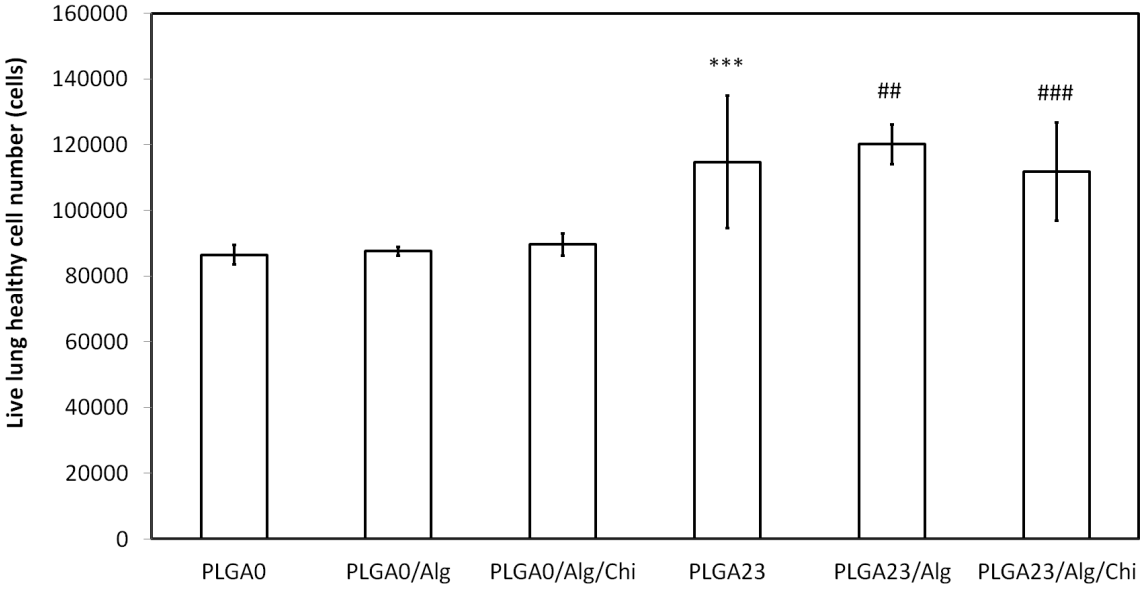

Fig. 4.7. One-day total live cell numbers of primary small airway lung healthy epithelial cells cultured on the various substrates. Data are expressed as the mean ± SEM; N=3. *** $p<0.1$ compared to PLGA0; ## $p<0.05$ compared to PLGA0/Alg; ### $p<0.1$ compared to PLGA0/Alg/Chi.

4.3.7. Breast adenocarcinoma cell (MCF-7) responses

4.3.7.1. Breast adenocarcinoma cell proliferation

One-day measurements of viable breast adenocarcinoma cell numbers were conducted to further investigate the effects of surface chemistry and surface topography on breast cancer cells in addition to lung carcinoma cells. The alginate self assembly monolayer demonstrated a significant influence on breast cancer cell proliferation (Fig.

4.8.). Specifically, PLGA0/Alg had 39% less viable cells than PLGA0, and 31% less than PLGA0/Alg/Chi. Similarly, PLGA23/Alg also showed a significantly lower live cell number compared to PLGA23 and PLGA23/Alg/Chi, 31% and 41% less, respectively. However, there was no statistically significant difference between unmodified and chitosan monolayer modified PLGA surfaces. Furthermore, when comparing various PLGA surfaces with same chemistry but differenct surface patterns, no significant difference was observed between nano-smooth and nanopatterned PLGA surfaces. However, PLGA0/Alg and PLGA23/Alg both showed significantly lower breast cancer cell numbers compared to any other PLGA substrate. Here, breast cancer cells showed a pronounced dependence on surface chemistry as alginate inhibited breast cancer cell proliferation the most.

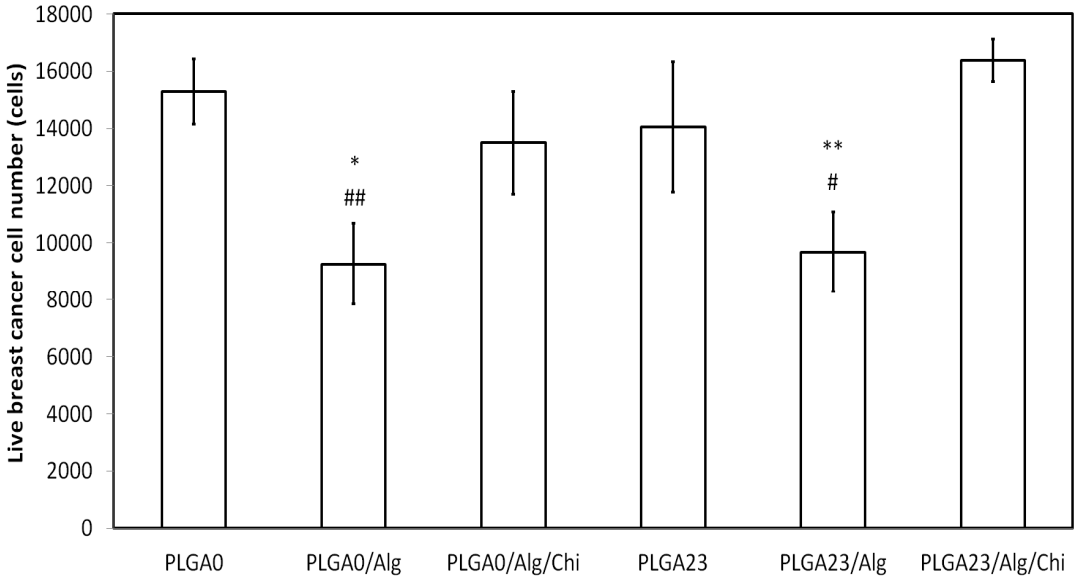

Fig. 4.8. One-day total live cell numbers of breast adenocarcinoma epithelial cells cultured on the various PLGA substrates. Data are expressed as mean ± SEM; N=3. *p<0.01 compared to PLGA0; ## p<0.05 compared to PLGA0/Alg/Chi; **p<0.05 compared to PLGA23; # p<0.01 compared to PLGA23/Alg/Chi.

4.3.7.2. Breast adenocarcinoma cell VEGF synthesis

The total VEGF concentration secreted by breast adenocarcinoma cells after one-day of culturing on the various chemically modified nano-smooth and nanopatterned PLGA surfaces is shown in Fig. 4.9. Similar to the results of breast cancer cell proliferation in Section 4.3.5.1., an alginate self assembled monolayer modified PLGA decreased VEGF secretion from breast cancer cells and thus inhibited the bioactivity of breast cancer cells. Specifically, PLGA0/Alg showed statistically significant 10% and 6% less total VEGF content compared to PLGA0 and PLGA0/Alg/Chi, respectively. Similarly, the cells on the alginate modified 23 nm patterned PLGA surface (PLGA23/Alg) also demonstrated significantly lower VEGF concentrations than PLGA23 and PLGA23/Alg/Chi, 9% and 6% less, respectively. Furthermore, between the substrates with the same chemistry but different topography, on the average, PLGA23, PLGA23/Alg and PLGA23/Alg/Chi showed slightly lower VEGF concentration than PLGA0, PLGA0/Alg and PLGA0/Alg/Chi, although these differences were not statistically significant. Here, surface chemistry and surface topography both affected the VEGF secretion from breast cancer cells, however, surface chemistry played a more significant role than surface topography when both factors were presented.

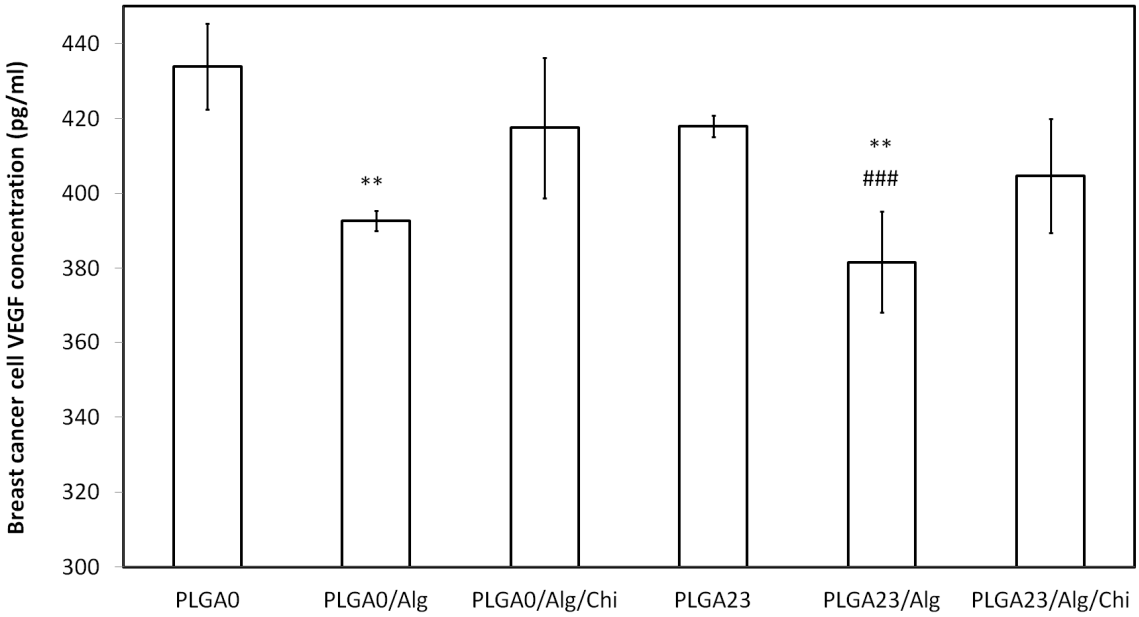

Fig. 4.9. VEGF secreted by breast adenocarcinoma cells (MCF-7) cultured on the various PLGA substrates after one day. Data are expressed as the mean ± SEM; N=3. **$p < 0.05$ compared to PLGA0; ### $p < 0.01$ compared to PLGA23.

4.3.8. Breast healthy cell (HEMpiC) proliferation

Prior results from this study indicated that alginate self assembled monolayer modified PLGA decreased breast adenocarcinoma cell proliferation and VEGF secretion. However, for cancer tissue replacement by healthy tissue, it is also important to investigate the interactions of healthy breast cells with chemistry modified nanopatterned PLGA surfaces. For this, live HEMpiC cell numbers were determined and the results are presented in Fig. 4.10. Comparing the surfaces with the same topography but different surface chemistry, PLGA0/Alg statistically improved 15% viable breast healthy cell number compared to PLGA0/Alg/Chi after one day. However, PLGA23 had significantly (22%) more viable HEMpiC cell numbers compared to PLGA23/Alg after one day.

These results revealed that a chitosan self assembled monolayer decreased healthy breast cell proliferation, and alginate also induced a slight decrease in healthy breast cell proliferation. In addition, comparing PLGA substrates with the same chemistry but different surface topography, no significant difference was observed between nano-smooth and nanopatterned substrates. Similar to breast adenocarcinoma cells, surface chemistry played a significant role on healthy breast cell growth than surface topography.

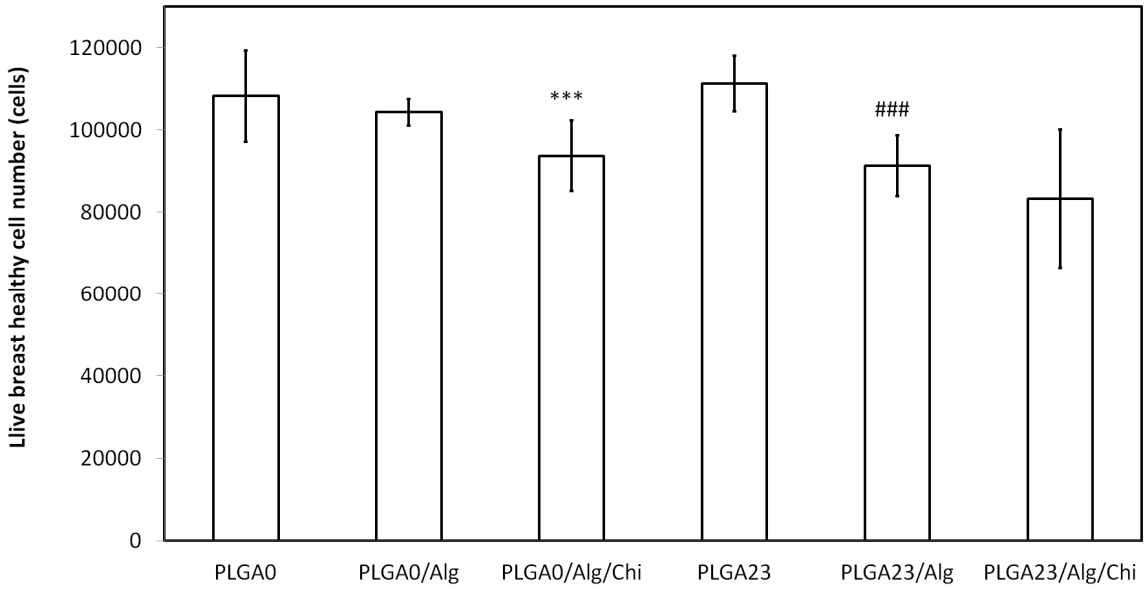

Fig. 4.10. Three-day total live cell numbers of HEMpiC (normal breast epithelial cells) cultured on the various PLGA substrates. Data are expressed as mean ± SEM; N=3. *** $p<0.1$ compared to PLGA0/Alg; ### $p<0.1$ compared to PLGA23.

4.3.9. Nominal VEGF per cell for lung and breast cancer cells

Furthermore, after normalizing VEGF concentration and total live cell numbers on PLGA0, nominal VEGF per cell was obtained on the various substrates as shown in table 2.3. After one-day, lung cancer cells on all the chemically or nanopatterned

modified substrates exhibited low norminal VEGF per cell compared to PLGA0. Moreover, lung cancer cells on PLGA23/Alg had the lowest nominal VEGF per cell and had only 0.43 nominal VEGF per cell compared to nano-smooth PLGA. These results indicated that both the surface nanopattern and chemistry modification decreased lung cancer cell bioactivity, especially lung cancer cells on PLGA23/Alg were significantly less bioactive and secreted much less VEGF. However, further investigation on breast cancer cells indicated that the significant decrease on alginate self assembled substrates resulted from the total decreased breast cancer cell number, but not from the decreased VEGF secretion per cell. Another possible reason is that here only the live cell numbers were used to calculate the nominal VEGF per cell, however the VEGF collected from the culture media may have also included the VEGF secreted by apoptotic or dead cells before their death. In this way, the VEGF concentration was not the real content secreted by the live cancer cells and, thus, the nominal VEGF per cell may have been exaggerated.

Table 4.3. One-day nominal VEGF per cell on the various substrates

Sample	PLGA0	PLGA0/Alg	PLGA0/Alg/Chi	PLGA23	PLGA23/Alg	PLGA23/Alg/Chi
Normalized lung cancer cell VEGF concentration*	1.00	0.88	0.91	0.92	0.83	1.04
Normalized total live lung cancer cell number**	1.00	1.35	1.30	1.48	1.94	1.74
Nominal VEGF per lung cancer cell***	**1.00**	**0.65**	**0.70**	**0.62**	**0.43**	**0.60**
Normalized breast cancer cell VEGF concentration	1.00	0.90	0.96	0.96	0.88	0.93
Normalized total live breast cancer cell number	1.00	0.61	0.88	0.92	0.63	1.07
Nominal VEGF per breast cancer cell	**1.00**	**1.50**	**1.09**	**1.04**	**1.39**	**0.87**

*Normalized VEGF concentration obtained by normalizing all the VEGF concentration on PLGA0/Alg, PLGA0/Alg/Chi, PLGA23, PLGA23/Alg and PLGA23/Alg/Chi to the concentration on PLGA0; **normalized total live cell obtained by normalizing all the total live cell numbers on PLGA0/Alg, PLGA0/Alg/Chi, PLGA23, PLGA23/Alg and PLGA23/Alg/Chi to the total live cell number on PLGA0; ***nominal VEGF per cell obtained by dividing the normalized VEGF concentration by normalized total live cell number.

4.4. Discussion

4.4.1. Surface chemical modification of PLGA substrates by LBL deposition

LBL deposition of alginate and chitosan has been demonstrated as a facile and versatile technique for the chemical modification of a wide range of surfaces [143, 153]. Moreover, alginate and chitosan have been demonstrated to be biocompatible, biodegradable, antifouling and antitumor, thus, could be ideal candidates for the chemical modification of biomaterial surfaces. As demonstrated in this study, LBL deposition of alginate and chitosan on nano-smooth and nanopatterned PLGA surfaces has effectively altered surface chemistry, surface wettability and surface topography. The deposition of alginate induced an increase in surface roughness values on both nano-smooth and nanopatterned PLGA. However, the further deposition of chitosan produced less roughened surfaces. Moreover, the results here indicated that the LBL depositon treatment using alginate and chitosan could readily alter PLGA surface wettability. The deposition of alginate and chitosan monolayers decreased the hydrophobicity of PLGA which was expected since both alginate and chitosan are hydrophilic. This result agrees with the analysis of surface chemistry on the various substrates (from FTIR), that polar groups of –OH, $–COO^-$ and $–NH_2$ were more hydrophilic and rendered the surface less hydrophobic.

4.4.2. The effects of LBL deposition on lung cancer and healthy cell functions

In the present study, variable surface chemistry, surface wettability and surface topography were obtained by LBL deposition of alginate and chitosan on nano-smooth

and nanopatterned PLGA surfaces, and moreover, the influence of these surface properties on lung carcinoma cell behaviors was evaluated. One-day cell proliferation results indicated that more lung cancer cells grew on alginate and chitosan deposited PLGA surfaces. The increase could be attributed to the increased hydrophilicity of alginate and chitosan surfaces, considering that more hydrophilic surfaces may lead to better cell spreading and promote cell proliferation. In addition, LBL deposition altered surface roughness and surface charge, thus, the increased lung carcinoma cell proliferation on alginate and chitosan deposited substrates can be the result of the collective influence of various properties.

Another important significant finding of this study was that an alginate deposited surface largely decreased the ability of lung carcinoma cells secreting VEGF. No matter whether nano-smooth and nanopatterned PLGA surfaces, alginate deposited surfaces had significantly lower VEGF concentration which strongly suggested anti-cancer properties of alginate. Moreover, PLGA23/Alg demonstrated a larger decrease of VEGF from PLGA0 compared to both PLGA0/Alg and PLGA23, suggesting that surface chemistry and surface nanotopography both had a remarkable influence on VEGF secretion of lung carcinoma cells. Further investigations on the nominal VEGF per cell revealed that this decrease can be attributed to the significantly decreased lung cancer cell bioactivity on PLGA23/Alg which provided a negative impact on lung cancer cell growth.

In addition, lung healthy cell responses on various PLGA surfaces were also investigated here and interestingly, noticeable different results were observed. After one-day of culture, PLGA23, PLGA23/Alg and PLGA23/Alg/Chi all showed significantly higher viable cell numbers compared to PLGA0, PLGA0/Alg and PLGA0/Alg/Chi, no

matter the surface chemistry. Obviously, more rough surfaces increased lung healthy cell proliferation. However, as the surface roughness and surface chemistry altered, similar live cell numbers were observed among PLGA0, PLGA0/Alg and PLGA0/Alg/Chi (also PLGA23, PLGA23/Alg and PLGA23/Alg/Chi), suggesting that alginate and chitosan may have the ability to decrease lung healthy cell proliferation. Thus, two opposite influences of surface roughness and surface chemistry interacted together to determine cell growth. Here, it was further confirmed than nanotopography can have positive influences on lung healthy cell behaviors.

4.4.3. The effects of LBL deposition on breast cancer and healthy cell functions

Importantly, in addition to lung cancer and lung healthy cell responses, breast cancer and breast healthy cell behaviors on the various LBL deposited surfaces were also reported. In some aspects, the breast cells demonstrated a different correlation with various surface properties compared to lung cells. One-day cell proliferation results indicated that alginate deposited PLGA surfaces, no matter surface roughness, inhibited breast cancer cell proliferation, resulting in significantly lower viable cell numbers than pure PLGA and chitosan-terminated PLGA. Alginate has been reported to have anti-tumor effect depending on the composition of the homopolymer of l,4-linked β-D-mannuronic acid (MM-block) and α-L-guluronic acid (GG-block) in alginates, i.e., alginates with a higher content of MM-block exhibited higher antitumor activity than those with a lower content and a high MM-block content may be required for the development of the antitumor activity of the polymer [147]. However, the anti-cancer properties of alginate to lung cancer and breast cancer haven’t been widely investigated

and reported. In the present study, the negatively charged alginate substrates inhibited VEGF secretion of both lung and breast cancer cells, suggesting that alginate may be a potential candidate as surface coating or modification on anti-cancer biomaterials. The secretion of VEGF by lung cancer and breast cancer cells has been effectively inhibited by alginate, especially when surface nanopatterns were present. On the average, both lung cancer and breast cancer cells on PLGA23/Alg demonstrated lower VEGF concentrations compared to PLGA0/Alg. Therefore, it is safe to conclude that the collective effect of nanopatterns and surface chemistry has been achieved on PLGA23/Alg, which allows for the complete control of PLGA surface properties to achieve specific purposes of directing cancer cell functions. Overall, PLGA23/Alg was recognized as the best candidate of anti-cancer cell-biomaterial interface to both lung cancer and breast cancer.

Moreover, breast healthy cell proliferation on various PLGA surfaces was investigated and unfortunately, the alginate and chitosan both inhibited breast healthy cell growth. However, although PLGA23 enhanced breast healthy cell proliferation as described in Chapter 3, the positive effect of 23 nm featured surface topographies was not observed here. PLGA23/Alg and PLGA23/Alg/Chi did not show higher live breast healthy cell numbers compared to PLGA0/Alg and PLGA0/Alg/Chi. This result suggested that the nanopattern effect may have been masked by surface chemistry and breast healthy cells did not successfully sense the nanopatterns underlying the self assembly monolayer. Therefore, further studies need to be conducted to create the effective combination of surface chemistry and surface topography to positively influence breast healthy cell functions.

4.5. Conclusions

In this chapter, LBL deposition of alginate and chitosan was used to modify surface chemistry and surface roughness of nano-smooth and nanopatterned PLGA surfaces. Results indicated that the LBL self assembly effectively altered PLGA surface chemistry, surface topography and decreased the hydrophobicity of PLGA surfaces. Alginate deposited PLGA surfaces exhibited anti-cancer properties, significantly decreasing lung cancer cell and breast cancer cell VEGF synthesis. Furthermore, alginate modified PLGA inhibited breast cancer cell proliferation, whereas it showed no significant influence on lung carcinoma cell proliferation. However, breast healthy cell demonstrated a strong correlation to surface topography, and the 23 nm surface featured PLGA surfaces (no matter what surface chemistry) promoted lung healthy cell proliferation. The results of this part of the dissertation provided important information of cell responses mediated by surface chemistry in addition to surface topography and an effective surface chemistry (alginate self assembly monolayer) was discovered to inhibit cancer cell VEGF secretion. It is believed that surface chemistry and surface topography could be effectively combined to generate expected influences on various cell lines of value for healthy tissue replacement of cancerous tissue.

Chapter 5 The Correlation of PLGA Nanometer Surface Properties with Lung and Breast Cell Functions

5.0. Preface

In the last three chapters, the impact of PLGA nanotopographies on lung healthy and carcinoma and breast healthy and adenocarcinoma cell functions (such as adhesion, proliferation, apoptosis, morphology and VEGF secretion) was systematically studied. The results over all the time periods tested revealed that cancer cells can recognize and respond differently to nanotopographies compared to flat topographies, as different cell lines showed dramatically different cell behaviors on the same PLGA nanotopography. Similarly, the role of nanoscale topography in controlling various cell functions has been observed in an increasing number of studies on other cell lines [43, 52, 154-156]. However, the relevant mechanism(s) behind these cell behaviors on nanostructured material surfaces has not been well understood especially for lung and breast cancer cells. This study was designed to do just that as it created various PLGA surfaces either with i) different topographies but the same chemistry or ii) different chemistry but the same topography. Specifically, in the present chapter, the correlation of material surface properties (including surface topography, surface chemistry, surface wettability, surface

charge, and surface free energy) with cell functions were systematically investigated. First, various PLGA surfaces were characterized by AFM to investigate surface nanotopographies and surface area quantitatively in an effort towards understanding how surface properties affect various cell functions. Second, PLGA surface wettability and surface free energy were examined in order to correlate how surface wettability and surface free energy are related to initial protein adsorption that controls cell responses. Lastly, ELISA experiments were performed to quantify the adsorption of two important proteins (fibronectin and vitronectin) involved in cell adhesion and subsequent cell functions. In summary, this part of the thesis will report on nanotopography-mediated cancer and healthy cell functions in relationship to surface properties and protein adsorption, depicting some possible clues behind topography-mediated cell functions.

5.1. Introduction

Great attention has been paid to exploring the cell-material interface in biomaterial science, as many studies have revealed that the physiochemical properties of an implant has a large impact on regulating cell behavior and functions [129, 157-159]. In particular, many studies have shown the effects of substrate topography or roughness [54, 55, 160], surface chemistry [161], surface charge [162], and surface free energy [161] on cell morphology, adhesion, migration, proliferation, and gene expression. Here, the present studies have demonstrated that nanotopographies (as small as 23 nm) inhibited both lung cancer and breast cancer cell functions and enhanced lung healthy and breast healthy cell proliferation. Also, changing roughness is easier and is more likely to be cleared by the FDA faster than changing chemistry. Therefore, topography is of specific

interest because of the great potential in the application of ideal anticancer implants. However, the effect of nanoscale topography on cancer and normal cell functions has not been throughly understood to date. Especially, the infinite number of potential combinations of cell types, biomaterial compositions, and topographical patterns have increased the difficulty in extricating the precise interaction mechanisms between implants and cell responses [163]. For example, in addition to the myriad of different topographical cues intentionally presented to cells, all materials contain topographies. In addition, the functional, behavioral, and morphological differences between cell types imply that distinct cell types may respond differently to topographical cues [164].

A possible mechanism suggests that substrate nanotopographical discontinuities lead to preferential protein adsorption, and subsequent protein patterning [163]. Patterned protein deposition has been observed on substrates modified to have topographical cues and such proteins were found to be effective in patterning cells [165-167]. Particularly, in this study, the 23 nm PLGA surface topography has patterns on a similar size scale as proteins, which could have an important effect on directing protein deposition due to the suitable “dock-in” sites. Morever, protein adsorption and subsequent bioactivity are highly related to cell responses including adhesion, proliferation, morphology, and apoptosis. For example, it was observed that avidin adsorption on polystyrene increased with surface roughness on nanometer-size topographical patterns most likely caused by the increase of the effective surface area [136]. Another study revealed that significantly greater quantity of vitronectin adsorbed on nanophase ceramics compared to convetional ceramics, which, subsequently, may have contributed to the observed enhanced adhesion of osteoblasts [168]. Similarly, it was also found that more fibronectin (a protein which

promotes osteoblast adhesion) adsorption occurred on RNT (rosette nanotubes) coated hydrogels than uncoated hydrogels and osteoblast adhesion and proliferation were subsequently greatly enhanced on RNT coated biomimetic nanoscale hydrogels [169]. In this study, PLGA surface properties (including surface topography or roughness, surface chemistry, surface charge, and surface energy) were changed systematically by creating different nano size surface features and subsequent protein adsorption may hace been greatly affected. Therefore, studying the amount of protein adsorbed on nanotopographies could be an important clue to uncover the mechanisms of the novel topography-mediated cell responses observed here.

In addition, it is claimed that if the topographical effect was assessed using substrates of same chemistry, the process of cell sensing and adapting to topographies (such as focal adhesions, protein secretion, gene expression, cell-matrix signal pathways, etc.) may play an important role in determining cell fates [1]. Especially, isotropic nanotopographies could direct more cell functions with relatively less dramatic changes in cell shape. Specifically, it was found that a separation of ≥ 73 nm between cell adhesive gold nanodots coated with cyclic RGDfK peptide resulted in limited MC3T3-osteoblast attachment and spreading, and dramatically reduces the formation of focal adhesion and actin stress fibers [4]. Another study by Matthew *et al.* [77] indicated that 13 nm high islands increased fibroblast functions compared to planar surfaces through the gene up-regulation, notably in the areas of cell signaling, proliferation, cytoskeleton, and production of extracellular matrix proteins. Also, it has been proposed that the cell nucleus can turn the mechanical cues arising from nano topographically induced morphological changes into gene changes [170]. Moreover, during the cell sensing and

adaptation process, a topographical pattern determines what cell functions are regulated and the scale affects the degree to which that function is regulated.

With this in mind, studies presented in this chapter were designed to explore the correlation between the various surface properties and cell behaviors. Specifically, the impacts and correlation of surface topography and surface chemistry on cell functions were investigated. Moreover, the surface free energy of various substrates was calculated and its influence on cell functions was evaluated. Lastly, the adsorption of cell adhesion proteins (fibronectin and vitronectin) was measured and a strong relation between protein adsorption and cell responses was built.

5.2. Experimental

5.2.1. Fabrication of nanometer surface and LBL deposited nanometer surface PLGA films

PLGA surfaces with various topographies were fabricated following the same method described in Section 2.2.1. LBL deposited nanometer surface PLGA substrates were created using the method described in Section 4.2.1.

5.2.2. Atomic force microscopy

Atomic force microscopy (AFM) images of all the PLGA films created here were obtained in ambient air using AFM-MFP3D (Asylum Research, Santa Babara, CA) and sharp topped cantilevers with a K value, stiffness value, of 0.06 N/M. The AFM operated in contact mode at a scan rate of 256 lines/scan. The scan areas were 2 μm × 2 μm, 5 μm

× 5 μm, and 10 μm × 10 μm for each substrate. An image processing software of IGOR Pro 6.21 was used to analyze the results. For the analysis of topographical parameters, root mean square roughness R_{rms} and local geometric area (A_{geo}) were obtained for all the samples using images with scan area of 10 μm × 10 μm.

5.2.3. Determination of surface wettability and surface free energy

Contact angles on various nanopatterned and LBL deposited nanopatterned PLGA surfaces (PLGA0, LGA23, PLGA300 and PLGA400; PLGA0, PLGA0/Alg, PLGA0/Alg/Chi, PLGA23, PLGA23/Alg and PLGA23/Alg/Chi) were measured through the sessile drop shape method under ambient conditions. Contact angles of three different liquids (deionized water, glycerol and formamide) were measured (see Table 5.1). 3 μL of the test liquid was dropped onto the substrate and the liquid drop was photographed and analyzed by a drop shape analyzer (Easy Drop FM40, Kruss, Germany). Contact angles on at least three different regions on each sample were measured and averaged.

Owens-Wendt method was used to calculate surface free energy of nano-smooth and nanopatterned samples utilizing the results of the contact angle measurements [171]. Briefly, the contact angles of two measuring liquids would yield two equations in the form of Eqn. 5.1, with different values of the constant coefficients. Therefore, two linear equations are obtained in the following form and used to calculate the surface free energy of the various substrates:

$$\gamma_{SL}=(1+\cos\theta)\,\gamma_L=2\,(\gamma_S^{d}\,\gamma_L^{d})^{1/2}+2\,(\gamma_S^{p}\,\gamma_L^{p})^{1/2} \qquad \text{(Eqn. 5.1)}$$

where γ_{SL} is the solid-liquid interfacial energy, θ is the contact angle between the solid and the measuring liquid; γ_L, γ_L^{d} and γ_L^{p} are the total, dispersive component and polar

component of the liquid surface tension, respectively, which are listed in Table 5.1; γ_S^d and γ_S^p are the dispersive and polar components of solid surface tension. It is assumed that the equalities $\gamma_S = \gamma_S^d + \gamma_S^p$ and $\gamma_L = \gamma_L^d + \gamma_L^p$ are valid while using Eqn. 5.1; that is, the total surface free energy of a sample is obtained by adding up the dispersive and polar components of the surfaces [172].

Table 5.1. Liquids and their values of the surface tension (γ_L, mN/m) at 20 °C used for contact angle and surface free energy measurements. γ_L^d and γ_L^p are the dispersive and polar components of γ_L, respectively (adapted from [172])

Liquid	Specifications	γ_L (mN/m)	γ_L^d (mN/m)	γ_L^p (mN/m)
Deionized water	Milipore systems	72.8	21.8	51
Glycerol	Sigma-Aldrich, >99%	64	34	30
Formamide	Fisher, ≥ 99.5%	58	39	19

5.2.4. Fibronectin and vitronectin adsorption

Adsorption of the cell adhesive protein fibronectin and vitronectin on the various PLGA surfaces (PLGA0, PLGA23, PLGA300, and PLGA400; PLGA0, PLGA0/Alg, PLGA0/Alg/Chi, PLGA23, PLGA23/Alg, and PLGA23/Alg/Chi) was measured by an enzyme-linked immunosorbent assay (ELISA). For this, all the PLGA substrates were soaked in DMEM supplemented with 10% FBS and 1% P/S (without cells) under standard cell culture conditions (5% CO_2, humidified air at 37°C) for 24 hrs. The PLGA substrates soaked in DMEM without FBS and P/S were used as background controls.

After 24 hrs, non-specific fibronectin and vitronectin adsorption on the substrates was removed by rinsing in phosphate buffered solution (PBS) and blocked by soaking in 2% bovine serum albumin (BSA, Sigma-Aldrich) for 1 hr. The absorbed fibronectin was then bound to a primary rabbit anti-bovine fibronectin antibody (Chemicon, AB2047) for 1 hr and the absorbed vitronectin bound to a primary rabbit anti-human vitronectin polyclonal antibody (Chemicon, AB19014) for 1 hr. The samples were further incubated with a secondary goat anti-rabbit antibody conjugated with horseradish peroxidase (Bio-Rad, 170-6515) for 1 h. After washing with 0.05% Tween 20 (Sigma-Aldrich), the amount of fibronectin and vitronectin absorption on various PLGA samples was measured with an ABTS kit (Vector Laboratories, SK-4500). The secondary antibody binding was detected using a microplate spectrophotometer at 405 nm (SpectraMax340PC, Molecular Devices). Experiments were run in duplicate (n=2) at three different times (N=3).

5.3. Results

5.3.1. Surface topography and surface roughness of various PLGA films

AFM images of the different surface topographies of nanopatterned PLGA surfaces are shown in Fig. 5.1. For PLGA0, PLGA23, PLGA300 and PLGA400, pattern sizes corresponded to the diameters of the PS beads used and PLGA23 showed pattern sizes less than 100 nm. Topographical results obtained from AFM confirmed the evolution of surface pattern sizes increasing with the diameters of the PS beads. Quantitative roughness values (R_{rms}) and real geometric surface areas of the nanopatterned PLGA surfaces are listed in Table 5.2. Specifically, PLGA0 had a much

smaller R_{rms} value than PLGA23, PLGA300 and PLGA400, but PLGA0 still had some nano scale roughness and, thus, was called nano-smooth PLGA surface in this thesis. In addition, as the pattern sizes increased from the 23 nm to 300 nm and 400 nm, the surface roughness values (R_{rms}) increased from 3.73 nm to 10.78 nm and 24.11 nm. Although the diameters of the patterns increased largely from nano scale (23 nm) to submicro scale (300 nm and 400 nm), the relatively small change of roughness values (R_{rms}) could be attributed to the very slight alteration in vertical heights of the patterns when the horizontal diameters of the patterns were greatly changed. The surface geometric area values also showed that PLGA0, PLGA23, PLGA300 and PLGA400 had very similar surface area values (100 μm^2, 100.1 μm^2, 100.6 μm^2 and 102.3 μm^2) and further confirmed the very small alteration of vertical heights of the patterns when using largely different diameters of PS beads.

For the LBL deposited PLGA surfaces, the nanopattern remained on PLGA23/Alg and PLGA23/Alg/Chi, but the deposition of alginate and chitosan monolayers changed the surface roughness of PLGA0 and PLGA23. Specifically, the deposition of the alginate monolayer largely increased the surface roughness values of PLGA0 and PLGA23. However, the further deposition of the chitosan monolayer slightly decreased the surface roughness values. Thus, the surface roughness measurement revealed the following trend as: PLGA0<PLGA0/Alg/Chi<PLGA0/Alg and PLGA23<PLGA23/Alg/Chi<PLGA23/Alg. As expected, the deposition of alginate and chitosan monolayers altered the surface roughness at the same time as they changed surface chemistry. For PLGA0, the LBL deposition of alginate on the nano-smooth PLGA surface increased the surface roughness from 0.54 nm to 5.38 nm, but the

deposition of another monolayer of chitosan decreased the surface roughness to 3.31 nm. For PLGA23, although the LBL deposition changed the surface roughness values from 3.73 nm for PLGA23 to 7.41 nm and 5.01 nm for PLGA23/Alg and PLGA23/Alg/Chi, the tightly arrayed surface pattern was still observed from the AFM images of PLGA23/Alg and PLGA23/Alg/Chi. Again, the surface area values of the LBL deposited PLGA and non-modified PLGA were very similar, but a slight decrease was demonstrated from PLGA0/Alg to PLGA0/Alg/Chi, from PLGA23/Alg to PGA23/Alg/Chi. This result also agreed with the fact that the deposition of another monolayer of chitosan decreased the surface roughness of PLGA0/Alg and PLGA23/Alg. In this study, the deposition of the alginate and chitosan monolayer not only changed the surface chemistry, but it also altered the surface roughness.

Table 5.2. Surface roughness (R_{rms}) and local geometric area (S_{geo}) of all the samples measured by AFM (10×10 μm^2 scan area)

Sample	R_{rms} (nm)	S_{geo} (μm^2)
PLGA0	0.54	100.0
PLGA23	3.73	100.1
PLGA300	10.78	100.6
PLGA400	24.11	102.3
PLGA0/Alg	5.38	100.3
PLGA0/Alg/Chi	3.31	100.1
PLGA23/Alg	7.41	100.3
PLGA23/Alg/Chi	5.01	100.2

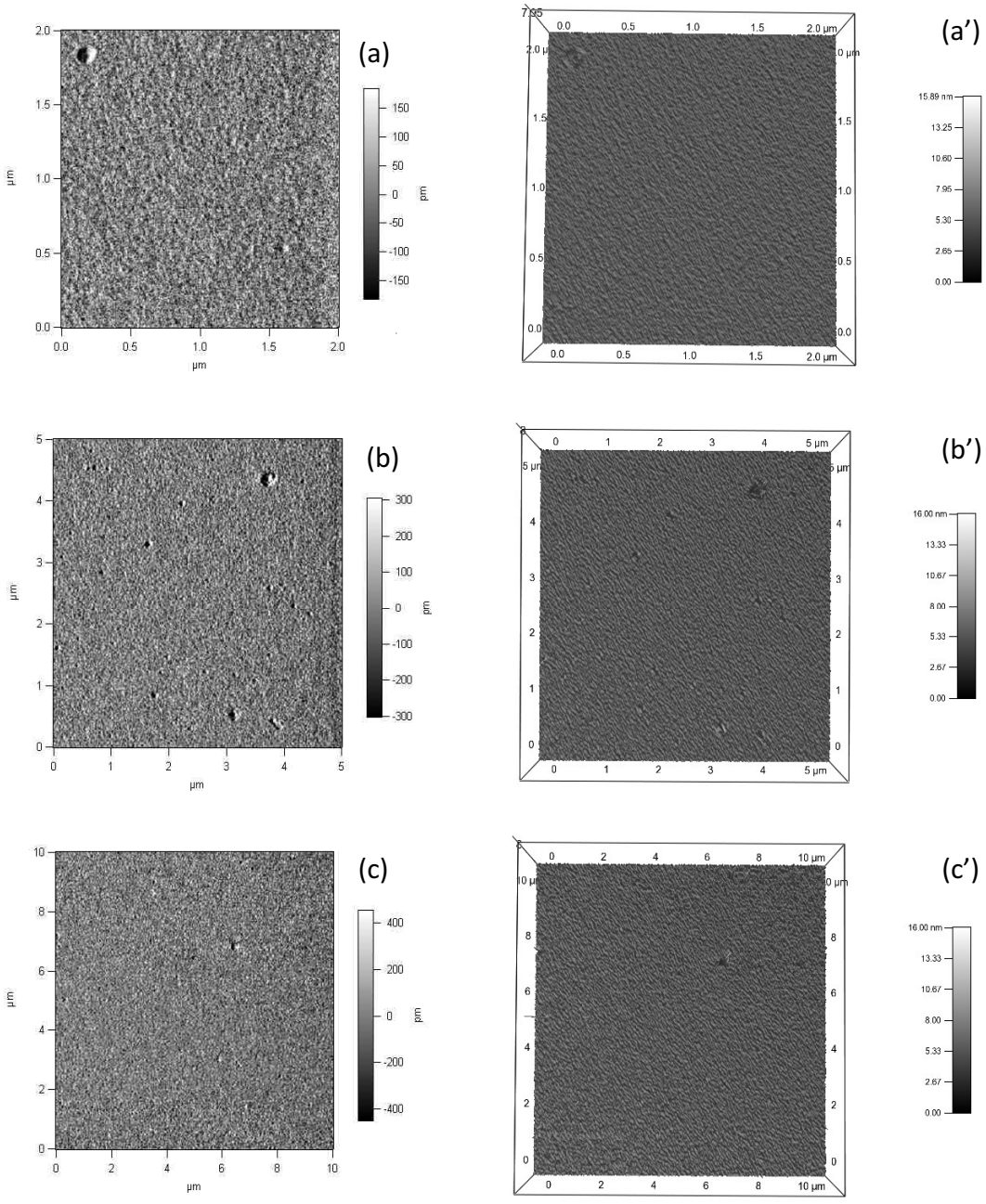

(Continued on next page)

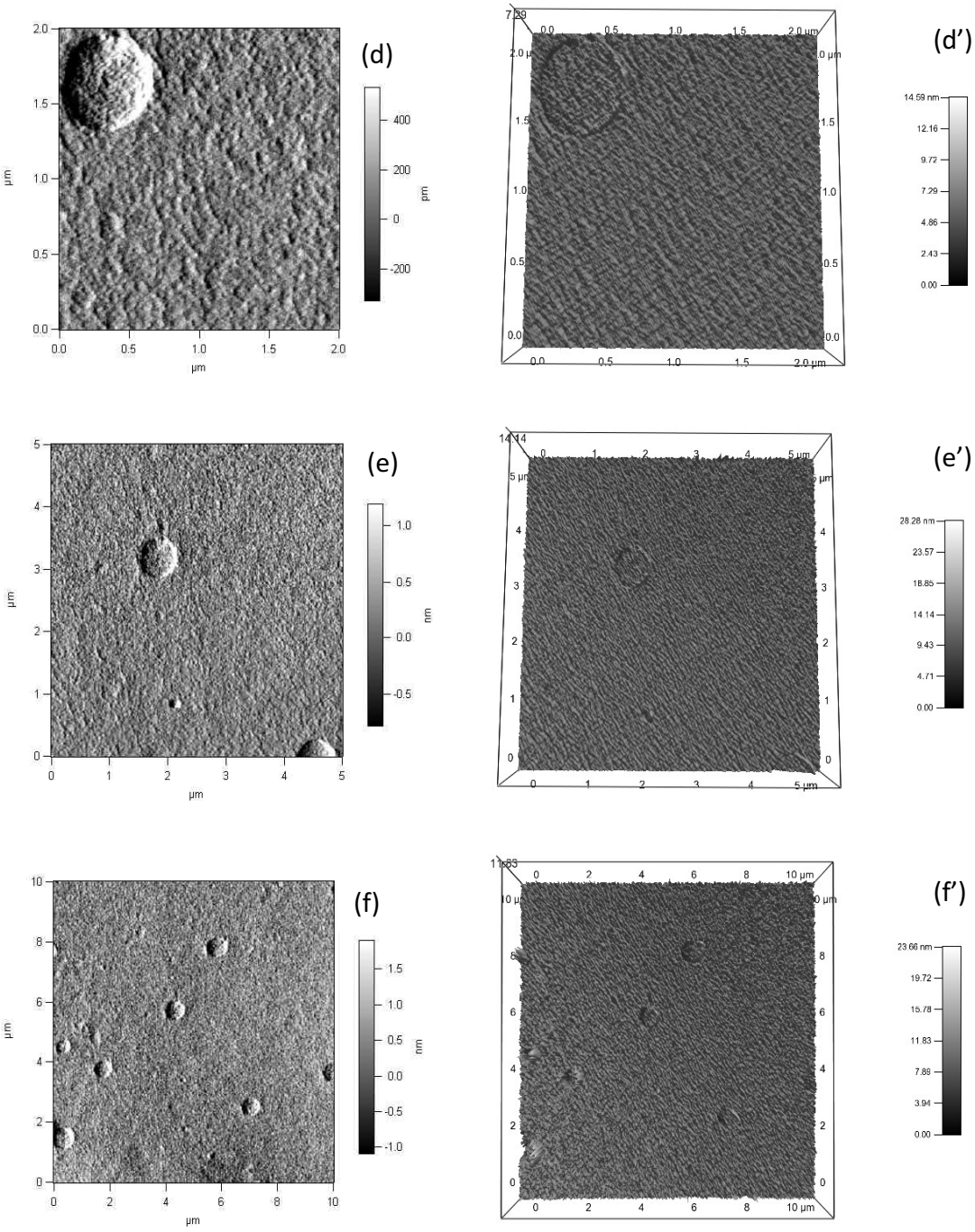

(Continued on next page)

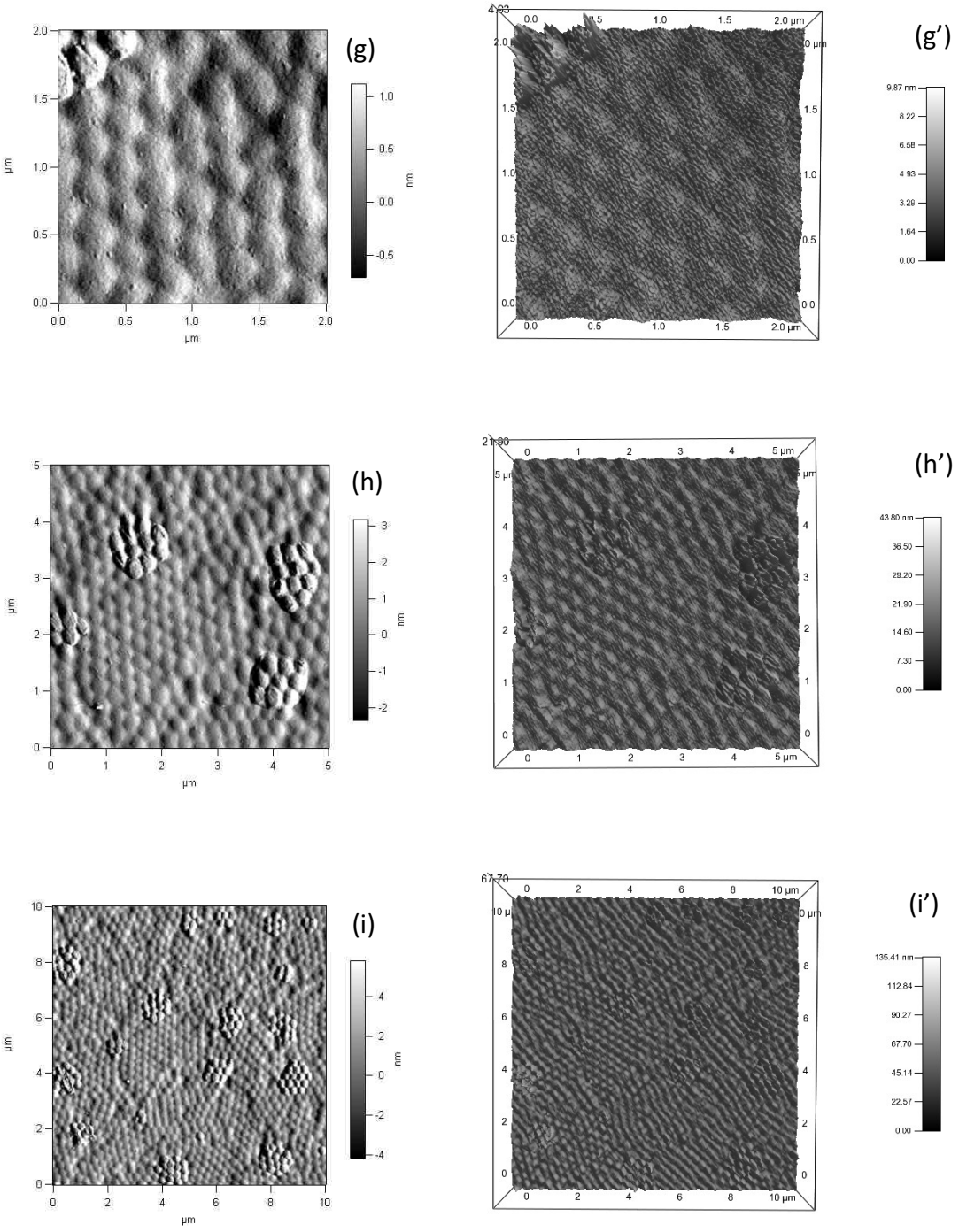

(Continued on next page)

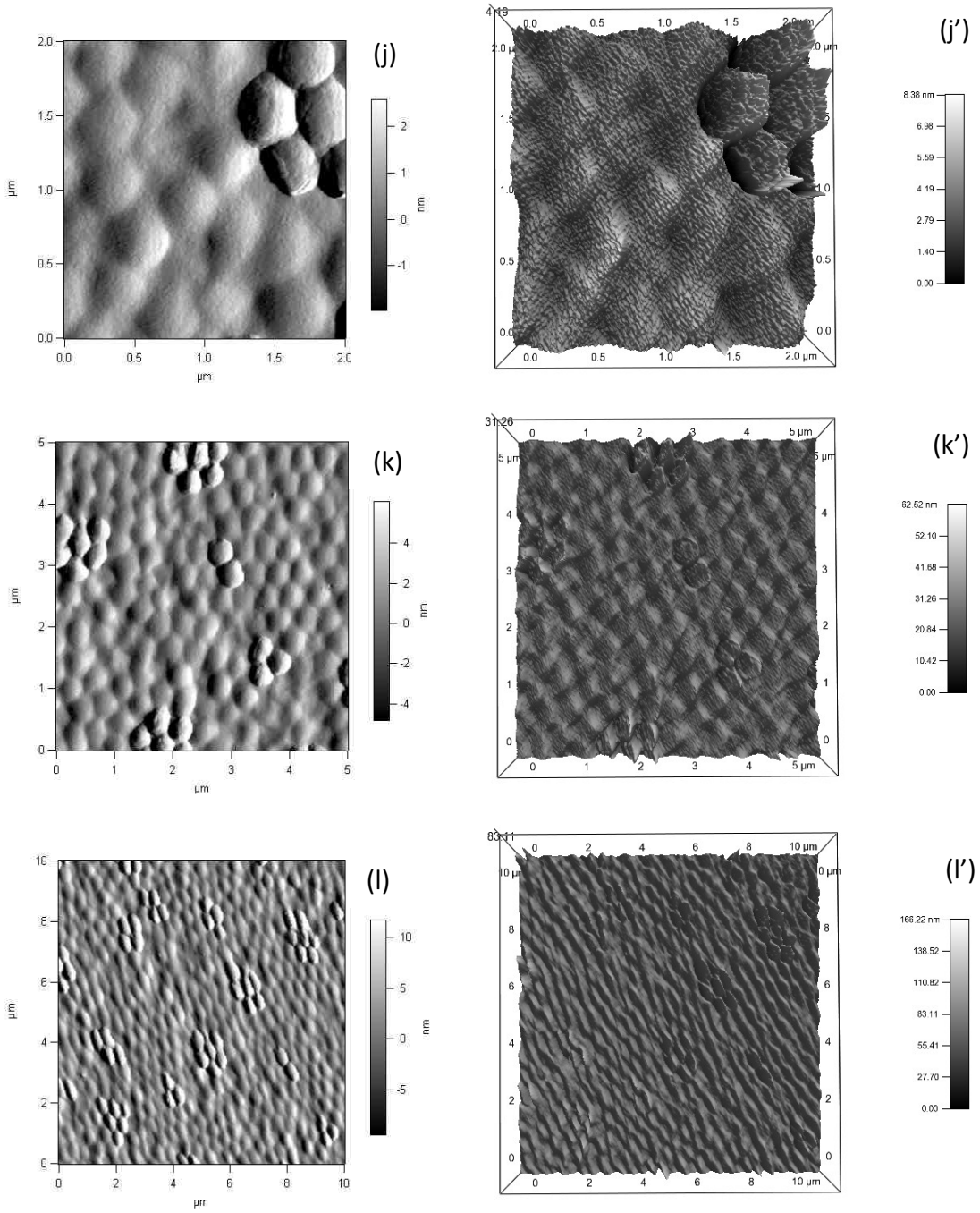

(Continued on next page)

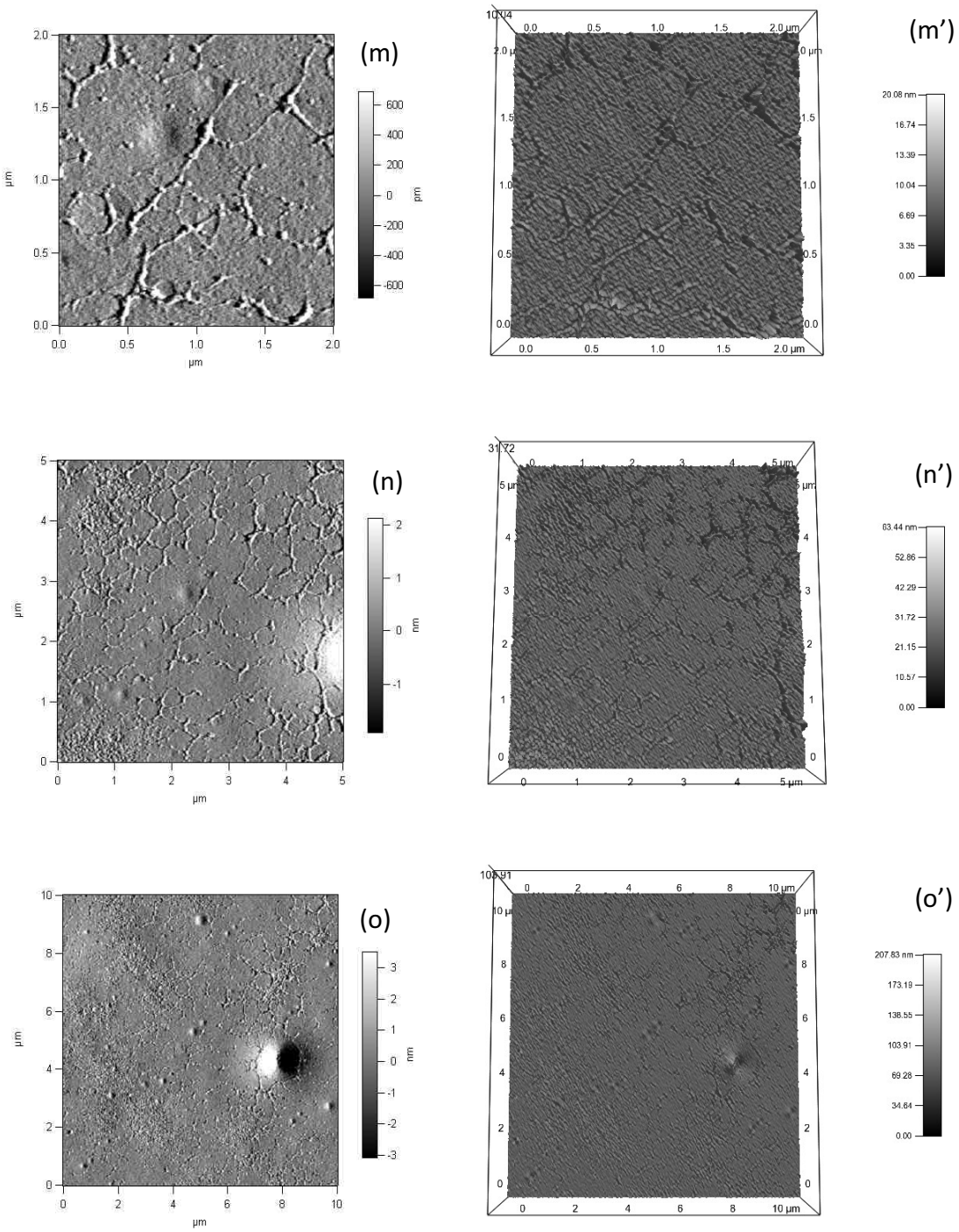

(Continued on next page)

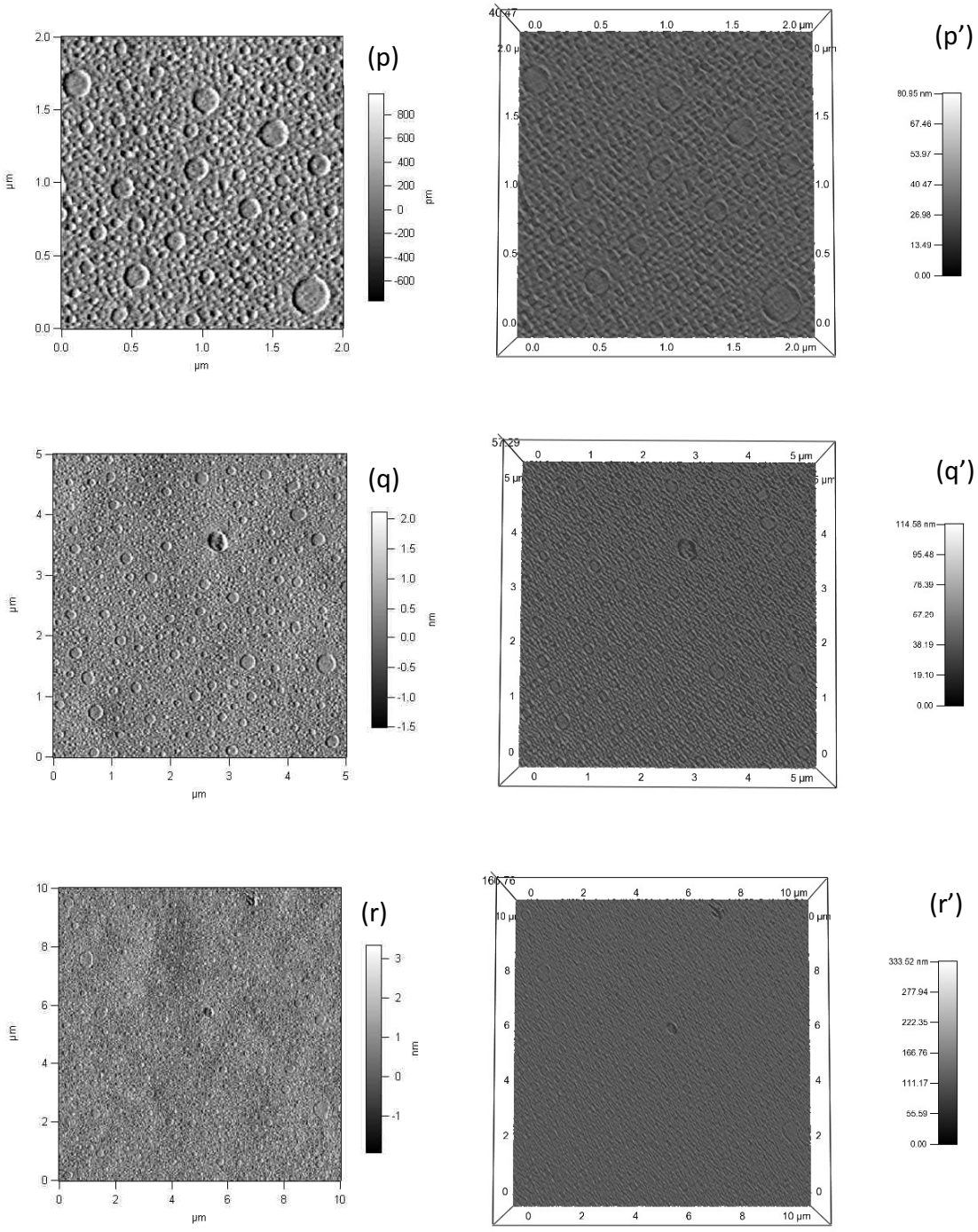

(Continued on next page)

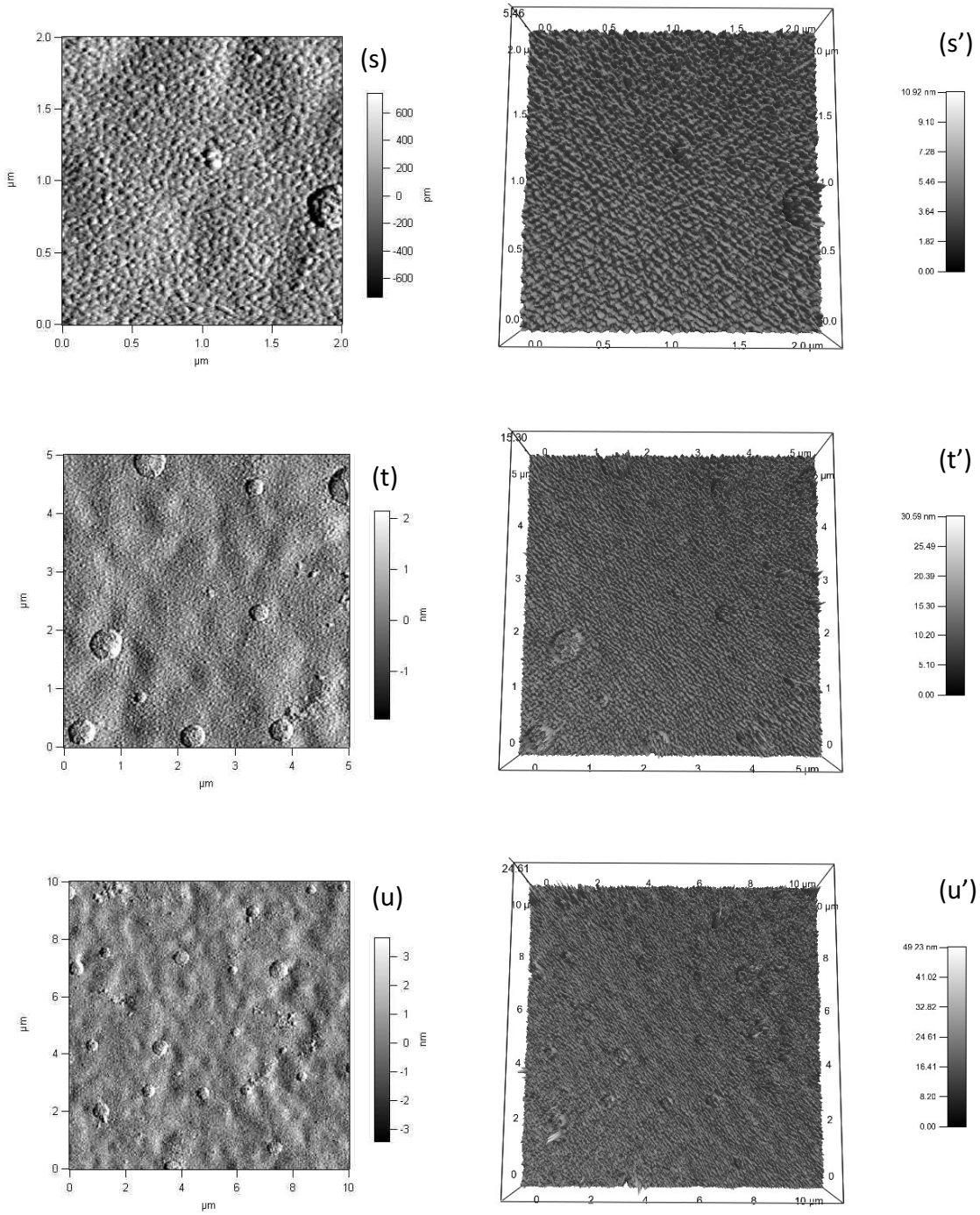

(Continued on next page)

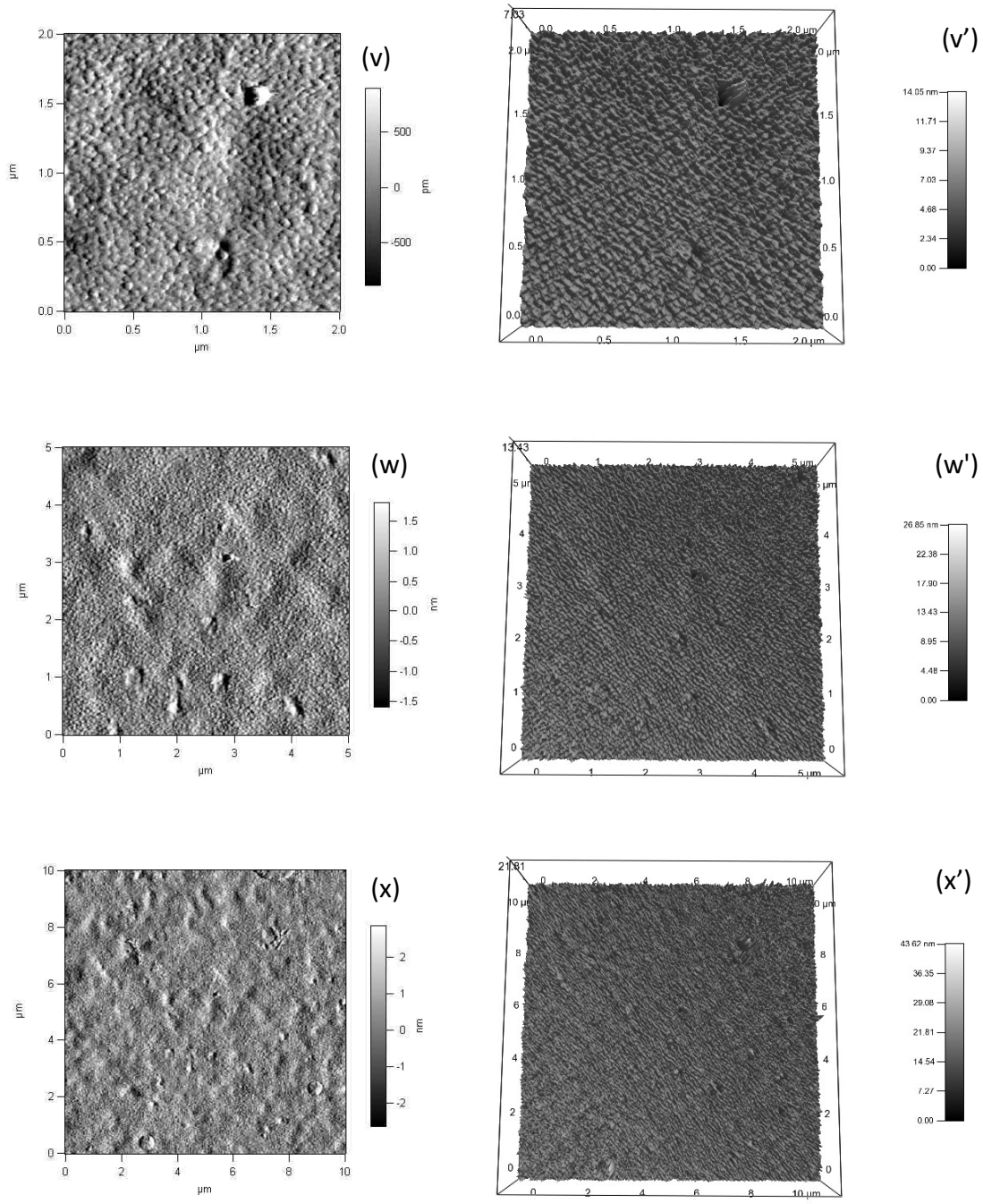

Fig. 5.1. 2 µm × 2 µm-, 5 µm × 5 µm -, and 10 µm ×10 µm 2D and 3D AFM images of PLGA0 (a, b, c and a', b' c'), PLGA23 (d, e, f and d', e', f'), PLGA300 (g, h, i and g', h', i'), PLGA400 (j, k, l and j', k' l'), PLGA0/Alg (m, n, o and m', n' o'), PLGA0/Alg/Chi (p, q, r and p', q', r'), PLGA23/Alg (s, t, u and s', t', u') and PLGA23/Alg/Chi (v, w, x and v', w', x').

5.3.2. Surface wettability and surface free energy

As shown in Table 5.3., although water contact angle measurements revealed slightly different results, the difference among PLGA0, PLGA23, PLGA300 and PLGA400 was statistical. All the nano-smooth and nanopatternd PLGA surfaces were hydrophobic (θ_{H2O}>90°). As nanopatterns were present on the PLGA, the surfaces became more hydrophilic with decreased water contact angles. Clearly, surface wettability can be influenced by surface topography, but the observed impact of topography on controlling PLGA surface wettability was slight while keeping the same surface chemistry. Surface free energy results of nano-smooth and nanopatterned PLGA calculated from Eqn. 5.1 using water and glycerol contact angles are shown in Fig. 5.2. Among all the PLGA substrates, PLGA300 revealed the highest surface free energy (17.9 mN/m), PLGA23 had the second highest (16.5 mN/m), and PLGA0 demonstrated the lowest surface free energy (13.6 mN/m). Generally, nanopatterned PLGA surfaces exhibited higher surface free energy than nano-smooth surface. Considering all the nano-smooth and nanopatterned PLGA had the same surface chemistry, this increase could be attributed to the surface nanotopographies.

Table 5.3. Contact angles measured by water and glycerol on nanopatterned substrates

Substrate	Contact angles measured by different liquids (°)	
	θ (H_2O)	θ (Glycerol)
PLGA0	98.1 ± 0.4	94.9 ± 1.8
PLGA23	93.8 ± 1.8	94.5 ± 2.3
PLGA300	91.6 ± 1.6	92.4 ± 2.6
PLGA400	96.6 ± 0.5	97.7 ± 2.7

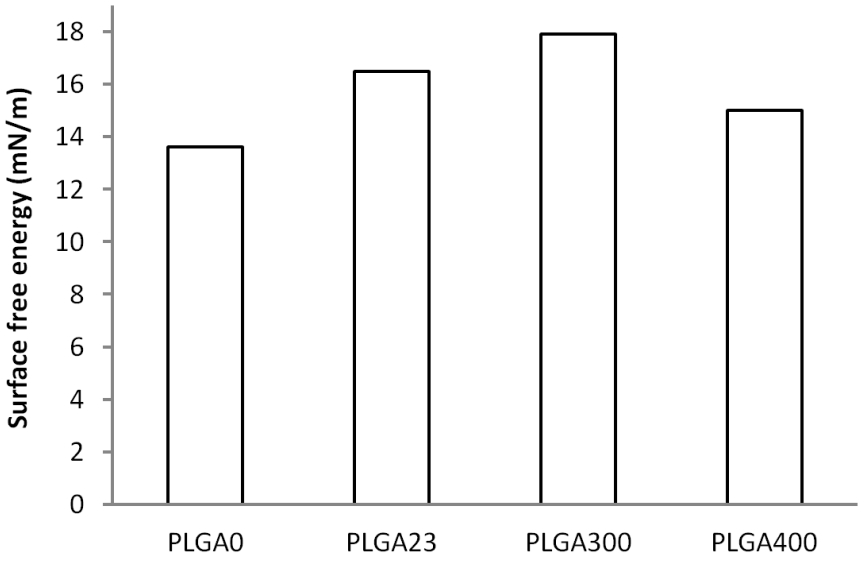

Fig. 5.2. Calculated surface free energy (using contact angle results of water and glycerol) of PLGA0, PLGA23, PLGA300 and PLGA400.

The contact angle results on alginate and chitosan deposited PLGA substrates are shown in Table 5.4. Clearly, the deposition of alginate and chitosan on PLGA surfaces decreased the water contact angles compared to the pure PLGA surfaces, indicating increased water wettability. This result is obvious since both alginate and chitosan are more hydrophibic than PLGA, resulting in increased water wettability than pure PLGA surfaces. Moreover, the increase in hydrophibility on nanopatterned surfaces (PLGA23/Alg and PLGA23/Alg/Chi) was more significant than that on nano-smooth surfaces (PLGA0/Alg and PLGA0/Alg/Chi). Here, the deposition of alginate and chitosan changed both surface chemistry and surface roughness, which both could contribute to the alteration of surface wettability.

Table 5.4. Contact angles measured by water and formamide on LBL deposited substrates

Substrate	Contact angles measured by different liquids (°)	
	θ (H_2O)	θ (Formamide)
PLGA0	98.1 ± 0.4	72.8 ± 1.8
PLGA0/Alg	90.8 ± 0.9	56.5 ± 2.9
PLGA0/Alg/Chi	87.4 ± 0.6	59.3 ± 1.8
PLGA23	93.8 ± 1.8	61.9 ± 2.9
PLGA23/Alg	76.3 ± 2.2	61.3 ± 3.0
PLGA23/Alg/Chi	68.5 ± 1.4	45.9 ± 3.6

5.3.3. Fibronectin and vitronnectin adsorption

Cell adhesive protein adsorption on nanopatterned PLGA surfaces demonstrated different adsorption features for fibronectin and vitronectin (Fig. 5.3). Results of fibronectin adsorption indicated little difference between nano-smooth and nanopatterned PLGA surfaces. Specifically, PLGA23 showed significantly 20% more fibronectin adsorption compared to PLGA0. However, no significant difference was demonstrated between PLGA0, PLGA300 and PLGA400. Vitronectin adsorption revealed a significant difference between nano-smooth and nanopatterned PLGA surfaces. PLGA23, PGA300 and PLGA400 all showed significantly higher vitronectin adsorption than that on PLGA0, 13%, 30% and 26%, respectively. Among the nanopatterned PLGA surfaces, vitronectin adsorption on PLGA300 was slightly higher than that on PLGA23 and PLGA300, although the difference was not statistically significant.

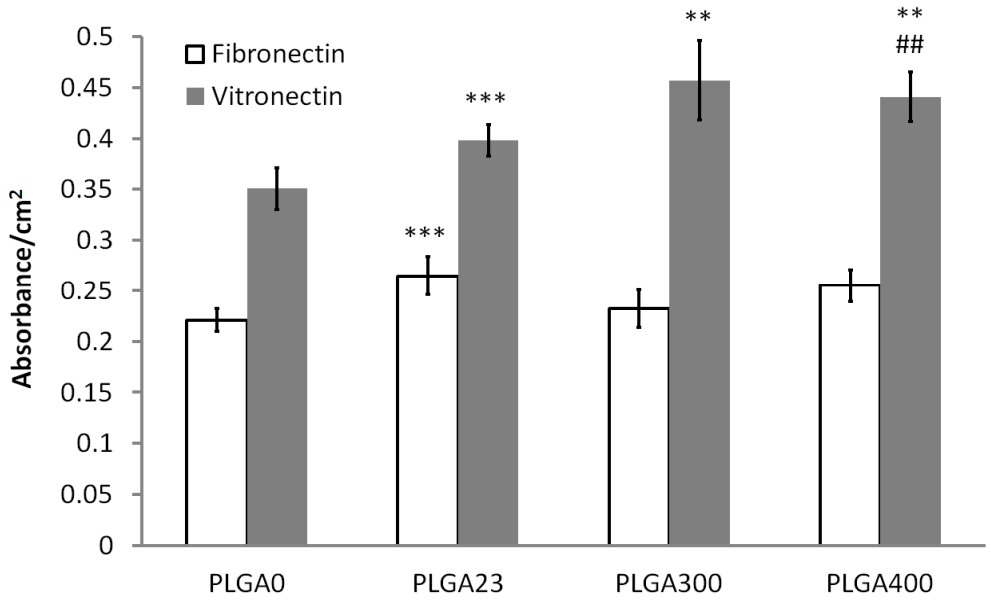

Fig. 5.3. Fibronectin and vitronectin adsorption per substrate size (expressed by light absorbance) on PLGA0, PLGA23, PLGA300 and PLGA400 measured by the enzyme-linked immunosorbent assay (ELISA). Data are expressed as mean ± SEM (N=3). **p<0.05 and ***p<0.1 compared to PLGA0; ## p<0.05 compared to PLGA23.

Fibronectin and vitronectin adsorption on the LBL deposited PLGA surfaces are presented in Fig. 5.4. Results revealed decreased vitronectin adsorption but increased fibronectin adsorption on alginate and chitosan deposited surfaces (i.e., PLGA0/Alg. PLGA0/Alg/Chi, PLGA23/Alg and PLGA23/Alg/Chi) compared to untreated pure PLGA surfaces (i.e., PLGA0 and PLGA23). Specifically, PLGA0/Alg, PLGA0/Alg/Chi, PLGA23/Alg and PLGA23/Alg/Chi all exhibited significantly lower vitronectin adsorption than that on PLGA0 and PLGA23. As a result, although PLGA23 had higher vitronectin adsorption than PLGA0, PLGA23/Alg demonstrated significantly 36% lower vitronectin adsorption compared to PLGA0. However, fibronectin adsorption results

exhibited the opposite trend as alginated and chitosan deposited surfaces had increased fibronectin adsorption compared to pure PLGA surfaces. PLGA0/Alg and PLGA0/Alg/Chi both showed significantly higher fibronectin adsorption than that on PLGA0, 31% and 63% more, respectively. However, the increase in fibronectin adsorption on the nanopatterned surfaces was not as significant as the increase on nano-smooth substrates. PLGA23/Alg/Chi showed significantly 12% more vitronectin adsorption compared to PLGA23. No significant difference was observed between PLGA23 and PLGA23/Alg. The results indicated that surface chemistry played an important role on protein adsorption, which may have partially masked the influence of nanotopography on the nanopatterned surfaces.

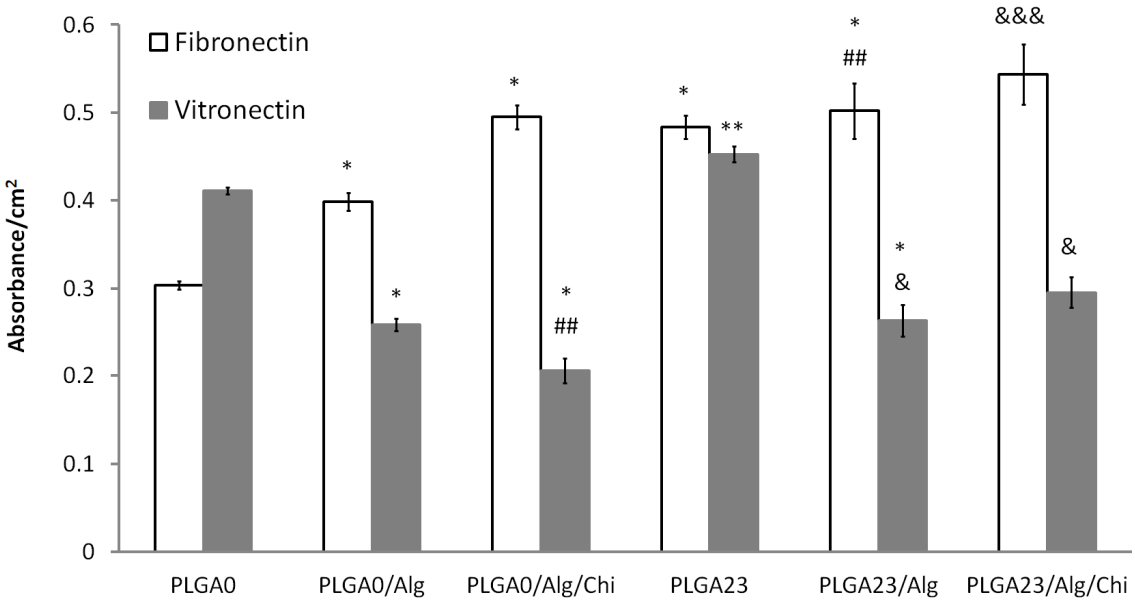

Fig. 5.4. Fibronectin and vitronectin adsorption per substrate size (expressed by light absorbance) on PLGA0, PLGA0/Alg, PLGA0/Alg/Chi, PLGA23, PLGA23/Alg and PLGA23/Alg/Chi measured by the enzyme-linked immunosorbent assay (ELISA). Data are expressed as mean ± SEM (N=3). *$p<0.01$ and **$p<0.05$ compared to PLGA0; ## $p<0.05$ compared to PLGA0/Alg; & $p<0.01$ and &&& $p<0.1$ compared to PLGA23.

5.4. Discussion

5.4.1. Surface nanopattern mediated cell functions

5.4.1.1 The impact of protein adsorption on cell adhesion

In chapter 2, four-hour lung cancer cell adhesion showed enhanced cell adhesion densities on PLGA23, PLGA300 and PLGA400 compared to nano-smooth PLGA surfaces. Here, greater adsorption of the cell adhesive proteins on these substrates revealed a possible mechanism for the increased cell adhesion on nanopatternd PLGA

surfaces. It is known that proteins immediately adsorb on the biomaterial surfaces once a biomaterial is in contact with a protein containing solution and cells subsequently recognize this initial layer of proteins to initiate integrin-mediated adhesion [173]. Fibronectin and vitronectin have been recognized as two major adhesion proteins to mediate cell-biomaterial adhesion. A study by Lafrenie *et al.* [118] found that A549 cells were deficient in vitronectin receptor αvβ3 but did express fibronectin receptor. However, another study showed that A549 cells did express integrin αvβ3 [174]. In this way, it is reasonable to expect that A549 cell adhesion had a significant dependence on fibronectin but maybe limited dependence on vitronectin. PLGA23, PLGA300 and PLGA400 had significantly higher vitronectin adsorption than that on nano-smooth PLGA, whereas only PLGA23 showed significantly higher fibronectin adsorption compared to PLGA0. This result suggested that both fibronectina and vitronectin preferentially and competitively adsorbed onto various PLGA surfaces. The reason for the observed increase in select protein adsorption resulted from the alterations in surface topography from a conventional to a nanopatterned surface. Greater surface wettability was shown on nanopatterned PLGA surfaces and this increase could be linked to the greater protein adsorption. A study by Kooten *et al.* [175] found that assembled fibronectin matrix was higher on the polystyrene substrates with higher wettability exposed to plasma treatment to increase oxygen surface incorporation, and subsequent endothelial cell proliferation increased with increasing oxygen incorporation. In addition, as the nanometer surface roughness increase, there is a greater charge density at the surface which can adsorb greater quantities of proteins [173]. The present study in this dissertation further confirmed the effects nanotopography alone can have on protein adsorption. As a result,

this increase in vitronectin and fibronetin adsorption on nanopatterned PLGA led to the greater lung cancer cell adhesion compared to nano-smooth PLGA.

However, the adhesion of breast adenocarcinoma cells showed a different dependence on protein adsorption and significantly higher MCF-7 cells were observed on PLGA23 compared to PLGA0. MCF-7 cells were shown to have a great affinity and bound well to both fibronectin and vitronectin [176, 177], and, thus, MCF-7 cell adhesion could be related to the adsorption of both fibronectin and vitronectin. In Chapter 3, breast cancer cells showed a significantly higher adhesion density on PLGA23 than that on PLGA0, PLGA300 and PLGA400. This increase can arise from the greater protein adsorption of both fibronectin and vitronectin on PLGA23 compared to PLGA0. However, although PLGA300 and PLGA400 had greater vitronectin adsorption than PLGA0, the breast cancer cell adhesion density was not promoted on PLGA300 and PLGA400. The possible reason could be that the conformation and biological activities of vitronectin coated on nanopatterned PLGA was not favorable to breast cancer cell adhesion. Importantly, a study by Underwood *et al.* [178] provided evidence that antibodies specific to a cell attachment region of fibronectin bound preferentially to the conformation of fibronectin on the more hydrophilic tissue culture polystyrene compared to untreated hydrophobic polystyrene. In contrast, antibodies specific to the cell-binding region in vitronectin displayed slightly increased binding to vitronectin coated on hydrophobic polystyrene. Here, the nanopatterned PLGA was more hydrophilic compared to nano-smooth PLGA, which may limit the conformation and bioactivity of adsorbed vitronectin and, thus, breast cancer cell adhesion was not promoted on PLGA300 and PLGA400.

5.4.1.2. The correlation between PLGA surface energetics and cell responses

Surface free energy was calculated from contact angles in this study and nanopatterned PGA had higher surface free energy than nano-smooth PLGA. In this study, the influence of surface topography on cell responses was independently studied by introducing nanopatterns but with the same surface chemistry through a deliberately designed experiment. Therefore, alterations in surface topography had a slight effect on surface wettability and surface free energy and resulted in slight increase in surface free energy on nanopatterned PLGA.

Surface free energy has been known to significantly influence cell attachment, spreading and proliferation. Here, both PLGA23 and PLGA300 had higher surface free energy compared to PLGA0 and PLGA400, suggesting high cell adhesivity and spreading. There was evidence that substrates with higher surface free energy have more potential to cause “wetting” of cell aggregates on their surfaces and induce cell spreading and cell proliferation [171, 172]. A study by Yang *et al.* [172] provided evidence that there was a strong correlation between cell responses and the surface free energy and found that nanocrystalline diamond which was treated with NH_3 plasma had the highest free energy and exhibited the best osteoblast responses, whereas the worst osteoblast responses was found on the lowest surface free energy diamond surface which was treated by H_2 plasma. Also, the cell proliferation density is related to cell adhesion as more cell adhesion means subsequent more cell proliferation. Thus, improved cell proliferation can be expected on the surfaces with higher cell adhesion and surface free energy. As a result, lung carcinoma cells indicated enhanced proliferation density on both PLGA23 and PLGA300 and breast adenocarcinoma cells showed increased proliferation

density on PLGA23. Moreover, improved protein adsorption on nanopatterned PLGA surface may also related to higher surface free energy, and small change in protein adsorption can have a profound influence on cell adhesion and proliferation.

5.4.1.3. The relationship of PLGA surface properties and cell functions

The surface properties of various PLGA surfaces and corresponding cell behaviors are summarized in Table 5.5. Clearly, different cell functions (including adhesion, proliferation, apoptosis and VEGF secretion) showed varied cell responses to surface nanotopography. Both lung cancer and breast cancer cells exhibited decreased cell adhesion and proliferation density on PLGA0 and PLGA400 compared to PLGA23 and PLGA300. However, four cell lines (lung cancer cell, lung normal cell, breast cancer cell and breast normal cell) all had higher cell proliferation density on PLGA23 compared to PLGA0. As discussed above, cell adhesion and proliferation was related to protein adsorption and surface free energy influenced by surface topography. PLGA23 had nanoscale surface roughness comparable to the dimensions of proteins, which was favorable for the protein conformation and bioactivity due to the suitable “dock-in” sites. Moreover, the increased surface free energy of PLGA23 can promote the dispersion of cell aggregates and cell adhesivity to the material surface, and thus high cell adhesion and proliferation was observed on 23 nm topographical surfaces.

However, although PLGA23 showed higher cell adhesion and proliferation density, a higher percentage of cell apoptosis and decreased VEGF secretion was discovered on PLGA23 after further investigation of critical cell bioactivity indicators. For both lung cancer and breast cancer cells, a greater percentage of cancer cell apoptosis

occurred on PLGA23. Moreover, the secretion VEGF, an essential growth factor for cancer growth and development, also revealed that cancer cells on PLGA23 secreted the least VEGF. Clearly, the lack of VEGF could significantly inhibit the growth of cancer cells and thus limit the formation of tumors. It is known that nanotopography can alter the gene express profiles of various cell types [163] and influence integrin-mediated signaling cascades [1]. The proposed hypothetical model showing how the surface nanotopography direct cancer cell fates is presented schematically in Figure 5.5. Cell interactions with ECM are mediated by integrins that control cell gene expression, apoptosis and growth factor synthesis in a synergistic manner. The predicted size of surface occupancy by the head of an integrin heterodimer is about 10 nm in diameter [124, 179]. This suggested that a 23 nm tightly arrayed semispherical pattern would restrict the clustering of integrins and the following formation of focal adhesion and actin stress fibers through disordering the assembly of intergins by continuous protrusions. Therefore, 23 nm patterns severely limit intergrin activation and cell-biomaterial communication, resulting in dramatically reduced cell spreading, proliferation and migration and eventually cell apoptosis. However, larger surface patterns (especially PLGA400) had relatively much larger size compared to integrins, and, thus, clustering of integrins could be allowed to form on the pattern surface or spacing of patterns. The activated integrins could effectively promote the formation of focal adhesions and actin stress fibers, resulting in cell spreading and proliferation. However, experiments will be needed to identify this proposed hypothetical model.

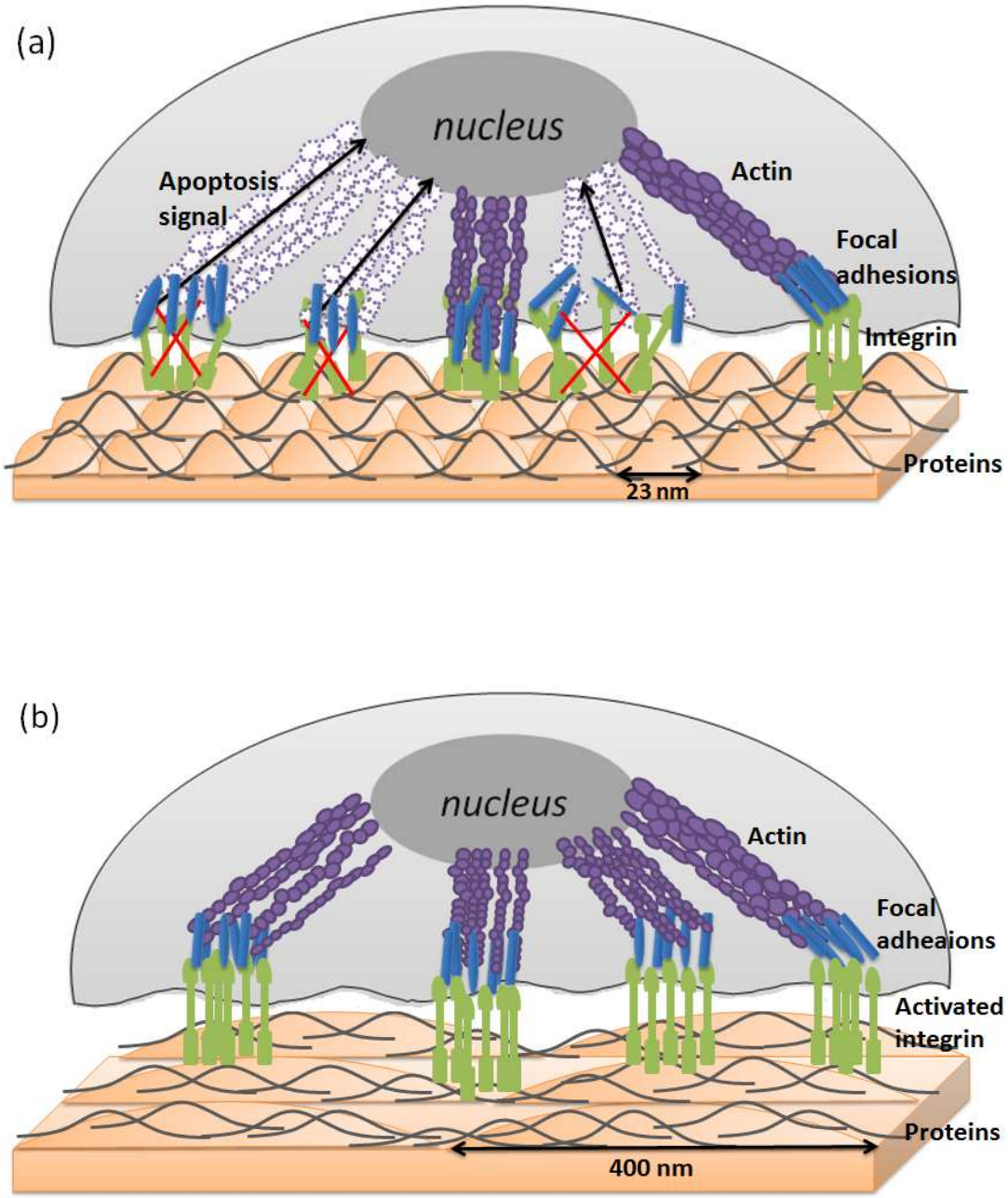

Fig. 5.5. Schematic presentation of nanopatterns which direct cancer cell apoptosis: (a) 23 nm patterns severely limit intergrin clustering and activation, resulting in dramatically reduced cell spreading, proliferation and eventually cell apoptosis; (b) 400 nm surface patterns support clustering and activation of integrins, resulting in assembly of actin stress fibers and signaling to the nucleus.

Table 5.5. Surface properties and corresponding optimal cell functions of nano-smooth and nanopatterned PLGA samples

Substrate			PLGA0	PLGA23	PLGA300	PLGA400
Surface properties	Surface roughness R_{rms} (nm)		0.54	3.73	10.78	24.11
	Surface free energy (mN/m)		13.60	16.49	17.91	15.02
	Protein adsorption	Fibronectin (absorbance/cm^2)	0.22	0.26	0.23	0.25
		Vitronectin (absorbance/cm^2)	0.35	0.40	0.46	0.44
Cell responses	Cell adhesion	Lung cancer cell	Low adhesion density	-	-	-
		Breast cancer cell	Low adhesion density	-	Low adhesion density	Low adhesion density
	Cell proliferation	Lung cancer cell	Low proliferation density	-	-	Low proliferation density
		Lung healthy cell	-	High live cell number	High live cell number	-
		Breast cancer cell	-	-	Low proliferation density	Low proliferation density
		Breast normal cell	-	High live cell number	-	-
	Apoptosis	Lung cancer cell	-	High apoptosis percentage	-	-
		Breast cancer cell	-	High apoptosis percentage	-	-
	VEGF secretion	Lung cancer cell	-	Low VEGF secretion	-	-
		Breast cancer cell	-	Low VEGF secretion	-	-

* "-" represents cell responses not optimal for corresponding combination of cells and substrates

5.4.2. Nanopattern and LBL monolayer mediated cell functions

5.4.2.1. The impact of surface properties on protein adsorption

This study showed that the adsorption of the cell adhesive proteins fibronectin and vitronectin was significantly influenced by the alteration in surface chemistry. Altered surface properties (surface chemistry, surface wettability, surface charge) and competitive adsorption of fibronectin and vitronectin on substrate surfaces could be responsible for the altered protein adsorption. In the present study, the deposition of alginate and chitosan increased the hydrophilicity of substrate surfaces. This is expected as both alginate and chitosan are hydrophilic and, thus, LBL deposition on PLGA surfaces increased hydrophilicity. Fibronectin showed a strong affinity to more hydrophilic surfaces as more fibronectin adsorbed on the alginate and chitosan deposited surfaces. Some studies also discovered that hydrophilic substrates absorbed more fibronectin molecules than hydrophobic substrates. For example, Sousa *et al.* [180] found that fibronectin displayed higher affinity for the pure titanium with a titanium oxide layer, the more hydrophilic one, and lower for the TiO_2 sputtered on Si substrate, the more hydrophobic one. Another study also showed that the amounts of serum proteins, including fibronectin, adsorbed from serumcontaining medium were larger to more hydrophilic plasma-treated polytetrafluoroethylene surfaces than those adsorbed to more hydrophobic unmodified polytetrafluoroethylene [181]. However, no consistent conclusion has been established since other studies also revealed increased fibronectin binding on more hydrophobic surfaces [182, 183]. For instance, increased fibronectin binding and more rapid adsorption kinetics were observed on hydrophobic silanized-silica in contrast to hydrophilic silica [183]. Moreover, the increased fibronectin

adsorption could be attributed to other surface properties in addition to surface wettability. The fibronectin adsorption result clearly indicated that positively charged chitosan-terminated films adsorbed higher amount of fibronectin adsorption in comparison to negatively charged alginated-terminated surfaces. This observation can be well explained by the strong electrostatic attraction between negatively charged proteins (i.e., fibronectin and vitronectin) and positively charged chitosan at or near the substrate surfaces. Similar observation has also been reported by Wittmer *et al.* [184] on LBL (poly (L-lysine) and dextran sulfate) assembly multilayer films.

However, vitronectin adsorption exhibited the opposite trend in comparison to fibronectin adsorption and less vitronectin adsorbed on alginate- and chitosan-terminated substrates. Here, vitronectin exhibited a preference for more hydrophobic surfaces. Similarly, Toromanov *et al.* [185] reported that vitronectin adsorbed in increasing amount as the hydrophobicity of the substrate increases (the fraction of -OH groups decreases). In addition, electrostatic interactions could play an important role in vitronectin adsorption. Because vitronectin bears a net negative charge, the anionic alginate-terminated surfaces tended to adsorbed less protein than the cationic chitosan-terminated surfaces. However, more vitronectin adsorption was still observed on PLGA0/Alg in comparison to PLGA0/Alg/Chi. Complex competitive adsorption of fibronectin with vitronectin may be responsible for the observed results. Fibronectin has been shown to adsorb more than vitronectin onto same substrates under competitive condition [186]. Here, it is also observed that more fibronectin adsorbed on the alginate- and chitosan-terminated surfaces, leading to the binding sites for vitronectin decrease and less vitronectin adsorb

onto these surfaces under the presence of competitive proteins (i.e., fibronectin and vitronectin).

5.4.2.2. The impact of surface properties on cell proliferation

Lung carcinoma cells exhibited higher cell proliferation on alginate- and chitosan-terminated substrates compared to pure unmodified PLGA. This result can be well explained by the increased fibronectin adsorption on these surfaces. Since lung cancer cells express fibronectin receptor but are deficient in vitronectin receptor αvβ3 [118], the increased fibronectin adsorption could induce more lung cancer cell adhesion and subsequent cell proliferation. Moreover, fibronectin could be reorganized in an extracellular matrix-like structure on more hydrophilic surfaces by cells [105], and extensive rearranging of fibronectin molecules can happen on hydrophilic surfaces, whereas, on hydrophobic substrates, the rearrangement is restricted due to a higher binding force between the protein and surface [187]. Thus, high lung cancer cell proliferation was observed on more hydrophilic surfaces with more fibronectin adsorption in this study.

However, breast cancer cells showed the lowest cell proliferation only on alginate-terminated surfaces (PLGA0/Alg and PLGA23/Alg). This observation can be well explained by the total least protein adsorption of fibronectin and vitronectin on PLGA0/Alg and PLGA23/Alg. Since MCF-7 express both fibronectin and vitronectin receptors [188], cell proliferation can be affected by the adsorption of both fibronectin and vitronectin. In Fig. 5.4, on the average, alginate-terminated surface had the least total

protein adsorption including fibronectin and vitronecin (PLGA0/Alg<PLGA0/Alg/Chi<PLGA0, PLGA23/Alg<PLGA23/Alg/Chi<PLGA23), and decreased protein adsoprtion on alginate-terminated substrates had potential to decrease breast cancer cell adhesion and further less live cells were observed on these surfaces.

5.4.2.3. The correlation between surface properties and cell functions

The surface properties and cell functions of various substrates are summarized in Table 5.6. Clearly, through the deposition of alginate and chitosan on PLGA surfaces, surface properties and corresponding cell functions were significantly changed. Both positive and negative impacts were observed on cancer and healthy cells. Lung cancer cell proliferation increased on alginate- and chitosan-terminated surfaces, while breast cancer cell proliferation was significantly decreased on alginate-terminated surfaces. The possible reason was related to surface protein (fibronectin and vitronectin) adsorption as discussed above. However, lung healthy cell proliferation exhibited little correlation with surface chemistry but a significant correlation with surface nanopatterns. Lung healthy cell proliferation was significantly increased on nanopatterned substrates (PLGA23, PLGA23/Alg and PLGA23/Alg/Chi) no matter what surface chemistry compared to substrates without nanopatterns (PLGA0, PLGA0/Alg and PLGA0/Alg/Chi). However, for breast healthy cells, alginate- and chitosan-terminated substrates revealed significantly lower cell proliferation compared to corresponding pure PLGA substrates. Moreover, chitosan exhibited more profound inhibition on breast healthy cell

proliferation in comparison to alginate. The mechanism(s) of these phenomena need to be clarified in the future study.

More importantly, further investigation on VEGF secretion showed that alginate had a negative effect on both lung cancer and breast cancer cells. On alginate-terminated surfaces (PLGA0/Alg and PLGA23/Alg), lung cancer and breast cancer cells had significantly lower VEGF concentrations compared to any other substrates. Here, alginate-terminated surfaces showed anti-cancer properties which could be attributed to the chemistry of alginate since alginate has exhibited anti-tumor properties to other cancer cells as described in *Introduction* section of this chapter. Moreover, cancer cells on PLGA23/Alg revealed slightly lower VEGF concentration than PLGA0/Alg. This result indicated that surface nanopattern and surface chemistry simultaneously inhibited cancer cell VEGF secretion, but surface chemistry still played a leading role. Inhibition of VEGF has been recognized as a novel approach for cancer therapy. However, in some cases where chemistry change needs to be avoided, surface nanotopography could be an ideal candidate to inhibit cancer cell functions since only physical changes introduced and no any pharmacy or chemistry used.

Table 5.6. Surface properties and corresponding optimal cell functions of nanopatterned and LBL deposited substrates

Substrate			PLGA0	PLGA0/Alg	PLGA0/ Alg/Chi	PLGA23	PLGA23/Alg	PLGA23/ Alg/Chi
Surface Properties	Surface chemistry		PLGA	alginate	chitosan	PLGA	alginate	chitosan
	Water contact angle (°)		98.1	90.8	87.4	93.8	76.3	68.5
	Protein adsorption	Fibronectin (absorbance/cm^2)	0.30	0.40	0.49	0.48	0.50	0.54
		vitronectin (absorbance/cm^2)	0.41	0.26	0.21	0.45	0.26	0.29
Cell responses	Cell proliferation	Lung cancer cell	Low live cell number	-*	-	Low live cell number	-	-
		Lung healthy cell	-	-	-	High live cell number	High live cell number	High live cell number
		Breast cancer cell	-	Low live cell number	-	-	Low live cell number	-
		Breast healthy cell	High live cell number	-	-	High live cell number	-	-
	VEGF secretion	Lung cancer cell	-	Low VEGF concentration	-	-	Low VEGF concentration	-
		Breast cancer cell	-	Low VEGF concentration	-	-	Low VEGF concentration	-

* "-" represents cell responses not optimal for corresponding combination of cells and substrates

5.5. Conclusions

This chapter summarizes the surface properties and cell functions on all the substrates with nanopattern or LBL coating. Surface topography and roughness, surface free energy and protein adsorption was believed to play profound roles on regulating cell functions. It was concluded that cell adhesive protein adsorption can affect cancer cell adhesion and subsequent cell proliferation. Moreover, it was believed that surface free energy was related to cell spreading and cell proliferation. However, competitive roles were present to cells when positive or negative impacts were induced by different factors. In addition, on alginate- and chitosan-terminated substrates, surface roughness, surface chemistry and surface charge all had significant influence on cell functions and especially, alginate-terminated nanopatterned substrates exhibited optimal cancer cell behaviors. Clearly, these results provided important guidance and cues for designing custom biomaterials to achieve specific goals.

Chapter 6 Conclusions and Future Directions

This dissertation systematically investigated cancer and healthy cell responses on nanopatterned PLGA substrates, and further chemistry modification on nanopatterned PLGA and cell responses to these modified substrates. As a result, it generated a large amount of useful information to guide the design and fabrication of ideal anti-cancer implants. Here, an ideal anti-cancer biomaterial surface is proposed based on the conclusions of this dissertation and future directions are pointed out for the further development of this field.

6.1. Ideal anti-cancer implants for lung cancer

This dissertation demonstrated that 23 nm surface featured PLGA can induce lung cancer cell apoptosis and decrease their VEGF secretion probably due to the inhibition of integrin clustering by 23 nm protrusions. However, PLGA23 increased lung cancer cell adhesion and proliferation since more fibronectin was absorbed on nanopatterned surfaces. Further chemistry modification by LBL deposition of alginate and chitosan was expected to decrease fibronectin adsorption, unfortunately, fibronectin adsorption was not decreased on these chemistry modified surfaces. However, the VEGF secretion of lung cancer cells on alginate deposited surfaces was further decreased compared to PLGA23. Therefore, based on these conclusions, the ideal anti-cancer implants for lung cancer have

the following properties: nanopatterns (less than 100 nm), low fibronectin adsorption and low surface free energy. For the future, decreasing fibronectin adsorption on nanopatterned PLGA should be the focus for fabricating ideal implants for lung cancers. However, a challenging problem arises when designing surfaces to achieve multiple purposes since when changing one surface property other surface properties change simultaneously. The combination and balance of these surface properties are important for designing anti-cancer surfaces for lung cancer. The studies and conclusions in this dissertation provided a large amount of guidance and cues for achieving this goal.

6.2. Ideal anti-cancer implants for breast cancer

As demonstrated in this dissertation, breast cancer cell responses to PLGA substrates are strongly correlated to the various surface properties of PLGA. Breast cancer cell apoptosis was induced on 23 nm surface featured PLGA and VEGF secretion also decreased on PLGA23. The anti-cancer properties of nanopatternded PLGA were determined by the pattern size as patterns less than 100 nm (e.g., 23 nm surface featured PLGA) had desirable effects on apoptosis and VEGF, whereas nanopatterns with larger pattern sizes (e.g., 400 nm surface featured PLGA) showed no anti-cancer properties. However, breast cancer cell adhesion and proliferation again increased on PLGA23 due to the increased vitronectin adsorption and higher surface free energy on PLGA23. Fortunately, after further modification of PLGA surface with alginate, the vitronectin adsorption on alginate-terminated PLGA23 was largely decreased and, thus, breast cancer cell proliferation on PLGA23/Alg was inhibited significantly.

Clearly, it is important to design implants for specific purposes when the cell responses of different cell lines are different to the same surface properties. For example, if the main purpose of the implants is to kill or inhibit cancer cells, surfaces with nanopatterns, low protein adsorption and low surface free energy should be exploited. However, if healthy cells are expected to grow on the implant surfaces, the surface properties should be designed to have high protein adsorption and surface free energy. This dissertation provided important information for the design of desirable implant interfaces.

6.2. Future directions

For future directions, responses of multiple types of cells under competitive conditions to nanopatterned PLGA need to be studied. Many different cell types are in contact with the implants *in vivo*, so it is reasonable to investigate more lung tissue or breast tissue related cell responses on the nanopatterned PLGA under competitive conditions. For example, co-culturing of cancer cells and breast cells could be an important step for the full evaluation of a new anti-cancer implant material.

Secondly, investigating anti-cancer ability of LBL deposited nanopatterned PLGA with multiple layers is also important due to the consideration of stability and anti-cancer efficiency of LBL modification on nanopatterned PLGA. Moreover, the exploring of LBL deposition on 300 nm or 400 nm patterned PLGA surfaces and the collective influence of surface chemistry and surface patterns on cancer/healthy cell functions could be another important future direction.

Thirdly, a better understanding of mechanism(s) behind the cells responses to the nanopatterned and also chemistry modified PLGA substrates is needed. Importantly, it is better to investigate the effects of surface properties on cell functions independently and then, the way how to effectively combine the optimal surface properties needs to be determined to achieve specific purposes.

Lastly, animal studies to determine the *in vivo* biological responses of nanopatterned and chemistry modified PLGA substrates need to be conducted to evaluate the biocompatibility and anti-cancer properties of these substrates. For example, human lung cancer or breast cancer cells can be injected subcutaneously into mice. When the tumor volumes reach a specific size, animals can be implanted with the nanopatterned PLGA substrates. After pre-determined time, incisional biopsies, scanning electron microscopy, fluorescence microscopy, etc., can be used to observe tumor size and morphology to evaluate the anti-cancer properties of the implanted substrates.

In summary, for the first time, lung cancer and breast cancer cell responses on nanopatterned PLGA (including chemistry modified PLGA) have been systematically investigated and the correlation between surface properties and cell functions has been well established in this dissertation. Overall, alginate-terminated PLGA substrates with 23 nm surface patterns are the best material created in this study for anti-cancer (specifically, lung cancer and breast cancer) implants. This dissertation provided a large amount of information to the field of anti-cancer implant application and further research of nanopatterned anti-cancer implants and their application in clinical practice could be based on this dissertation.

Bibliography

1. Lim, J.Y. and H.J. Donahue, *Cell sensing and response to micro- and nanostructured surfaces produced by chemical and topographic patterning.* Tissue Engineering, 2007. **13**(8): p. 1879-1891.
2. Rosenberg, M.D., *Cell Guidance by Alterations in Monomolecular Films.* Science, 1963. **139**(3553): p. 411-.
3. Rosenberg, M.D., *Long-Range Interactions between Cell and Substratum.* Proceedings of the National Academy of Sciences of the United States of America, 1962. **48**(8): p. 1342-1349.
4. Arnold, M., et al., *Activation of integrin function by nanopatterned adhesive interfaces.* Chemphyschem, 2004. **5**(3): p. 383-388.
5. Tzvetkova-Chevolleau, T., et al., *The motility of normal and cancer cells in response to the combined influence of the substrate rigidity and anisotropic microstructure.* Biomaterials, 2008. **29**(10): p. 1541-1551.
6. Bellin, M.F., et al., *Liver Metastases - Safety and Efficacy of Detection with Superparamagnetic Iron-Oxide in Mr-Imaging.* Radiology, 1994. **193**(3): p. 657-663.
7. Cormode, D.P., et al., *Nanotechnology in medical imaging: probe design and applications.* Arterioscler Thromb Vasc Biol, 2009. **29**(7): p. 992-1000.
8. Corot, C., et al., *Recent advances in iron oxide nanocrystal technology for medical imaging.* Advanced Drug Delivery Reviews, 2006. **58**(14): p. 1471-1504.
9. Corot, C., et al., *Comparison of different types of blood pool agents (P792, MS325, USPIO) in a rabbit MR angiography-like protocol.* Investigative Radiology, 2003. **38**(6): p. 311-319.
10. Harisinghani, M.G., et al., *Noninvasive detection of clinically occult lymph-node metastases in prostate cancer.* New England Journal of Medicine, 2003. **348**(25): p. 2491-U5.
11. Hyafil, F., et al., *Ferumoxtran-10-enhanced MRI of the hypercholesterolemic rabbit aorta - Relationship between signal loss and macrophage infiltration.* Arteriosclerosis Thrombosis and Vascular Biology, 2006. **26**(1): p. 176-181.
12. Walczak, P., et al., *Dual-modality monitoring of targeted intraarterial delivery of mesenchymal stem cells after transient ischemia.* Stroke, 2008. **39**(5): p. 1569-1574.
13. Medarova, Z., et al., *In vivo imaging of siRNA delivery and silencing in tumors.* Nature Medicine, 2007. **13**(3): p. 372-377.
14. Sharma, P., et al., *Nanoparticles for bioimaging.* Adv Colloid Interface Sci, 2006. **123-126**: p. 471-85.
15. Yang, Y.H., et al., *Amperometric glucose biosensor based on a surface treated nanoporous ZrO2/chitosan composite film as immobilization matrix.* Analytica Chimica Acta, 2004. **525**(2): p. 213-220.
16. Hikage, M., et al., *Nano-imaging of the lymph network structure with quantum dots.* Nanotechnology, 2010. **21**(18): p. -.

17. Garguilo, J.M., et al., *Fibrinogen adsorption onto microwave plasma chemical vapor deposited diamond films.* Diamond and Related Materials, 2004. **13**(4-8): p. 595-599.
18. Wong, H.L., et al., *A new polymer-lipid hybrid nanoparticle system increases cytotoxicity of doxorubicin against multidrug-resistant human breast cancer cells.* Pharmaceutical Research, 2006. **23**(7): p. 1574-1585.
19. Schiffelers, R.M., et al., *Cancer siRNA therapy by tumor selective delivery with ligand-targeted sterically stabilized nanoparticle.* Nucleic Acids Research, 2004. **32**(19).
20. Jain, P.K., I.H. El-Sayed, and M.A. El-Sayed, *Au nanoparticles target cancer.* Nano Today, 2007. **2**(1): p. 18-29.
21. Zhong, W.W., *Nanomaterials in fluorescence-based biosensing.* Analytical and Bioanalytical Chemistry, 2009. **394**(1): p. 47-59.
22. Vo-Dinh, T., L.R. Allain, and D.L. Stokes, *Cancer gene detection using surface-enhanced Raman scattering (SERS).* Journal of Raman Spectroscopy, 2002. **33**(7): p. 511-516.
23. Fu, C.C., et al., *Characterization and application of single fluorescent nanodiamonds as cellular biomarkers.* Proceedings of the National Academy of Sciences of the United States of America, 2007. **104**(3): p. 727-732.
24. Yu, X., et al., *High-resolution MRI characterization of human thrombus using a novel fibrin-targeted paramagnetic nanoparticle contrast agent.* Magnetic Resonance in Medicine, 2000. **44**(6): p. 867-872.
25. Nakajima, M., et al., *Nano-sized fluorescent particles as new tracers for sentinel node detection: Experimental model for decision of appropriate size and wavelength.* Cancer Science, 2005. **96**(6): p. 353-356.
26. Sirivisoot, S. and T.J. Webster, *Multiwalled carbon nanotubes enhance electrochemical properties of titanium to determine in situ bone formation.* Nanotechnology, 2008. **19**(29): p. -.
27. Cui, Y., et al., *Nanowire nanosensors for highly sensitive and selective detection of biological and chemical species.* Science, 2001. **293**(5533): p. 1289-1292.
28. Vogelstein, B. and K.W. Kinzler, *Cancer genes and the pathways they control.* Nature Medicine, 2004. **10**(8): p. 789-799.
29. Fong, K.M., et al., *Lung cancer - 9: Molecular biology of lung cancer: clinical implications.* Thorax, 2003. **58**(10): p. 892-900.
30. Vanraemdonck, D.E., A. Schneider, and R.J. Ginsberg, *Surgical-Treatment for Higher Stage Non-Small-Cell Lung-Cancer.* Annals of Thoracic Surgery, 1992. **54**(5): p. 999-1013.
31. Cavalieri, E., et al., *Catechol estrogen quinones as initiators of breast and other human cancers: Implications for biomarkers of susceptibility and cancer prevention.* Biochimica et Biophysica Acta (BBA) - Reviews on Cancer, 2006. **1766**(1): p. 63-78.
32. Jarde, T., et al., *Molecular mechanisms of leptin and adiponectin in breast cancer.* European Journal of Cancer, 2011. **47**(1): p. 33-43.
33. Smith, T.L., *Breast cancer: current and emerging trends in detection and treatment*. 2006: The Rosen Publishing Group, Inc.

34. D'Amico, T.A., et al., *Lung and heart-lung transplantation in patients with end-stage cystic fibrosis: The Stanford experience - Discussion.* Annals of Thoracic Surgery, 2002. **74**(1): p. 17-18.
35. Shennib, H., *Sublobar resection for lung cancer.* European Journal of Cardio-Thoracic Surgery, 1999. **16**: p. S61-S63.
36. Read, R.C., G. Yoder, and R.C. Schaeffer, *Survival after Conservative Resection for T1-N0-M0 Non-Small-Cell Lung-Cancer.* Annals of Thoracic Surgery, 1990. **49**(3): p. 391-400.
37. Nyren, O., et al., *Cancer Risk after Hip-Replacement with Metal Implants - a Population-Based Cohort Study in Sweden.* Journal of the National Cancer Institute, 1995. **87**(1): p. 28-33.
38. Brinton, L.A. and S.L. Brown, *Breast implants and cancer.* Journal of the National Cancer Institute, 1997. **89**(18): p. 1341-1349.
39. Nemecek, J.A.R. and V.L. Young, *How Safe Are Silicone Breast Implants.* Southern Medical Journal, 1993. **86**(8): p. 932-944.
40. McGregor, D.B., et al., *Evaluation of the carcinogenic risks to humans associated with surgical implants and other foreign bodies - a report of an IARC Monographs Programme Meeting.* European Journal of Cancer, 2000. **36**(3): p. 307-313.
41. Flemming, R.G., et al., *Effects of synthetic micro- and nano-structured surfaces on cell behavior.* Biomaterials, 1999. **20**(6): p. 573-588.
42. Denbraber, E.T., et al., *Effect of Parallel Surface Microgrooves and Surface-Energy on Cell-Growth.* Journal of Biomedical Materials Research, 1995. **29**(4): p. 511-518.
43. Dunn, G.A. and A.F. Brown, *Alignment of Fibroblasts on Grooved Surfaces Described by a Simple Geometric Transformation.* J Cell Sci, 1986. **83**: p. 313-340.
44. den Braber, E.T., et al., *Orientation of ECM protein deposition, fibroblast cytoskeleton, and attachment complex components on silicone microgrooved surfaces.* Journal of Biomedical Materials Research, 1998. **40**(2): p. 291-300.
45. Fewster, S.D., et al., *Precise Ultrafine Surface Texturing of Implant Materials to Improve Cellular Adhesion and Biocompatibility.* Nanobiology, 1994. **3**(3-4): p. 201-210.
46. Fujimoto, K., et al., *Cell activation by the micropatterned surface with settling particles.* Journal of Biomaterials Science-Polymer Edition, 1997. **8**(11): p. 879-891.
47. Harrington, D.A., et al., *Branched peptide-amphiphiles as self-assembling coatings for tissue engineering scaffolds.* Journal of Biomedical Materials Research Part A, 2006. **78A**(1): p. 157-167.
48. Hajicharalambous, C.S., et al., *Nano- and sub-micron porous polyelectrolyte multilayer assemblies: Biomimetic surfaces for human corneal epithelial cells.* Biomaterials, 2009. **30**(23-24): p. 4029-4036.
49. Thapa, A., et al., *Nano-structured polymers enhance bladder smooth muscle cell function.* Biomaterials, 2003. **24**(17): p. 2915-2926.

50. Miller, D.C., et al., *Endothelial and vascular smooth muscle cell function on poly(lactic-co-glycolic acid) with nano-structured surface features.* Biomaterials, 2004. **25**(1): p. 53-61.
51. Pattison, M.A., et al., *Three-dimensional, nano-structured PLGA scaffolds for bladder tissue replacement applications.* Biomaterials, 2005. **26**(15): p. 2491-2500.
52. Park, G.E., et al., *Accelerated chondrocyte functions on NaOH-treated PLGA scaffolds.* Biomaterials, 2005. **26**(16): p. 3075-3082.
53. Bakeine, G.J., et al., *Design and fabrication of large area nano-structured substrates for use in pancreatic beta-cell engineering.* Microelectronic Engineering, 2009. **86**(4-6): p. 1468-1472.
54. Tsukiyama, S., et al., *Enhanced cell survival and yield of rat small hepatocytes by honeycomb-patterned films.* Japanese Journal of Applied Physics, 2008. **47**(2): p. 1429-1434.
55. Ranjan, A. and T.J. Webster, *Increased endothelial cell adhesion and elongation on micron-patterned nano-rough poly(dimethylsiloxane) films.* Nanotechnology, 2009. **20**(30): p. -.
56. Ferraz, N., et al., *Influence of nanoporesize on platelet adhesion and activation.* Journal of Materials Science-Materials in Medicine, 2008. **19**(9): p. 3115-3121.
57. Burns, K., C. Yao, and T.J. Webster, *Increased chondrocyte adhesion on nanotubular anodized titanium.* Journal of Biomedical Materials Research Part A, 2009. **88A**(3): p. 561-568.
58. Bakeine, G.J., et al., *Design, fabrication and evaluation of nanoscale surface topography as a tool in directing differentiation and organisation of embryonic stem-cell-derived neural precursors.* Microelectronic Engineering, 2009. **86**(4-6): p. 1435-1438.
59. Lipski, A.M., et al., *The effect of silica nanoparticle-modified surfaces on cell morphology, cytoskeletal organization and function.* Biomaterials, 2008. **29**(28): p. 3836-3846.
60. Chen, Y.C., et al., *Induction and regulation of differentiation in neural stem cells on ultra-nanocrystalline diamond films.* Biomaterials, 2010. **31**(21): p. 5575-5587.
61. Oakley, C. and D.M. Brunette, *The Sequence of Alignment of Microtubules, Focal Contacts and Actin-Filaments in Fibroblasts Spreading on Smooth and Grooved Titanium Substrata.* J Cell Sci, 1993. **106**: p. 343-354.
62. den Braber, E.T., et al., *Quantitative analysis of cell proliferation and orientation on substrata with uniform parallel surface micro-grooves.* Biomaterials, 1996. **17**(11): p. 1093-1099.
63. Webb, A., et al., *Guidance of Oligodendrocytes and Their Progenitors by Substratum Topography.* J Cell Sci, 1995. **108**: p. 2747-2760.
64. Clark, P., et al., *Cell guidance by ultrafine topography in vitro.* J Cell Sci, 1991. **99 (Pt 1)**: p. 73-7.
65. Teixeira, A.I., et al., *Epithelial contact guidance on well-defined micro- and nanostructured substrates.* J Cell Sci, 2003. **116**(10): p. 1881-1892.
66. Johansson, F., et al., *Axonal outgrowth on nano-imprinted patterns.* Biomaterials, 2006. **27**(8): p. 1251-1258.

67. Choi, C.H., et al., *Cell interaction with three-dimensional sharp-tip nanotopography.* Biomaterials, 2007. **28**(9): p. 1672-1679.
68. Yang, F., et al., *Electrospinning of nano/micro scale poly(L-lactic acid) aligned fibers and their potential in neural tissue engineering.* Biomaterials, 2005. **26**(15): p. 2603-2610.
69. Shin, H.J., et al., *Electrospun PLGA nanofiber scaffolds for articular cartilage reconstruction: mechanical stability, degradation and cellular responses under mechanical stimulation in vitro.* Journal of Biomaterials Science-Polymer Edition, 2006. **17**(1-2): p. 103-119.
70. Dalby, M.J., et al., *Nucleus alignment and cell signaling in fibroblasts: response to a micro-grooved topography.* Experimental Cell Research, 2003. **284**(2): p. 274-282.
71. Nomura, S., et al., *Cell culture on nanopillar sheet: Study of HeLa cells on nanopillar sheet.* Japanese Journal of Applied Physics Part 2-Letters & Express Letters, 2005. **44**(37-41): p. L1184-L1186.
72. Dalby, M.J., et al., *Investigating filopodia sensing using arrays of defined nano-pits down to 35 nm diameter in size.* International Journal of Biochemistry & Cell Biology, 2004. **36**(10): p. 2005-2015.
73. Lee, K.Y., et al., *Nanoscale adhesion ligand organization regulates osteoblast proliferation and differentiation.* Nano Letters, 2004. **4**(8): p. 1501-1506.
74. Green, A.M., et al., *Fibroblast response to microtextured silicone surfaces: Texture orientation into or out of the surface.* Journal of Biomedical Materials Research, 1994. **28**(5): p. 647-653.
75. Hunt, J.A., et al., *Laser surface modification of polymers to improve biocompatibility.* Journal of Materials Science-Materials in Medicine, 1995. **6**(12): p. 813-817.
76. Lim, J.Y., et al., *Human foetal osteoblastic cell response to polymer-demixed nanotopographic interfaces.* Journal of the Royal Society Interface, 2005. **2**(2): p. 97-108.
77. Dalby, M.J., et al., *Increasing fibroblast response to materials using nanotopography: morphological and genetic measurements of cell response to 13-nm-high polymer demixed islands.* Experimental Cell Research, 2002. **276**(1): p. 1-9.
78. Yang, S.M., et al., *Nanomachining by colloidal lithography.* Small, 2006. **2**(4): p. 458-475.
79. Andersson, A.S., et al., *Nanoscale features influence epithelial cell morphology and cytokine production.* Biomaterials, 2003. **24**(20): p. 3427-3436.
80. Dalby, M.J., et al., *Attempted endocytosis of nano-environment produced by colloidal lithography by human fibroblasts.* Experimental Cell Research, 2004. **295**(2): p. 387-394.
81. Rich, A. and A.K. Harris, *Anomalous Preferences of Cultured Macrophages for Hydrophobic and Roughened Substrata.* J Cell Sci, 1981. **50**(Aug): p. 1-7.
82. Puleo, D.A. and A. Nanci, *Understanding and controlling the bone-implant interface.* Biomaterials, 1999. **20**(23-24): p. 2311-2321.
83. Wilson, C.J., et al., *Mediation of biomaterial-cell interactions by adsorbed proteins: A review.* Tissue Engineering, 2005. **11**(1-2): p. 1-18.

84. Jr., R.A.F., *Nanomedicine, Volume IIA:Biocompatibility*.
85. Anderson, J.M., *Biological responses to materials.* Annual Review of Materials Research, 2001. **31**: p. 81-110.
86. Anderson, J.M., *Inflammatory response to implants.* ASAIO Trans, 1988. **34**(2): p. 101-7.
87. Ahmad, S., *Host response - IgA - peacemaker in the gut.* Nature Reviews Microbiology, 2008. **6**(1): p. 4-4.
88. Fathi, M.H., et al., *In vitro corrosion behavior of bioceramic, metallic, and bioceramic-metallic coated stainless steel dental implants.* Dental Materials, 2003. **19**(3): p. 188-198.
89. Merritt, K. and J.J. Rodrigo, *Immune response to synthetic materials - Sensitization of patients receiving orthopaedic implants.* Clin Orthop Relat Res, 1996(326): p. 71-79.
90. Blank, J., *biological performance of materials: fundamentals of biocompatibility*.
91. Alexander, P., Horning, E. S., *Carcinogenesis, mechanisms of action.*
92. Webster, T.J., *Nanotechnology for the regeneration of hard and soft tissues*. 2007, Hackensack, N.J. ; London: World Scientific. xxi, 237 p.
93. Khang, D., et al., *Nanotechnology for regenerative medicine.* Biomedical Microdevices, 2010. **12**(4): p. 575-587.
94. Dulgar-Tulloch, A.J., R. Bizios, and R.W. Siegel, *Human mesenchymal stem cell adhesion and proliferation in response to ceramic chemistry and nanoscale topography.* Journal of Biomedical Materials Research Part A, 2009. **90A**(2): p. 586-594.
95. Boyan, B.D., et al., *Surface roughness mediates its effects on osteoblasts via protein kinase A and phospholipase A(2).* Biomaterials, 1999. **20**(23-24): p. 2305-2310.
96. Khang, D., et al., *Enhanced fibronectin adsorption on carbon nanotube/poly(carbonate) urethane: Independent role of surface nano-roughness and associated surface energy.* Biomaterials, 2007. **28**(32): p. 4756-4768.
97. Discher, D.E., P. Janmey, and Y.L. Wang, *Tissue cells feel and respond to the stiffness of their substrate.* Science, 2005. **310**(5751): p. 1139-1143.
98. Ulrich, T.A., E.M.D. Pardo, and S. Kumar, *The Mechanical Rigidity of the Extracellular Matrix Regulates the Structure, Motility, and Proliferation of Glioma Cells.* Cancer Research, 2009. **69**(10): p. 4167-4174.
99. Itoh, S., et al., *Enhanced bone ingrowth into hydroxyapatite with interconnected pores by electrical polarization.* Biomaterials, 2006. **27**(32): p. 5572-5579.
100. Chou, L.S., et al., *Substratum Surface-Topography Alters Cell-Shape and Regulates Fibronectin Messenger-Rna Level, Messenger-Rna Stability, Secretion and Assembly in Human Fibroblasts.* J Cell Sci, 1995. **108**: p. 1563-1573.
101. Keselowsky, B.G., D.M. Collard, and A.J. Garcia, *Integrin binding specificity regulates biomaterial surface chemistry effects on cell differentiation.* Proceedings of the National Academy of Sciences of the United States of America, 2005. **102**(17): p. 5953-5957.
102. Keselowsky, B.G., D.M. Collard, and A.J. Garcia, *Surface chemistry modulates focal adhesion composition and signaling through changes in integrin binding.* Biomaterials, 2004. **25**(28): p. 5947-5954.

103. Zhou, J., et al., *Layer by layer chitosan/alginate coatings on poly(lactide-co-glycolide) nanoparticles for antifouling protection and Folic acid binding to achieve selective cell targeting.* Journal of Colloid and Interface Science, 2010. **345**(2): p. 241-247.
104. Yang, L., B.W. Sheldon, and T.J. Webster, *The impact of diamond nanocrystallinity on osteoblast functions.* Biomaterials, 2009. **30**(20): p. 3458-3465.
105. Altankov, G. and T. Groth, *Reorganization of Substratum-Bound Fibronectin on Hydrophilic and Hydrophobic Materials Is Related to Biocompatibility.* Journal of Materials Science-Materials in Medicine, 1994. **5**(9-10): p. 732-737.
106. McHale, G., et al., *Topography driven spreading.* Physical Review Letters, 2004. **93**(3): p. 036102.
107. Goldenberg, N.M. and B.E. Steinberg, *Surface Charge: A Key Determinant of Protein Localization and Function.* Cancer Research, 2010. **70**(4): p. 1277-1280.
108. Qiu, Q., et al., *Attachment, morphology, and protein expression of rat marrow stromal cells cultured on charged substrate surfaces.* Journal of Biomedical Materials Research, 1998. **42**(1): p. 117-127.
109. Hallab, N.J., et al., *Cell adhesion to biomaterials: Correlations between surface charge, surface roughness, adsorbed protein, and cell morphology.* Journal of Long-Term Effects of Medical Implants, 1995. **5**(3): p. 209-231.
110. Carpenter, J., D. Khang, and T.J. Webster, *Nanometer polymer surface features: the influence on surface energy, protein adsorption and endothelial cell adhesion.* Nanotechnology, 2008. **19**(50): p. -.
111. Carpenter, J., D. Khang, and T.J. Webster, *Nanometer polymer surface features: the influence on surface energy, protein adsorption and endothelial cell adhesion.* Nanotechnology, 2008. **19**(50).
112. Webster, T.J., R.W. Siegel, and R. Bizios, *Osteoblast adhesion on nanophase ceramics.* Biomaterials, 1999. **20**(13): p. 1221-7.
113. Wang, X.H., et al., *Covalent immobilization of chitosan and heparin on PLGA surface.* International Journal of Biological Macromolecules, 2003. **33**(1-3): p. 95-100.
114. Zhang, Y.J., W. Li, and K.J. Chen, *Application of two-dimensional polystyrene arrays in the fabrication of ordered silicon pillars.* Journal of Alloys and Compounds, 2008. **450**(1-2): p. 512-516.
115. Cayre, O.J. and V.N. Paunov, *Fabrication of microlens arrays by gel trapping of self-assembled particle monolayers at the decane-water interface.* Journal of Materials Chemistry, 2004. **14**(22): p. 3300-3302.
116. Haginoya, C., M. Ishibashi, and K. Koike, *Nanostructure array fabrication with a size-controllable natural lithography.* Applied Physics Letters, 1997. **71**(20): p. 2934-2936.
117. Liu, H. and T.J. Webster, *Nanomedicine for implants: A review of studies and necessary experimental tools.* Biomaterials, 2007. **28**(2): p. 354-369.
118. Lafrenie, R.M., et al., *Up-Regulated Biosynthesis and Expression of Endothelial-Cell Vitronectin Receptor Enhances Cancer Cell-Adhesion.* Cancer Research, 1992. **52**(8): p. 2202-2208.

119. Gentile, F., et al., *Cells preferentially grow on rough substrates.* Biomaterials, 2010. **31**(28): p. 7205-7212.
120. Tsai, W.B. and J.H. Lin, *Modulation of morphology and functions of human hepatoblastoma cells by nano-grooved substrata.* Acta Biomaterialia, 2009. **5**(5): p. 1442-1454.
121. El-Said, W.A., et al., *Analysis of effect of nanoporous alumina substrate coated with polypyrrole nanowire on cell morphology based on AFM topography.* Ultramicroscopy, 2010. **110**(6): p. 676-681.
122. Martinez, E., et al., *Effects of artificial micro- and nano-structured surfaces on cell behaviour.* Annals of Anatomy-Anatomischer Anzeiger, 2009. **191**(1): p. 126-135.
123. Yang, L., et al., *Understanding osteoblast responses to stiff nanotopographies through experiments and computational simulations.* Journal of Biomedical Materials Research Part A, 2011. **97A**(4): p. 375-382.
124. Park, J., et al., *Nanosize and vitality: TiO2 nanotube diameter directs cell fate.* Nano Letters, 2007. **7**(6): p. 1686-1691.
125. Hanahan, D. and R.A. Weinberg, *The hallmarks of cancer.* Cell, 2000. **100**(1): p. 57-70.
126. Bergers, G. and L.E. Benjamin, *Tumorigenesis and the angiogenic switch.* Nature Reviews Cancer, 2003. **3**(6): p. 401-410.
127. Dunn, K.W., P.N. Hall, and C.T.K. Khoo, *Breast Implant Materials - Sense and Safety.* British Journal of Plastic Surgery, 1992. **45**(4): p. 315-321.
128. Steinbach, B.G., et al., *Breast Implants, Common Complications, and Concurrent Breast Disease.* Radiographics, 1993. **13**(1): p. 95-118.
129. Vazquez, G. and A. Pellon, *Polyurethane-coated silicone gel breast implants used for 18 years.* Aesthetic Plastic Surgery, 2007. **31**(4): p. 330-336.
130. Brook, M.A., *Platinum in silicone breast implants.* Biomaterials, 2006. **27**(17): p. 3274-3286.
131. Kwon, K.W., et al., *Label-free, microfluidic separation and enrichment of human breast cancer cells by adhesion difference{*. Lab on a Chip, 2007. **7**(11): p. 1461-1468.
132. Keon Woo, K., et al. *Label-Free, Microfluidic Separation of Human Breast Carcinoma and Epithelial Cells by Adhesion Difference*. in *Solid-State Sensors, Actuators and Microsystems Conference, 2007. TRANSDUCERS 2007. International*. 2007.
133. Barr, S., E. Hill, and A. Bayat, *Patterning of novel breast implant surfaces by enhancing silicone biocompatibility, using biomimetic topographies.* Eplasty, 2010. **10**: p. e31.
134. Dalby, M.J., A. Hart, and S.J. Yarwood, *The effect of the RACK1 signalling protein on the regulation of cell adhesion and cell contact guidance on nanometric grooves.* Biomaterials, 2008. **29**(3): p. 282-289.
135. Bell, G.I. and E.C. Anderson, *Cell Growth and Division .I. A Mathematical Model with Applications to Cell Volume Distributions in Mammalian Suspension Cultures.* Biophysical Journal, 1967. **7**(4): p. 329-&.

136. Blanco, E.M., M.A. Horton, and P. Mesquida, *Simultaneous investigation of the influence of topography and charge on protein adsorption using artificial nanopatterns.* Langmuir, 2008. **24**(6): p. 2284-2287.
137. Erickson, H.P., *Size and Shape of Protein Molecules at the Nanometer Level Determined by Sedimentation, Gel Filtration, and Electron Microscopy.* Biological Procedures Online, 2009. **11**(1): p. 32-51.
138. Kerr, J.F., A.H. Wyllie, and A.R. Currie, *Apoptosis: a basic biological phenomenon with wide-ranging implications in tissue kinetics.* Br J Cancer, 1972. **26**(4): p. 239-57.
139. Einspahr, J.G., et al., *Expression of vascular endothelial growth factor in early cutaneous melanocytic lesion progression.* Cancer, 2007. **110**(11): p. 2519-27.
140. Iyer, S., et al., *Atomic force microscopy detects differences in the surface brush of normal and cancerous cells.* Nat Nanotechnol, 2009. **4**(6): p. 389-93.
141. Wybourne, M.N., et al., *Creation of biomolecule arrays by electrostatic immobilization on electron-beam-irradiated polystyrene thin films.* Nanotechnology, 1996. **7**(3): p. 302-305.
142. Huang, M., E. Khor, and L.Y. Lim, *Uptake and cytotoxicity of chitosan molecules and nanoparticles: Effects of molecular weight and degree of deacetylation.* Pharmaceutical Research, 2004. **21**(2): p. 344-353.
143. Croll, T.I., et al., *A blank slate? Layer-by-layer deposition of hyaluronic acid and chitosan onto various surfaces.* Biomacromolecules, 2006. **7**(5): p. 1610-22.
144. Meng, X.N., et al., *Characterisation of fibronectin-mediated FAK signalling pathways in lung cancer cell migration and invasion.* Br J Cancer, 2009. **101**(2): p. 327-334.
145. Razina, T.G., et al., *Comparative Evaluation of the Efficiency of Various Alginate Forms under Conditions of an Oncological Experiment.* Bulletin of Experimental Biology and Medicine, 2011. **152**(2): p. 231-235.
146. Fujihara, M., et al., *Purification and Chemical and Physical Characterization of an Antitumour Polysaccharide from the Brown Seaweed Sargassum-Fulvellum.* Carbohydrate Research, 1984. **125**(1): p. 97-106.
147. Fujihara, M. and T. Nagumo, *An Influence of the Structure of Alginate on the Chemotactic Activity of Macrophages and the Antitumor-Activity.* Carbohydrate Research, 1993. **243**(1): p. 211-216.
148. Otterlei, M., et al., *Induction of Cytokine Production from Human Monocytes Stimulated with Alginate.* Journal of Immunotherapy, 1991. **10**(4): p. 286-291.
149. Qi, L.F., Z.R. Xu, and M.L. Chen, *In vitro and in vivo suppression of hepatocellular carcinoma growth by chitosan nanoparticles.* European Journal of Cancer, 2007. **43**(1): p. 184-193.
150. Lin, S.Y., et al., *Chitosan prevents the development of AOM-induced aberrant crypt foci in mice and suppressed the proliferation of AGS cells by inhibiting DNA synthesis.* Journal of Cellular Biochemistry, 2007. **100**(6): p. 1573-1580.
151. Kato, Y., H. Onishi, and Y. Machida, *Contribution of chitosan and its derivatives to cancer chemotherapy.* In Vivo, 2005. **19**(1): p. 301-310.
152. Zhu, X.S., et al., *Comparative toxicity of several metal oxide nanoparticle aqueous suspensions to Zebrafish (Danio rerio) early developmental stage.*

Journal of Environmental Science and Health Part a-Toxic/Hazardous Substances & Environmental Engineering, 2008. **43**(3): p. 278-284.
153. Zhou, J., et al., *Layer by layer chitosan/alginate coatings on poly(lactide-co-glycolide) nanoparticles for antifouling protection and Folic acid binding to achieve selective cell targeting.* J Colloid Interface Sci, 2010.
154. Lu, J., et al., *Improved endothelial cell adhesion and proliferation on patterned titanium surfaces with rationally designed, micrometer to nanometer features.* Acta Biomaterialia, 2008. **4**(1): p. 192-201.
155. Amaral, M., et al., *Nanocrystalline diamond: In vitro biocompatibility assessment by MG63 and human bone marrow cells cultures.* Journal of Biomedical Materials Research Part A, 2008. **87A**(1): p. 91-99.
156. Woo, K.M., et al., *Nano-fibrous scaffolding promotes osteoblast differentiation and biomineralization.* Biomaterials, 2007. **28**(2): p. 335-343.
157. Tran, P.A., et al., *Opportunities for nanotechnology-enabled bioactive bone implants.* Journal of Materials Chemistry, 2009. **19**(18): p. 2653-2659.
158. Slenters, T.V., et al., *Silver coordination compounds as light-stable, nano-structured and anti-bacterial coatings for dental implant and restorative materials.* Journal of Materials Chemistry, 2008. **18**(44): p. 5359-5362.
159. MacDonald, D.E., et al., *Thermal and chemical modification of titanium-aluminum-vanadium implant materials: effects on surface properties, glycoprotein adsorption, and MG63 cell attachment.* Biomaterials, 2004. **25**(16): p. 3135-46.
160. Khang, D., et al., *Selective adhesion and mineral deposition by osteoblasts on carbon nanofiber patterns.* Int J Nanomedicine, 2006. **1**(1): p. 65-72.
161. Scotchford, C.A., et al., *Growth of human osteoblast-like cells on alkanethiol on gold self-assembled monolayers: The effect of surface chemistry.* Journal of Biomedical Materials Research, 1998. **41**(3): p. 431-442.
162. Chung, T.H., et al., *The effect of surface charge on the uptake and biological function of mesoporous silica nanoparticles 3T3-L1 cells and human mesenchymal stem cells.* Biomaterials, 2007. **28**(19): p. 2959-2966.
163. Bettinger, C.J., R. Langer, and J.T. Borenstein, *Engineering Substrate Topography at the Micro- and Nanoscale to Control Cell Function.* Angewandte Chemie-International Edition, 2009. **48**(30): p. 5406-5415.
164. Hoffman-Kim, D., J.A. Mitchel, and R.V. Bellamkonda, *Topography, Cell Response, and Nerve Regeneration.* Annual Review of Biomedical Engineering, Vol 12, 2010. **12**: p. 203-231.
165. Tang, Q., et al., *Formation and characterization of protein patterns on the surfaces with different properties.* Synthetic Metals, 2004. **147**(1-3): p. 247-252.
166. Zemla, J., et al., *Selective Protein Adsorption on Polymer Patterns Formed by Self-Organization and Soft Lithography.* Biomacromolecules, 2009. **10**(8): p. 2101-2109.
167. Tan, J.L., et al., *Simple approach to micropattern cells on common culture substrates by tuning substrate wettability.* Tissue Engineering, 2004. **10**(5-6): p. 865-872.

168. Webster, T.J., et al., *Specific proteins mediate enhanced osteoblast adhesion on nanophase ceramics.* Journal of Biomedical Materials Research, 2000. **51**(3): p. 475-483.
169. Zhang, L., et al., *Arginine-glycine-aspartic acid modified rosette nanotube-hydrogel composites for bone tissue engineering.* Biomaterials, 2009. **30**(7): p. 1309-1320.
170. Dalby, M.J., *Topographically induced direct cell mechanotransduction.* Medical Engineering & Physics, 2005. **27**(9): p. 730-742.
171. Lamour, G., et al., *Neuronal adhesion and differentiation driven by nanoscale surface free-energy gradients.* Biomaterials, 2010. **31**(14): p. 3762-3771.
172. Yang, L., et al., *Altering surface energy of nanocrystalline diamond to control osteoblast responses.* Journal of Materials Chemistry, 2012. **22**(1): p. 205-214.
173. Miller, D.C., K.M. Haberstroh, and T.J. Webster, *Mechanism(s) of increased vascular cell adhesion on nanostructured poly(lactic-co-glycolic acid) films.* Journal of Biomedical Materials Research Part A, 2005. **73A**(4): p. 476-484.
174. Heikkila, O., et al., *Integrin alpha V beta 6 is a high-affinity receptor for coxsackievirus A9.* Journal of General Virology, 2009. **90**: p. 197-204.
175. van Kooten, T.G., H.T. Spijker, and H.J. Busscher, *Plasma-treated polystyrene surfaces: model surfaces for studying cell-biomaterial interactions.* Biomaterials, 2004. **25**(10): p. 1735-1747.
176. Blumenthal, R.D., H.J. Hansen, and D.M. Goldenberg, *Inhibition of adhesion, invasion, and metastasis by antibodies targeting CEACAM6 (NCA-90) and CEACAM5 (Carcinoembryonic antigen).* Cancer Research, 2005. **65**(19): p. 8809-8817.
177. Hiscox, S., et al., *Src kinase promotes adhesion-independent activation of FAK and enhances cellular migration in tamoxifen-resistant breast cancer cells.* Clinical & Experimental Metastasis, 2007. **24**(3): p. 157-167.
178. Underwood, P.A., J.G. Steele, and B.A. Dalton, *Effects of Polystyrene Surface-Chemistry on the Biological-Activity of Solid-Phase Fibronectin and Vitronectin, Analyzed with Monoclonal-Antibodies.* J Cell Sci, 1993. **104**: p. 793-803.
179. Takagi, J., et al., *Global conformational rearrangements in integrin extracellular domains in outside-in and inside-out signaling.* Cell, 2002. **110**(5): p. 599-611.
180. Sousa, S.R., P. Moradas-Ferreira, and M.A. Barbosa, *TiO2 type influences fibronectin adsorption.* Journal of Materials Science-Materials in Medicine, 2005. **16**(12): p. 1173-1178.
181. Dekker, A., et al., *Adhesion of Endothelial-Cells and Adsorption of Serum-Proteins on Gas Plasma-Treated Polytetrafluoroethylene.* Biomaterials, 1991. **12**(2): p. 130-138.
182. Campillo-Fernandez, A.J., et al., *Analysis of the Biological Response of Endothelial and Fibroblast Cells Cultured on Synthetic Scaffolds with Various Hydrophilic/Hydrophobic Ratios: Influence of Fibronectin Adsorption and Conformation.* Tissue Engineering Part A, 2009. **15**(6): p. 1331-1341.
183. Iwamoto, G.K., et al., *Fibronectin Adsorption Detected by Interfacial Fluorescence.* Journal of Colloid and Interface Science, 1985. **106**(2): p. 459-464.
184. Wittmer, C.R., et al., *Fibronectin terminated multilayer films: Protein adsorption and cell attachment studies.* Biomaterials, 2007. **28**(5): p. 851-860.

185. Toromanov, G., et al., *Vitronectin activity on polymer substrates with controlled -OH density.* Polymer, 2010. **51**(11): p. 2329-2336.
186. Barrias, C.C., et al., *The correlation between the adsorption of adhesive proteins and cell behaviour on hydroxyl-methyl mixed self-assembled monolayers.* Biomaterials, 2009. **30**(3): p. 307-316.
187. Renner, L., et al., *Fibronectin displacement at polymer surfaces.* Langmuir, 2005. **21**(10): p. 4571-4577.
188. Nista, A., et al., *Functional role of alpha 4 beta 1 and alpha 5 beta 1 integrin fibronectin receptors expressed on adriamycin-resistant MCF-7 human mammary carcinoma cells.* International Journal of Cancer, 1997. **72**(1): p. 133-141.